The Use of Landsat Thematic Mapper in the Study of Landuse/Cover and Water Quality Relationships

Lubna Ahmad Shihadeh

Thesis submitted to the Faculty of
Virginia Polytechnic Institute and State University
in partial fulfillment of the requirements for the degree of
Master of Science
in
Biological Systems Engineering

Mary Leigh Wolfe
James B. Campbell
W. Cully Hession

September 10, 2010
Blacksburg, Virginia

Key Words: Remote sensing, Landuse/cover change, Water quality, Chromaticity

The Use of Landsat Thematic Mapper in the Study of Landuse/Cover and Water Quality Relationships

Lubna Ahmad Shihadeh

Abstract

In Jordan, the fourth driest country in the world, demand for water exceeds available water resources. The annual per capita water availability is 145 Cubic Meter (CM) per year, which is below the international poverty line of 500 CM/year. The increasing water deficit year-on-year poses serious future threat that will impact many sectors. Water quantity and quality are essential issues in Jordan and more efforts are needed to find new water resources, and to protect and improve the available resources.

This research seeks to study the relationship between Landuse/cover change and water quality in reservoirs in Jordan. Landuse changes were detected by using Landsat Thematic Mapper (TM) images obtained for King Talal reservoir in 1990 and 2006 and for Karameh reservoir in 1998 and 2006. Geometric correction and supervised classification were utilized in ERDAS software. Turbidity levels within the two reservoirs were estimated by the chromaticity technique and were compared to measured data from previous reports for both reservoirs. Remote sensing was successful in detecting the changes in landuse in both areas. The estimated turbidity levels correlated moderately well with measured data from previous reports for the same reservoirs; it was difficult to directly relate a specific Landuse/cover for turbidity levels. Limitations were defined as data collection and quality problems, in addition to some theoretical issues about using Landsat for this study.

ACKNOWLEDGMENTS

First of all, thanks to Allah for making this possible.

I would like to thank Dr. Mary Leigh Wolfe for her knowledge and support both academically and financially while serving as my major advisor. Thanks also go to my other committee members Dr. James B. Campbell, and Dr. W. Cully Hession for their assistance and support. Their instruction and mentorship has greatly helped in my research, and made my graduate experience successful one in many ways.

Also, I would like to thank Dr. Ali Al-Qudah, Dr. Mohammad Al-Smadi, Dr. Mustafa Al-Qaisi, Dr. Suhail Al-Wahsheh, Dr. Javier Osorio, and Sally Walker for their continuous support and help.

Many thanks for all the Biological Systems Engineering staff, friends, and graduate students.

DEDICATION

To my parents, Dad, Mr. Ahamad Shihadeh and Mom, Madam Safieh Abu-Zaied, thank you for being a great source of support and encouragement, prayers and many more. Any achievement in my life is a direct result of you sacrifices and your excellent parenting. Without you, this wouldn't have been possible.

To my husband, Shouib, I would like to say that your dedication and support throughout the life and this research project have had a great impact on me and helped me to continue working when I had a down moment in my school work. Thanks because of you my dream become true.

To my brothers, Dr. Wisam Shihadeh, Dr. Mohamad Shihadeh, my sisters, Wafa, Fida and Lina you have encouraged me to keep moving forward all the time.

To all my friends in Jordan and in the United States.

In the memory of my father in law, Dr. Nouh Al-Qudah for his support and care for me during this work

TABLE OF CONTENTS

LIST OF FIGURES

LIST OF TABLES

1 INTRODUCTION

1.1 Problem statement

Jordan is the fourth driest country in the world. Demand for water exceeds Jordan's available water resources. Access to a safe water supply is an essential requirement. In 2007 the demand exceeded resources by 638 Million Cubic Meter (MCM)/year and the allocations exceeded resources by 73 MCM (Ministry of Water and Irrigation, 2008). The annual per capita water availability is 145 Cubic Meter (CM)/year. This is far below the international poverty line of 500 CM/year. Water is an essential commodity for municipal, industrial and agricultural uses. The increasing water deficit year-on-year poses a serious future threat that will impact all sectors. A serious effort must be made at all levels: individuals, private and public sectors. The future challenges on water demand are enormous. Any unexpected population growth due to regional instability, as was the case during the past decades, would increase water demand and impact the plans to reach a balanced demand and supply.

In a country such as Jordan that is poor in water resources, dams become a good way to store and collect water from rainfall and rivers flow and provide it for different uses. Dams provide 33% (317 MCM) of the total amount of water needed for domestic use, agriculture, and industry. More efforts are needed to find new surface-water resources, such as building new dams, and to protect and improve the available resources. In addition, dams can improve the areas around them with respect to agriculture, tourism, and groundwater recharge.

Many dams were built to increase the water supply. King Talal Reservoir (KTR) is one of the largest projects in Jordan. The reservoir capacity is about 86 MCM. The dam height is 108 m and the catchment area is 3000 km^2. The reservoir is used to irrigate about 100 km^2 in the Jordan Valley. The population of the catchment area is about half of the kingdom population, which is distributed in Amman, Zarqa, Sweileh, Rusaifeh, Baka'a and Jerash with several villages around these cities (Royal Scientific Society, 2001).

The influent water to the reservoir is a mixture of rainfall, spring water, and domestic and industrial waste. These influent waters lead to degradation in the water quality of the reservoir

and reduce its usefulness as a major source of water in Jordan. Since the reservoir is now used for irrigation purposes, the monitoring activities are necessary to help keep the KTR effluent within the standards for irrigation water quality (Royal Scientific Society, 2006). Also, these monitoring activities will help forecasting the water quantity and quality which is necessary to establish precautionary measures to protect against any anticipated problems.

This research will focus also on Karameh Dam, which was built in 1997 with a capacity of 55 MCM, in Jordan Valley area to supply water for domestic, irrigation and recreation. The dam was constructed in spite of warnings from experts that this dam would fail (Salameh, 2004). Now, 13 years after its construction, the dam fails to fulfill its purposes because of the limited sources available to fill it and water is of bad quality. The government is paying the depreciation, capital, and operating costs of this project while realizing no benefit.

Monitoring water quality of reservoirs is important, especially for poor and dry countries like Jordan to sustain the quality and the potability of the water resource. The adverse effects of point or non-point source pollutants on the water quality of water resources should be controlled and reduced. The uncontrolled landuse/cover in the vicinity of the reservoirs is deteriorating the water quality of vital potable sources of water in Jordan and actions should be taken to improve the water quality and control the changes in landuse/cover.

Although field measurements provide correct information at a certain time and at a particular location, this method becomes expensive and incapable of monitoring the water quality of the entire source of a very large area at certain periods. Sensors placed on remote sensing platforms, to sense the earth surface at various resolutions, offer significant advantages to monitor water quality parameters of large water bodies by taking the most accurate and contemporary measurements over large regions.

1.2 Objectives

1. To evaluate the potential for developing landuse/cover maps for Jordan by using remote sensing techniques.
2. To quantify the changes in landuse/cover in dam areas in Jordan.

3. To determine if changes in water quality can be detected using remote sensing techniques.
4. To identify the relationship between the changes in landuse/cover and reservoir water quality over a period of time using remote sensing data.

1.3 Jordan background

1.3.1 Geography

Jordan, officially the Hashemite Kingdom of Jordan, is an Arab country in southwest Asia spanning the southern part of the Syrian Desert down to the Gulf of Aqaba. It shares borders with Syria to the north, Iraq to the northeast, the West Bank to the west, and Saudi Arabia to the east and south. It shares control of the Dead Sea with the West Bank, and the coastline of the Gulf of Aqaba Saudi Arabia, and Egypt. Much of Jordan is covered by desert, particularly the Arabian Desert; however the northwestern area, with the Jordan River, is regarded as part of the Fertile Crescent. The capital city of Amman is in the northwest.

Jordan consists of arid forest plateau in the east irrigated by oasis and seasonal-water streams with highland area in the west of arable land and Mediterranean evergreen forest. The Great Rift Valley of the Jordan River separates Jordan from the West Bank. The highest point in the country is Jabal Umm al Dami, located 1,854 meter (m) above sea level, while the lowest point is the Dead Sea at an elevation of - 408 m below sea level. Jordan is part of a region considered to be "the cradle of civilization" (Central Intelligence Agency, 2009).

1.3.2 Climate

The climate in Jordan varies between a very rainy season from November to March and semi-dry weather for the rest of the year. With hot, dry, and uniform summers, and cool, freezing, variable winters during which practically all of the precipitation occurs, the country has a Mediterranean-style climate. In general, the farther inland from the Mediterranean Sea, the greater the seasonal contrasts in temperature and rainfall decrease (Ministry of Water and Irrigation, 2008). Atmospheric pressures during the summer months are relatively uniform, whereas the winter months bring a succession of marked low pressure areas and accompanying

cold fronts. These cyclonic disturbances generally move eastward from over the Mediterranean Sea several times a month and result in sporadic precipitation.

Most of the East Bank receives less than 620 millimeter (mm)/year of rain (Figure 1.1) and is classified as a semi-dry region. In the eastern highlands of the Jordan Valley, precipitation ranges between 300 mm/year in the south to 500 mm/year or more in the northern section. The Jordan Valley, lying in the lee of high ground on the West Bank, forms a narrow climatic zone that receives up to 900 mm/year of rain in the northern reaches; rain dwindles to less than 120 mm/year at the head of the Dead Sea (Central Intelligence Agency, 2009).

Figure 1.1. Map of Jordan (Central Intelligence Agency, 2009)

The country's long summer reaches a peak during August. January is usually the coldest month. The fairly wide ranges of temperature during a 24-hour period are greatest during the summer months and have a tendency to increase with higher elevation and distance from the Mediterranean seacoast. Daytime temperatures during the summer months frequently exceed 29 °C (84.2 ˚F) and average about 32 °C (89.6˚F). In contrast, the winter months, September to March, bring moderately cool and sometimes very cold weather, averaging about 3.2 °C (37.8˚F) (Central Intelligence Agency, 2009). Except in the rift depression, frost is fairly common during

the winter; it may take the form of snow at the higher elevations of the northwestern highlands. Usually it snows a couple times in the winter in western Amman.

For a month or so before and after the summer dry season, hot, dry air from the desert, drawn by low pressure, produces strong winds from the south or southeast that sometimes reach gale force. Known in the Middle East by various names, including the Khamsin, this dry, sirocco-style wind is usually accompanied by great dust clouds. Its onset is heralded by a hazy sky, a falling barometer, and a drop in relative humidity to about 10 percent. Within a few hours there may be a 10 °C to 15 °C rise in temperature. These windstorms ordinarily last a day or so, cause much discomfort, and destroy crops by desiccating them.

The Shammal, another wind of some significance, comes from the north or northwest, generally at intervals between June and September. Remarkably steady during daytime hours but becoming a breeze at night, the Shammal may blow for as long as nine days out of ten and then repeat the process. It originates as a dry continental mass of polar air that is warmed as it passes over the Eurasian landmass. The dryness allows intense heating of the Earth's surface by the sun, resulting in high daytime temperatures that moderate after sunset (Central Intelligence Agency, 2009).

1.3.3 Water resources

Water supply and sanitation in Jordan is characterized by severe water scarcity, which has been exacerbated by forced immigration as a result of the 1948 Arab–Israeli War, the Six-Day War in 1967, the Gulf War of 1990, and the Iraq War of 2003. Jordan is considered as one of the ten most water scarce countries in the world (Ministry of Water and Irrigation, 2008). High population growth and the depletion of groundwater reserves are likely to aggravate the situation in the future. The country's major surface-water resources, the Jordan River and the Yarmouk River, are shared with Israel and Syria who leave only a small amount for Jordan (Ministry of Water and Irrigation, 2008). Groundwater resources in the country are overexploited, which causes pollution and depletion in the long term. The Jordanian government plans to bridge the gap between demand and supply through increased use of nonconventional water resources, such as desalinated water, wastewater reuse, and the Disi project, which features a 320 Kilometer (Km) long conveyor from the non-renewable Disi aquifer to the capital Amman.

The Red Sea-Dead Sea Canal project aims to provide desalinated water for people in Jordan. This Canal will channel 1.9 Billion Cubic Meter (BCM)/day from the Red Sea to the Dead Sea. In addition, the difference in altitude will enable the production of energy, which in turn will fuel desalination plants to be constructed in Jordan. The 850 MCM/year of desalinated water will be used for agriculture and urban water systems (Sharp, 2009) and the rest of the water will be used to recharge the Dead Sea. The idea of a regional joint project was raised more than a decade ago and is still under study (Sharp, 2009).

Despite Jordan's severe water scarcity, more than 97% of Jordanians have access to an improved water source and 93% have access to improved sanitation (Ministry of Water and Irrigation, 2008). This is one of the highest rates in the Middle East and North Africa (MENA); however, water supply is irregular and it is common to store water in rooftop tanks. The country seeks to increase cost recovery and efficiency of the water and sanitation sector through a number of new laws, a new tariff system, and a National Water Master Plan concerning infrastructure financing. The country relies largely on external donors (Central Intelligence Agency, 2009).

The Ministry of Water and Irrigation has the major role to lead the initiative to establish a Water Strategy for the future. This water strategy identifies many plans for Jordan’s future water and the actions that the Ministry will take to ensure that water is available for people, business, and nature (Ministry of Water and Irrigation, 2008).

Since the shortage of water resources in Jordan was first widely recognized in the early 1970’s, many strategies and measures have been proposed to alleviate and overcome it. These have included supply augmentation measures involving the construction of various hydraulic structures and the development of groundwater. However, no single action can remedy the nation's water shortage (Ministry of Water and Irrigation, 2008). Rather, an integrated approach will be adopted to enhance water availability, suitability, and sustainability. This approach requires that water be well managed and used as efficiently as possible, that demand be proficiently managed, that all available sources of water be developed, and that adverse impacts be mitigated through measures of environmental protection (Royal Scientific Society, 2006).

1.3.3.1 Surface water

The average amount of water from different basins is about 690 MCM/year. There are 15 basins located in different parts of Jordan (Ministry of Water and Irrigation, 2008). Surface water supplies contribute approximately 37% to Jordan's total water supply. Developed surface water in Jordan was estimated at 295 MCM in 2007 and projected to be 365 MCM by 2022 (Ministry of Water and Irrigation, 2008). Ten dams were constructed to store water that comes from rain and rivers.

1.3.3.2 Groundwater

Groundwater contributes approximately 54% of the total water supply and 80% of the drinking water (Ministry of Water and Irrigation, 2008). The unsustainable withdrawal of groundwater largely due to population growth and agricultural expansion is a major problem today. This has been made worse by the lack of enforcement of regulations on private sector well drilling and the near absence of controls on licensed abstraction rates. As water tables drop, pumping costs and salinity levels increase. Ten out of twelve water basins are over-pumped; groundwater is used at twice the recharge rate. Demand far exceeds supply and the deficit is increasing. Even with additional planned projects, demand will still exceed supply through 2022 (Ministry of Water and Irrigation, 2008).

1.3.3.3 Wastewater

The Water Authority of Jordan (WAJ) provides wastewater collection and treatment services to fourteen major populated areas. About four million people (62% of the population) are served by sewerage systems producing about 100 MCM/year of effluent that is being reused primarily in agriculture (Ministry of Water and Irrigation, 2008).

1.3.3.4 Brackish water

Several brackish springs have been identified in various parts of the country. Estimates of stored volumes of brackish groundwater for the major aquifers suggest vast resources, but not all of these quantities will be feasible for utilization because of the desalination cost (Ministry of Water and Irrigation, 2008).

1.3.4 Water strategy

H.M. King Abdullah II stated in 1999 that "Our water situation forms a strategic challenge that cannot be ignored. We have to balance between drinking water needs and industrial and irrigation water requirements. Drinking water remains the most essential and the highest priority issue" (Ministry of Water and Irrigation, 2008).

So Jordan found a new vision for a water strategy by the Ministry of Water and Irrigation (2008-2020) which aims to achieve the following goals:

a. "Adequate, safe, and secure drinking water supply."
b. "Greater understanding and more effective management of groundwater and surface water."
c. "Healthy aquatic ecosystems."
d. "A sustainable use of water resources, and implemented fair, affordable, and cost reflective water charges; Adaptation to increased population growth and economic development across the water sector and water users."
e. "Groundwater levels have dramatically declined showing that groundwater exploitation in the past was unsustainable. The abstracted amounts in each area need to be limited to the long-term sustainable amount."
f. "A sustainable water supply and demand balance must be secured. This means limiting and even reducing water consumption, while not ruling out new supply infrastructure."
g. "The economic development of the past two decades has created enormous pressures on the quality of ground and surface water resources. The process of deteriorating water quality must be halted. This requires that water sources are actively protected from pollution through actions of the Ministry of Water and Irrigation and other involved Ministries/Agencies (i.e. Ministry of Environment), such as setting up and implementing ground and surface water protection zones as well as through appropriate landuse planning which takes the need for water resources protection into account." (Ministry of Water and Irrigation, 2008)

1.3.5 Dams

Dam construction was a top priority of the Jordan development plans. Six dams were constructed in the period from 1967 to 2006 in the north and middle Jordan Valley with a total storage capacity of 160 MCM. These dams include Arab, Ziglab, King Talal, Karameh, Shueib, and Kafrein. Three other dams (Wala, Mujib, and Tannur) were constructed in the Southern Ghors with a total storage capacity of 57 MCM. Additional desert dams have been constructed in the highland and Badia areas with a total live storage of 30 MCM. Stored water from these dams is used for livestock and ground water recharge (Ministry of Water and Irrigation, 2008). Characteristics of the main dams in Jordan are listed in Table 1.1.

Table 1.1. Main dams in Jordan (Ministry of Water and Irrigation, 2008)

Location	Dam name	Construction	Cost MJD[a]	Type	Height (M)	Storage capacity MCM[b]	Annual Yield MCM[b]	Purpose
120 km north of Amman, (Yarmouk River)	Wehdeh	Completed in 2006	67	Roller compacted concrete (RCC)	87	110	81	Domestic& Irrigation
100 km south of Amman, (Wadi Mujib)	Mujib	Completed in 2003	45	RCC central section with overflow stepped spillway and earth fill wing embankments	62	31.2	17	Municipal & industry supply, & irrigation
60 km south of Amman, (Wadi Wala)	Wala	Completed in 2002	24	RCC central section with overflow stepped spillway and earth fill wing embankments	52	9.3	6	Municipal & industry supply, irrigation, and recharge
175 km south of Amman, (Wadi Hassa)	Tannur	Completed in 2001	23	RCC with overflow stepped spillway	60	16.8	8	Irrigation
Wadi Arab	Wadi Arab	Completed in 1986	20	Earth fill	83.5	16.8	16.8	Irrigation, municipal, & hydropower
Wadi Ziglab	Sharhabeel (Ziglab)	Completed in 1967	0.9	Earth fill	48	3.9	3.9	Irrigation
Zarqa river	King Talal	Completed in 1977	34	Earth fill	108	74	75	Irrigation

[a] MJD= Million Jordanian Dinar. (1.00 Jordanian Dinar = 1.408 U.S. Dollar, as of 1 September 2010) (Yahoo® Finance, http://finance.yahoo.com/currency-converter/)

[b] MCM= Million Cubic Meter.

2 LITERATURE REVIEW

This chapter is divided into four sections. The first section describes the characteristics of the available remotely sensed data. The second section talks about the preprocessing of the images and the data preparation. Sections three and four review the different remote sensing techniques used for monitoring landuse/cover change and water quality.

2.1 Remotely sensed data

2.1.1 Landsat

The Landsat series of satellites provides the longest continuous record of satellite-based observations. Landsat is an invaluable resource for monitoring global change and is a primary source of medium spatial resolution Earth observations used in decision-making (Chander et al., 2009). The Landsat Program began in early 1972 with the launch of the first satellite in the series. As technological capabilities increased, so did the amount and quality of image data captured by the various sensors onboard the satellites. Table 2.1 presents general information about each Landsat satellite.

Table 2.1. General information about each Landsat satellite (Chander et al., 2009)

Satellite	Sensor	Launch date	Decommission	Altitude Km	Inclination Degrees	Period Min	Repeat cycle Days	Crossing Time (a.m)
Landsat 1	MSS [a] and RBV[b]	July 23, 1972	January 7, 1978	920	99.20	103.34	18	9:30
Landsat 2	MSS and RBV	January 22, 1975	February 25, 1982	920	99.20	103.34	18	9:30
Landsat 3	MSS and RBV	March 5, 1978	March 31, 1983	920	99.20	103.34	18	9:30
Landsat 4	MSS and TM[c]	July 16, 1984	June 30, 2001	705	98.20	98.20	16	9:45
Landsat 5	MSS and TM	March 1, 1984	Operational	705	98.20	98.20	16	9:45
Landsat 6	ETM[d]	October 5, 1993	Did not achieve orbit					
Landsat 7	ETM+[e]	April 15, 1999	Operational	705	98.20	98.20	16	10:00
EO-1	ALI[f]	November 21, 2000	Operational	705	98.20	98.20	16	10:01

[a] MSS = Multispectral Scanner Sensor

[b] RBV = Return Beam Vidicon camera

[c] TM = Thematic Mapper sensor

[d] ETM = Enhanced Thematic Mapper sensor

[e] ETM+ = Enhanced Thematic Mapper Plus sensor

[e] ALI = Advanced Land Imager

2.1.1.1 Thematic Mapper sensor

Landsat Thematic Mapper (TM) is a sensor carried onboard Landsats 4 and 5 that has acquired images of the Earth nearly continuously from July 1982 to the present with a 16-day repeat cycle (United States Geological Survey, 2010). It has a temporal resolution and synoptic view, which makes it good for different types of studies, such as landuse change, water quality, and forest harvesting.

Landsat TM image data files consist of seven spectral bands (band designations) Table 2.2. The resolution is 30 meters for bands 1-5 and 7. Band 6 resolution (thermal infrared) is a collected 120 meters, but is resampled to 30 meters. The approximate scene size is 170 km north-south by 183 km east-west. Images have a radiometric resolution of 8-bits; therefore, pixel values range from 0 to 255.

Table 2.2. Characteristics of Landsat TM (United States Geological Survey, 2010)

Band Number	Data Recorded	Spectral Resolution (micrometers)	Spatial Resolution (meters)
Band 1	Blue	0.45-0.52	30
Band 2	Green	0.52-0.60	30
Band 3	Red	0.63-0.69	30
Band 4	Near IR	0.76-0.90	30
Band 5	Mid IR	1.55-1.75	30
Band 6	Thermal IR	10.40-12.50	120
Band 7	Mid IR	2.08-2.35	30

2.1.1.2 Multispectral scanner (MSS)

The spatial resolution of the multispectral scanner (MSS) sensor was approximately 79m (but often processed to pixel size of 60 m), with four bands ranging from the visible blue to the near- infrared (NIR) wavelengths. The MSS sensor on Landsat 3 (L3) included a fifth band in the thermal infrared wavelength, with a spectral range from 10.4 to 12.6 μm. The Landsat 1-3 MSS sensors used a band-naming convention of MSS-4, MSS-5, MSS-6, and MSS-7 for the blue, green, red, and NIR bands, respectively (Chander et al., 2009) .

2.1.1.3 Enhanced Thematic Mapper plus (ETM+)

The enhanced thematic mapper (ETM) and the enhanced thematic mapper plus (ETM+) sensors are on board Landsat 6 (L6) and Landsat 7 (L7), respectively. There are no data from the ETM sensor because L6 failed on launch. The L7 ETM+ sensor has a spatial resolution of 30 m for the six reflective bands and 60 m for the thermal band, and includes a panchromatic (pan) band with a 15 m resolution. L7 has a 378 gigabit (GB) Solid State Recorder (SSR) that can hold 42 minutes (approximately 100 scenes) (Chander et al., 2009).

2.2 Image preparation

2.2.1 Image registration

Images should be registered to one another with the best possible accuracy. Jensen (1995) recommends a root mean square error (RMSE) of 0.5 pixel or less, while Dai and Khorram (1998) suggest a RMSE of 0.2 pixel or less. Misregistration can cause false changes to appear on the change detection map, especially around class boundaries. Fuller et al. (1994) noted that even minor misregistration results in misclassification, especially with boundary pixels. They also stated that the misregistration results in a greater number of mixed pixels in the composite image, with up to 40% of the pixels representing mixed boundaries.

In order for the imagery to be compatible with other spatial data, a geographic rectification must be performed. Campbell (2007) mentioned geometric correction by resampling as another approach to image registration. In this method, the images are considered as an array of values and manipulated to create another array with the preferred geometry. This can be understood as an interpolation problem similar to those considered in other subjects. Campbell (2007) described three interpolation methods:

a. Nearest neighbor;
b. Bilinear interpolation; and
c. Cubic convolution.

The nearest neighbor resampling method is very simple; it computes new pixels as the value of the nearest pixel in the original image (Jonathan, 2001). This method is most common

because it is fast and does not lead to loss of information by smoothing (Kondratyev and Cracknell, 1998). However, there is the chance of repetition or omission of pixel digital numbers(Kondratyev and Cracknell, 1998). The nearest neighbor method may also result in some scan-line duplication (Itten and Meyer, 1993) .

Bilinear interpolation calculates a value for each pixel based upon the weighted average of the four nearest input pixels (Campbell, 2007), while cubic convolution interpolation uses a weighted average of values within a neighborhood that extends about two pixels in each direction. The bilinear and cubic methods smooth the data and therefore some data are lost. For example, the brightness values in the output image may differ from those in the input image. These methods may decrease the spatial resolution by averaging. Both the nearest neighbor (McGwire et al., 1996) and cubic convolution (Muller et al., 1998) methods are commonly used. In a study by Kovalick (1983) study, the nearest neighbor method was computationally the most efficient of the three methods.

2.2.2 Atmospheric correction

Errors in remote sensing data can be defined in different ways, including sensor calibration errors and atmospheric effects (Jensen et al., 1995). Solar radiation is basically unaffected as it travels through space. However, during the transmission through the atmosphere, it is selectively scattered and absorbed (Jensen et al., 1995). Atmosphere between the terrain and the remote sensing system can assign so much noise that the energy recorded no longer resembles the energy reflected by the terrain (Jensen et al., 1995). A result of atmospheric scattering is that fine detail in an image is lost (Richards, 1995). Because some types of scattering are wavelength dependent, the atmosphere will affect the bands differently (Bernstein et al., 1983; Richards, 1995), with the shorter wavelengths affected the most.

Atmospheric correction involves minimizing the effects of wavelength dependent scattering in imagery caused by haze and smoke. Different atmospheric scattering or haze removal techniques have been developed for use with digital remotely sensed data. The simplest method or most direct method is dark object subtraction (Chavez, 1975; Rowan, 1974; Vincent, 1972)Other methods are more sophisticated, using various atmospheric transmission models and in situ field data, and require specific targets to be present in the image (Ahern et al., 1977;

Otterman and Robinove, 1981). A major disadvantage with the more sophisticated techniques is that they require information other than the digital image data, e.g., path radiance and /or atmospheric transmission at several locations within the image area collected during the satellite over flight.

A method that uses in situ or ground-truth information is the most accurate in terms of correcting for atmospheric haze effects (Chavez, 1988) . However, users usually work with remotely sensed data that have already been collected. Because of that the simple dark-object subtraction technique can be used because it requires only information contained in the digital image data. This type of correction involves subtracting a constant digital number (DN) value from the entire digital image. This assumes a constant haze value throughout the entire image, and this is not the case always (Chavez, 1988). However, it does accomplish a first-order correction, which is better than no correction at all. A different constant is used for each spectral band.

According to Chavez (1988) most dark-object subtraction techniques assume that there are at least a few pixels within an image that should be black (0% reflectance). This assumption is made because in a single band there are a very large number of pixels. For example, for Landsat MSS and TM single-band images, there are over 7 million and 45 million pixels, respectively. Thus, there are usually some shadows due to topography or clouds in the image where the pixels should be completely dark. Ideally, if the atmosphere is clear, the imaging system should not detect any radiance at these shadow locations, and a DN value of zero should be assigned to them. However, because of atmospheric scattering, these shadowed areas will not be completely dark. Because of atmospheric scattering, the imaging system records a nonzero DN value at these apparently dark-shadowed pixel locations. This represents the DN value that should be subtracted from the particular spectral band to remove the first-order scattering component.

2.3 Monitoring Landuse/cover change using remote sensing

2.3.1 Remote sensing for monitoring Landuse/cover

Land cover change is one of the most significant disturbances to the regional environment (Vitousek, 1992). The cumulative effect of land cover and land use changes can impact global climate (Moran, 1993; Shukla et al., 1990), biogeochemical cycle (Detwiler and Hall, 1988; Lugo and Brown, 1992) , and biodiversity through habitat fragmentation (Skole and Tucker, 1993). It is vital to monitor land cover and land use change at regional and global scales. Land-cover change is closely related to the terrestrial surface material cycles and life-support processes (Liu et al., 2003). Monitoring landuse/cover change is complex when it is considered that in many areas historic land cover data are either of poor quality, or do not exist at all (Roberts et al., 1998). Even in the United States where a large amount of historic data exists, much of the data is incompatible because of differences in spatial resolution, accuracy, periodicity, file format, classification schemes, and availability (Gildea, 2000).

The lack of regular collection of ground truth data and the rapid changes made by humankind make the need for multitemporal data essential. Remote sensing plays an important role in linkage and analysis of temporal and spatial data, using techniques such as interpretation, detection, monitoring changes, and calculating areas. The Food and Agriculture Organization of the United Nations (FAO), for example, has put forward its land use/cover classification based on remote sensing data (Brent, 2002).

There have been many studies to monitor changes in landuse/cover and ecosystem. For example, Zhenqiang et al. (2004) studied the change in landuse/cover change and land degradation using remote sensing and GIS. In addition, in the last few decades, numerous examples of decreasing and disappearing freshwater lakes have been reported. Lake Chad, located in North Africa, and the Aral Sea, located in Central Asia, are two examples of lake disappearance that is linked to recent climatic events and intensified agricultural practices (Gorsevski, 2008). Similar examples at different spatio-temporal scales that have been recorded, where human activities are clearly among the primary drivers for the lake disappearances or decreases in water, are Ohrid and Prespa lakes (Gorsevski, 2008).

2.3.2 Remote sensing techniques for detection of Landuse/cover change

2.3.2.1 Image interpretation

Visual interpretation was the backbone of remote sensing when aerial photographs were the only remotely sensed images available (Center for Biodiversity and Conservation, 2010). Using visual signs, such as tone, texture, shape, pattern, and relationship to other objects, an observer can identify many features in an image. Methods to visually interpret satellite images are very similar to methods developed to interpret aerial photographs over 100 years ago (Center for Biodiversity and Conservation, 2010).

Visual interpretation was used in a study in Hengshan County located in north central China to discriminate between desertification and water erosion processes in remotely sensed images (Zhenqiang et al., 2004). To monitor the land use and land cover change and the land degradation, an image from 1991 was acquired by the TM sensor on board the Landsat-5 satellite, while images from 2002 were obtained by the ETM sensor on board the Landsat-7 satellite. Soil information was collected from the local government and digitized to produce soil maps. A digital elevation model (DEM) from the China Bureau of Surveying and Cartography was used to identify land forms and slope. The images were registered and interpreted. Land use/cover was classified with reference to the land classification suggested by Yuan (2002) and the technical standard for monitoring the environmental change around Beijing District. Using image interpretation and soil map, Zhenqiang et al. (2004) were able to draw two maps for landcover/use and land degradation.

The results showed that the monitored data may underestimate the potential danger of desertification (Zhenqiang et al., 2004). The difference between the monitored results and the traditional land survey result suggests a limited application of the images whose spatial resolution is less than 15 m in the studied area. It was also found that the surface width of most of the terrace field was not beyond 10 m, and the width of the slope ranges a quarter to half of the surface width. Consequently, the plant surface of the terrace field mixes together with the ridge of the field.

2.3.2.2 Image classification

Advances in technology have facilitated the development of classification algorithms to process imagery. Image classification is the process of sorting pixels into a finite number of individual classes, or categories, of data based on their pixel values. If a pixel satisfies a certain set of criteria, then the pixel is assigned to the class that corresponds to that criterion (Campbell, 2007).

In other words, classification is the process by which image pixels are grouped into classes with similar spectral attributes, and then each spectral class is assigned to an information class. However, those similar spectral classes do not necessarily represent a single or even similar information classes (Wayman, 2000). An example of classification is the grouping of urban and bare soil information classes into the same spectral class.

Image classification plays a big role in remote sensing and image analysis. The classification itself may be the goal of the study in some cases (Campbell, 2007).There are two ways to classify pixels into different categories: unsupervised and supervised classification. Next is the definition, advantages and limitations of both methods.

2.3.2.2.1 Unsupervised classification

Unsupervised classification can be defined as the identification of natural groups, or structures, within multispectral data (Al-Tamimi and Al-Bakri, 2005). Remotely sensed images are usually collected of spectral classes that are usually uniform with respect to brightness in several spectral channels. "Unsupervised classification is the definition, identification, labeling, and mapping of these natural classes" (Campbell, 2007). Unsupervised classification has many advantages such as, no prior knowledge of the region is required, human error is minimized since it is computer automated, and classes can be recognized as discrete units. However, this method has some limitations. Sometimes the analyst finds a problem matching spectral classes produced by the classification method to the informational classes that are needed by the user. In addition, the analyst has limited control over the classes and their identities, which makes it difficult to create specific informational classes if needed. Also, relationships between informational classes and spectral classes are not constant (Campbell, 2007).

Many studies demonstrate that the unsupervised classification technique was an effective approach for analyzing the direction, rate, and spatial pattern of land use change (Weng, 2001).

For example, Al-Tamimi and Al-Bakri (2005) assessed the accuracy of land use/cover maps derived from unsupervised classification techniques of Landsat TM imagery of the Ajloun area located in northwest Jordan. Image pre-processing techniques included geometric correction, resampling, registration, and determining the area of interest. Unsupervised classification was done, and outputs were merged and identified into four major classes. Accuracy of the classification was assessed based on ground visits. High classification accuracy was found for forested area, with variations in accuracy among the different classes. These variations were mainly attributed to the complex and fragmented patterns of cultivation and the scattered pattern of urban area. The study recommends the use of higher spatial and spectral resolution data to increase the level of accuracy.

2.3.2.2.2 Supervised classification

Supervised classification is closely controlled by the analyst. In this process, the analyst selects pixels that represent recognizable patterns. Knowledge of the data, the classes desired, and the algorithm to be used is required before selecting training samples. By identifying patterns in the imagery the user can "train" the computer system to identify pixels with similar characteristics. By setting priorities to these classes, the user supervises the classification of pixels as they are assigned to a class value. If the classification is accurate, then each resulting class corresponds to a pattern that was originally identified by the analyst. The selection of the training data is a significant step in supervised classification (Campbell, 2007).

Yuan et al. (2005) used supervised classification to monitor and map changes in landuse/cover in Minnesota. Multitemporal TM data for the seven-county Twin Cities Metropolitan Area of Minnesota acquired in 1986, 1991, 1998, and 2002 were prepared. Then supervised classification was performed. The results quantified the land cover change patterns in the metropolitan area and demonstrated the potential of multitemporal Landsat data and supervised classification method to provide an accurate, economical means to map and analyze changes in land cover over time that can be used as inputs to land management and policy decisions.

Supervised classification like any other methods has advantages and disadvantages. According to Campbell (2007) the advantages of supervised classification compared to the unsupervised classification are summarized as follows. For example, the analyst has control of

selecting informational classes to specific region, which is important to generate a classification for the specific purpose of comparison with different classification for the same area at different date. Also matching spectral categories with informational classes on the final map is not a problem. Finally, by examining training data, the analyst would be able to identify errors in classification.

Campbell (2007) described some of the limitations of supervised classification as follows. First, training data are usually defined with respect to informational classes first and then with respect to spectral classes. For example a training data that is 100% forest may be accurate with respect to it is informational class but still diverse with respect to density, shadow and therefore from a poor training data (Campbell, 2007). Second, supervised classification may not be able to recognize and represent special or unique categories not represented in the training data. And finally, selection of training data may be time consuming, expensive, and boring.

2.3.2.3 Change detection

Change detection can be defined as the "process of identifying differences in the state of an object or phenomenon by observing it at different times" (Singh, 1989). Remotely sensed imagery of a single region, acquired on at least two dates, can be used to identify changes that might have occurred in the interval between the two dates (Campbell, 2007). Significant effort has gone into the development of change detection methods using remotely sensed data (Jensen et al., 1995; Singh, 1989).

The challenge in change detection is using changes in digital spectral reflectance values to determine areas of true change over time. The basic principle in change detection using remote sensing data is that changes in land cover will result in changes in reflectance values that are distinguishable from changes caused by other factors, such as differences in atmospheric conditions, environmental conditions, solar illumination, and sun angle (Singh, 1989).

A critical prerequisite for application of change detection by remote sensing is the identification of suitable pairs of images representing the same region. Jensen (1995) mentioned that the sensor data used for spectral change detection should have consistent temporal, spatial, spectral, and radiometric resolutions. To reduce the misclassification due to differences in sun angle and seasonal differences, the analyst must assure that the two images are registered and

were acquired during the same season, at the same time of day and on or close to the required dates of the study. Images also should have no significant atmospheric effects. The two images must be compatible in every respect, including scale, geometry, and resolution; otherwise the change detection algorithm will interpret significant differences in image characteristics as changes on the landscape (Campbell, 2007).

Change detection techniques have been used to examine effects of land use changes caused by urban and suburban growth, effects of natural disasters (such as floods, forest and range fires), and impacts of insect infestations upon forest cover (Pyne, 2003). Gorsevski (2008) identified and assessed land use and land cover changes (LUCC) within the Ohrid and Prespa Lakes region between 1988 and 2000. Landsat-5 TM and Landsat-7 ETM+ imagery were used to monitor the changes in the lakes. The time period of the images agreed with the time when significant water decrease was observed from the lakes. Pre-processing of the images included geometric and radiometric correction, and the images were rectified to the Universal Transverse Mercator (UTM) projection system. An image differencing change detection technique was implemented to quantify the LUCC. The change detection technique is a simple pairwise comparison method based on the subtraction of two different time periods at the same location. Gorsevski (2008) implemented the standardized image differencing , which is based on z-scores using the visible blue bands. The visible blue bands were used for mapping water edges and forest types, differentiating between soil and plants, and identifying human made objects such as roads or buildings. Z-score thresholds were used to better understand the areas of true change. The findings were consistent with previous research showing that water level had decreased between 1988 and 2000.

Results showed that the most noticeable changes were due to the Albanian agricultural practices but also some other changes were due to harvesting, fire and urbanization (Gorsevski, 2008). Such changes would require further ground monitoring and meteorological or hydrological data analysis for accurate estimate of the water usage in relation to the LUCC. In addition, the remote sensing techniques used in the study with their relative simplicity and cost efficient analysis have the potential to support decision-makers in the real world mapping of sustainable lakes management (Gorsevski, 2008).

Similar studies have been performed in other parts of the world, including change detection of wetland Hongze Lake using a time series of remotely sensed imagery (Ruan et al., 2008). Three digital images acquired between 1979 and 2002 were preprocessed and registered; the ETM+ image of 2002 was classified using unsupervised classification techniques. Then change detection was used to identify the wetland trend change in time and space. The results showed that a great loss of wetland had occurred in the study area between 1979 and 2002 (Ruan et al., 2008).

2.4 Water-quality assessment using remote sensing

2.4.1 Previous studies

Concentrations of various suspended substances related to water quality have been successfully mapped using remote sensing (Schalles et al., 1998). Multispectral reflectance imagery has been used to determine parameters such as organic matter, secchi disk depth, and turbidity.

Remote sensing techniques, offering data acquisition over a long time period and for a broad spectral range, are considered advanced compared to the traditional methods for data acquisition (Manavalan et al., 1993). Spatial, spectral and temporal remote sensing data provide helpful and timely synoptic information (Goel and Jain, 1996). For example, analysis of remotely sensed images can be combined with ancillary data to determine the sources of nonpoint source pollution and soil erosion that may impact the hydrologic system.

Jain et al. (2002) found that remote sensing in water assessment can be cost effective and easy to use, requiring less time in analyzing the data, compared to the conventional methods, like in situ measurements. Some of the early research involving the remote sensing of water quality parameters came about in the early 1970's when aerial photography and other aerial images became available in large quantity (Agricultural Research Service, 2010; Schiebe and Ritchie, 1975). Researchers recognized after Landsat 1 was launched in July of 1972, that the multispectral imagery taken at regular time intervals by Landsat 1 over the US and many other places on Earth (Jensen, 2006) could be used to estimate and map water quality.

In 1975, a spectral response curve of water bodies for suspended sediment concentrations was determined by placing a boat carrying spectro-radiometers close to surface water to record the near noon sun reflectance of various Mississippi reservoirs (Schiebe and Ritchie, 1975). The best linear relationship between suspended sediment at the water surface and reflectance had a correlation coefficient of 0.9. The high correlation indicated that suspended sediments in surface water of reservoirs could be reliably estimated using remote sensing. However, at the time when this research was done, it did not have much of a practical application due to the lack of wide-spread hyperspectral data taken from either aerial or satellite based platforms.

In the late seventies, multispectral sensors on board the Landsat series of multispectral satellites were used to determine water circulation patterns and map the turbidity of open water by modeling field measurements with reflectance data. For example, Welby (1975) used MSS satellite images to study ocean currents along the North Carolina coast by looking at the spectral response changes due to the suspended matter.

Similar studies have been performed in other parts of the world including determination of siltation in the Aswan High Dam Reservoir (Smith et al., 1980). The study determined the surface area of the entire reservoir by totaling all pixels classified as water. Areas of extensive siltation were identified by comparing reflectance values in the green and red portions of the spectrum, and the amounts of deposition were determined through ground surveys. The resulting data were used to predict the distribution of silt deposits in the reservoir.

Vignolo et al. (2006) tracked the contaminated waters of Medrano Creek where it flows into Rio de la Plata (Argentina). Previous studies had shown that the water quality of Rio de la Plata at the outlet of Medrano Creek had decreased more than 50% as a source of water for human consumption. In this research, two spectral bands of the visible spectrum [0.45–0.52 mm (blue), 0.52–0.60 mm (green)] of satellite images obtained by LANDSAT 7 ETM+ were used to develop a model that predicts the water quality index (WQI) of surface waters in the study area. The model was validated using a data set of 12 physicochemical parameters obtained during 3 years. The results confirmed the potential of using satellite images to trace the organic contamination in freshwater systems and as tools for decision making in the management of water resources.

Many studies have been performed to measure lake water clarity. Secchi disk transparency (SDT) was found to be a cost-effective measure of water clarity (Nelson et al., 2003). However, in regions where there are thousands of lakes, sampling even a small proportion of those lakes for SDT year after year is cost excessive. Nelson et al. (2003) examined the ability of Landsat-7 ETM+ to measure water clarity across a large range of lakes. A regression model was developed to estimate SDT from Landsat data calibrated using 93 lakes in Michigan, USA. In addition, the influence of the distribution of SDT across the 93 calibration lakes on the model was examined. The study showed that the use of Landsat to measure water clarity was sensitive to the distribution of water clarity used in the calibration set.

In Minnesota, using similar remote sensing methods to those developed in the Michigan lakes study, a lake water-clarity/trophic state database was developed for more than 500 lakes in the Minneapolis and St. Paul metropolitan areas (Olmanson et al., 2000). The study used a total of 14 images from 1973 to 1998. Lakes were chosen that had data containing at least 20 ground observation points distributed over a wide area on well studied lakes. Models developed from these lakes were then applied to more lakes. Spatial patterns of seasonal and temporal trends in the turbidity were determined. Then a statistical analysis was done using GIS to determine the impact of landuse on water quality.

A similar study was performed by Coskun et al. (2008) to investigate the temporal assessment of the water quality changes of the Omerli watershed (Turkey). The study was mainly focused on the acquisition and analysis of the Satellite Probatoire de l'Observation de la Terre (SPOT) (1993), Indian Remote Sensing satellite (IRS) (1996 and 2000) and Landsat TM (2004, 2005, and 2006) satellite images that reflect the changes in the watershed utilizing the ground truth measurements. The water quality analysis of the drinking water reservoir within the watershed was investigated using 2006 Landsat TM satellite digital data. The results were compiled and compared with field measurements of total nitrogen (TN), total phosphorus (TP), chlorophyll a (CL) and total dissolved solids (TDS).

The observed reflectance showed a strong relationship with the water quality parameters and, thus, the satellite data proved to provide a useful index of TN, TP, CL and TDS. Moreover, the linkage between the water quality parameters and the individual band reflectance values were supported by multiple regressions (Coskun et al., 2008).

A comparison between final images from LANDSAT-5 TM data and water quality reference data was performed, and the results showed the polluted water carried by the creeks was displayed on satellite imagery (Coskun et al., 2008). The results made it possible for decision-makers to understand the main causes of the changes in the quality conditions of the reservoir.

2.4.2 Chromaticity technique

Chromaticity analysis, an established technique within colorimetry (measurement of color), defines the quality of color based on the hue and saturation of a color rather than on the brightness. The Commission International de l'Eclairage (CIE) in 1931 established a graphical representation of the quality of a color, enabling comparison of colors (Campbell, 2007). Chromaticity coordinates can be calculated for any visible light and represent the hue and saturation of color. Alfoldi and Munday (1977) defined a Landsat chromaticity diagram, similar to the CIE chromaticity diagram, except using MSS bands 4, 5, and 6 instead of the red, green, and blue primaries used for the CIE diagram.

Chromaticity analysis allows an average observer to duplicate the quality of any color by combining in the proper proportions the light from the three primary sources, red, green, and blue. The proportion of each primary source that combines to form another color is called a tristimulus value (Campbell, 2007).

Chromaticity analysis involves two steps. First, the tristimulus values are used to calculate chromaticity coordinates. This calculation is accomplished by defining three new quantities:

$$\boldsymbol{X} = \frac{\boldsymbol{X}}{\boldsymbol{X+Y+Z}} \qquad \text{Equ. (2.1)}$$

$$\boldsymbol{Y} = \frac{\boldsymbol{Y}}{\boldsymbol{X+Y+Z}} \qquad \text{Equ. (2.2)}$$

$$\boldsymbol{Z} = \frac{\boldsymbol{Z}}{\boldsymbol{X+Y+Z}} \qquad \text{Equ. (2.3)}$$

where:

X= tristimulus value for red

Y= tristimulus value for green

Z= tristimulus value for blue.

In actuality, only two of the quantities of X, Y, and Z are needed, because X+Y+Z = 1 (Campbell, 2007). X and Y are generally selected to represent the chromaticity coordinates of a color.

The second step is to represent the chromaticity of a color by plotting X and Y coordinates on the chromaticity diagram. The chromaticity coordinates for the visible spectrum are represented by the locus. The locus was developed by calculating chromaticity coordinates for the spectrum of colors and represents the spectrum of colors as defined by the CIE color matching test (Figure 2.1). The number next to each point represents the wavelength for that point. Equal proportions of X, Y and Z equal the white illuminant. E represents white or the point of equal energy on the diagram.

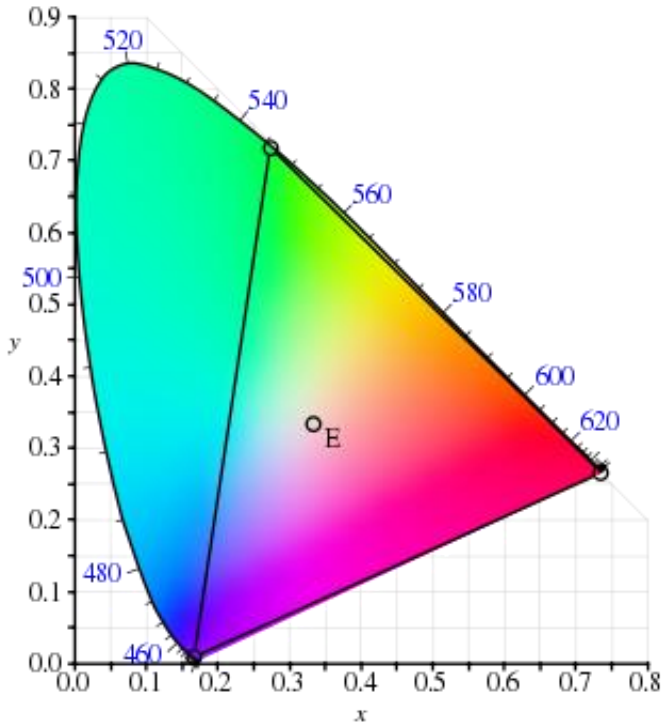

Figure 2.1. The CIE (RGB) primaries and location of primaries on the CIE 1931 xy chromaticity diagram (International Commission on Illumination, 1931)

2.4.3 Chromaticity and water-quality assessment

The potential ability of chromaticity analysis for monitoring water quality has been tested. Munday (1974) applied chromaticity analysis to estimate turbidity levels on Landsat imagery. Munday's research closely followed the procedure outlined in the previous section and used the same equations to calculate chromaticity coordinates for Landsat MSS data as a colorimetry (precise measurement of color) uses. Munday's application of chromaticity analysis to Landsat MSS data differs in one respect from colorimetry. Since the Landsat MSS does not have a spectral channel sensitive to blue light, data from the infrared band are substituted for blue.

Munday (1974) also eliminated MSS band 7 for water quality mapping because the wavelength of this band is highly absorbed by atmospheric water vapor. The remaining MSS bands 4, 5, and 6 are analogous to the x, y, and z tristimulus values for green, red, and blue, respectively. The near infrared wavelength of band 6 is substituted for the Z in this case. MSS digital numbers from each band are indicative of the brightness level reflected by a water body. Munday (1974) converted these MSS digital numbers to radiance values.

Only two coordinates need to be plotted on the chromaticity diagram. Again, X and Y are selected for this purpose. Plotted coordinates are compared to sediment locus (Figure 2.2). The points of the sediment locus are derived from pixels of known water quality and represent a wide range of sediment conditions in a water body. The far left point of the locus is near the point of equal energy. This position on the locus indicates radiance values for reflectance of water with high sediment content (Campbell, 2007). Each progressive step to the right on the sediment locus indicates a slightly different color for less turbid water. The far right position on the locus indicates clear water.

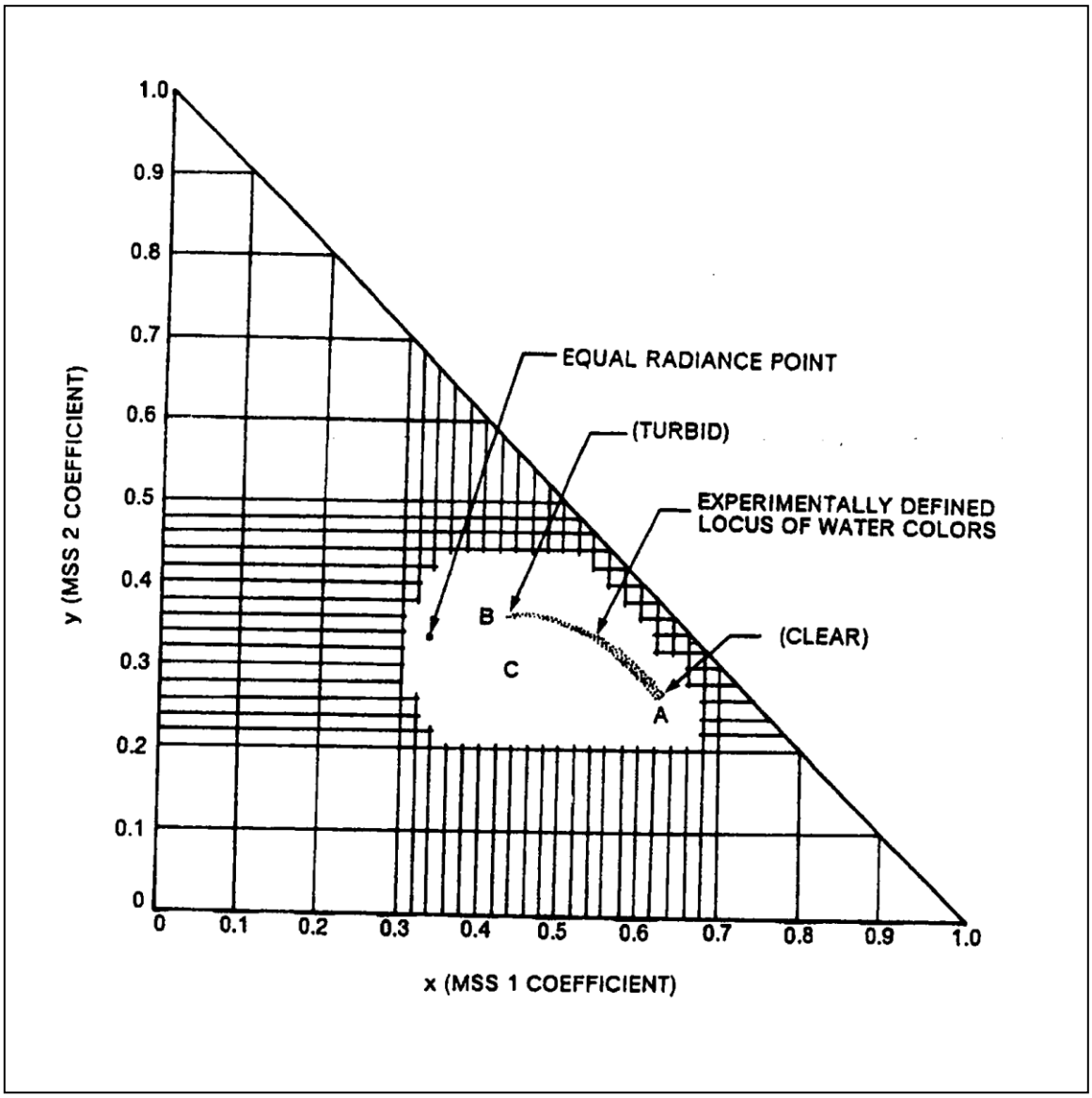

Figure 2.2. Chromaticity diagram space (Campbell, 2007)

The sediment locus may be explained by color additive mixture property within color theory. All points that lie within the two extremes of the locus are additive mixtures of either high sediment (the far left) or low sediment (the far right). If plotted chromaticity coordinates fall on the sediment locus, the coordinate pair was derived from a pixel with spectral qualities similar to that on the locus (Choubey, 1994).

In some cases, plotted coordinates fall below the locus. Such a location indicates a movement of the point toward the equal energy point. A position below the sediment locus is an indication of spectral impurity and can be caused by such factors as atmospheric variations, thin

clouds, air pollution, thin snow, and ice cover. Atmospheric correction is used to adjust points that do not fall on the locus (Campbell, 2007).

2.4.4 Early chromaticity research

The utility of chromaticity analysis has been tested in many areas. The Landsat chromaticity coordinates can be used to assess the turbidity of water bodies imaged by MSS (Campbell, 2007). Early work by Alfoldi (1977), Munday (1975), and Mather (1981) applied the chromaticity technique to estimate water quality levels from Landsat imagery. Munday and Alfoldi confirmed the accuracy and utility of chromaticity analysis for estimating water quality levels, while Mather applied the technique to coastal water with different geographic setting.

The goal of Alfoldi and Munday's (1977) research was to develop a Landsat water quality monitoring system using chromaticity analysis. This technique would require initial correlation of landsat data with water quality samples; thereafter, turbidity could be assessed on the basis of the initial calibration. Alfoldi and Munday (1977) built on previous research to combine the techniques of band normalization, chromaticity analysis, and atmospheric adjustments to Landsat data in order to determine sediment load and movement in the Minas Bay region, Bay of Fundy. Sediment levels were estimated by plotting brightness values (chromaticity coordinates) on a chromaticity diagram. Then the locations of these values were compared to the sediment locus, as an index to sediment levels.

The results of Alfoldi and Munday's (1977) study showed that chromaticity analysis of Landsat data was quite accurate in estimating the water quality of the Minas Bay region the upper Bay of Fundy. In a later study, Munday et al. (1979) confirmed the results of the Minas Bay study. Although the chromaticity techniques previously had been confirmed as a good water quality monitoring system, their research dealt with the impact of sediment size, chlorophyll, dissolved organic matter, solar angle, system noise and atmospheric adjustments on the position of chromaticity points within the diagram. Munday et al. (1979) concluded that such factors as sediment size, chlorophyll, dissolved organic matter, and solar angle had little effect on the position of chromaticity points; system noise was reduced through the averaging of four by six blocks of pixels; less error occurred in the middle range of particle size as compared with

extremely small or large sediment particles ; and the atmospheric adjustment of the chromaticity points improved the measurement of sediment levels over unadjusted chromaticity points.

Various studies have demonstrated the potential of remote sensing data for estimation of suspended sediment either qualitatively or quantitatively (Khorram et al., 1991; Lindeli et al., 1986; Nayak, 1983). For example, Indian Remote Sensing satellite (IRS) digital data in combination with field measurement were used to map distribution and concentration of suspended sediments along the Tamil Nadu coastal waters for monsoon and non-monsoon periods (Chauhan et al., 1996). Qualitative suspended sediment mapping was done for the entire Tamit Nadu coast while quantitative studies were taken at two selected sites. For qualitative mapping, both monsoon (17-12-90) and non- monsoon (18-4-90) season data were analyzed. The suspended sediment concentration (SSC) samples were collected on April 15, 1992 and March 10, 1992 around Ennore and Tuticorin coastal waters, respectively, synchronous to IRS-IA satellite overpass. These data were used for quantitative estimation of SSC using digital chromaticity technique. The study showed that the plumes of high suspended sediment concentration were contributed from the nearshore wetlands and river mouths and were finally diffuse towards the coast. Different classes of low to high SSC values ranging from less than 5 mg/L in offshore areas to 21 mg/L in nearshore were also delineated. Regression analysis of chromaticity transform of IRS data with suspended sediment data showed correlation coefficient of 0.78.

Similar studies have been performed in other parts of the world, including research conducted on Lake Garda (Italy) to confirm the benefit of using satellite images to monitor trophic status of water bodies, even in the absence of supporting in situ measurements (Zilioli and Brivio, 1997). Two Landsat-TM images, taken in April and August 1985 were used. Image processing gave radiance, reflectance, and chromaticity values. To make the multi-temporal analysis possible, a dark object subtraction technique was adopted to reduce differential haze effect between the two images. Results showed that satellite remote sensing scenes could be an effective tool for expeditious assessment of both spatial and temporal variation in water quality.

3 METHODOLOGY

3.1 Part One: Landuse/cover

3.1.1 Study area of King Talal Dam

The King Talal Dam (KTD) watershed is located in Jordan about 24-km northwest of the capital Amman. The drainage basin consists of a fifth order main stream called Zarqa River and two other tributaries, namely Ruman and Rumemin wadis. The catchment area is 3000 km^2 with a population of 2.439 million (Salameh, 1996), which is about half of the kingdom population and is distributed in Amman, Zarqa, Sweileh, Rusaifeh, Baka'a and Jerash with several villages around these cities (Royal Scientific Society, 2001). Precipitation falls in the winter season, which extends from October to May. Average annual precipitation over the basin varies considerably, from 400 mm on the west side to rarely exceeding 150 mm on the east side.

In 1977 it was agreed to construct King Talal Dam as the first trial on Zarqa River with a capacity of 56 MCM. Then, in 1987, the capacity of the dam was increased to 86 MCM, 78 MCM of which are used for irrigation purposes (Salameh, 1996). The height of the dam is 108 m. This dam is considered the most important water project in Jordan because the catchment area is the biggest in the country and because almost 50% of the population lives in this catchment (Ministry of Water and Irrigation, 2008). The water stored in the reservoir is used for irrigation of wide areas in the Ghor (Jordan valley). The area irrigated by water coming from the reservoir mixed with water coming through the King Abdullah channel is estimated to be 10,000 ha (Royal Scientific Society, 2001).

About 90% of the water supplied to the reservoir comes from the Zarqa River and about 10% comes from the Rumaimeen Valley. The Zarqa River flows from the east, bringing water from the effluent from Al Samra Wastewater Treatment plant (WWTP) and the treated and untreated effluents from industrial factories and farms located on the river's banks. The Rumaimeen Valley is located south of the reservoir. It was connected in 1988 to increase the flow into the reservoir (Royal Scientific Society, 2001). Other purposes for draining this valley into the reservoir were to study the effect of Baka'a wastewater plant on the water quality in this valley and on the water of the reservoir.

3.1.2 Study area of Karameh Dam

The Karameh Dam, an earth fill embankment, was constructed in 1997 on Wadi Mallaha (Salt Pan) in the Jordan Valley area to store water for irrigation during the dry season. The storage capacity of the reservoir is 55 MCM. Its catchment area measures 61.2 km^2 (Salameh, 2004), receiving average annual rainfall of 150 mm. In comparison, the annual potential evaporation in the area is 2450 mm (Ministry of Water and Irrigation, 2008).

The catchment area is relatively flat and is covered by the recent deposits of the Jordan Valley floor, possessing high porosity and permeability allowing rapid infiltration of rainwater. This results in very limited quantity of surface runoff. Therefore, in order to fill the reservoir, water from King Abdullah Canal, mainly fed from the Yarmouk River, was planned to be diverted. The dam area is covered by the Lisan Marl salty formation which was deposited at the bottom of the Lisan Lake, an ancestor lake of the present Dead Sea, which used to cover the entire Jordan Valley area. The Lisan Marl formation is only in the vicinity of the foothills area covered by thin (up to 100 m) recent alluvial sediments, otherwise it crops out at the surface, as it does in the dam site area.

The Karameh Dam was constructed in spite of the pre-construction experts' warnings that this dam project was questionable from the viewpoints of geology, hydrogeology, water salinity, and water resources to fill the dam (Salameh, 2004). Because of extremely high salinity not a single drop of water collected in the dam has been utilized.

3.1.3 Preprocessing of Landsat TM data

3.1.3.1 Registration of image to appropriate geographical coordinates

The May 2006 Landsat TM image and the 1990 images were obtained from the USGS Global Visualization Viewer (Glovis), with UTM projection zone 36 and used for both King Talal dam and Karameh dam. The 1990 image was rectified to the 2006 image using ERDAS Imagine software. Next, a polynomial geometric correction was applied to the source image (1990). Ground control points (GCPs) were chosen at specific locations on the source image and then matched on the reference image (2006). Ground control points help to establish the geometry and location of the output image in relation to an input image; it represents the process

of registering the image based on image coordinates. Ground points were chosen at easily identified targets, such as road intersections and field corners. The points were evenly distributed across the source image. Figure 3.1 displays the reference image with the ground control points.

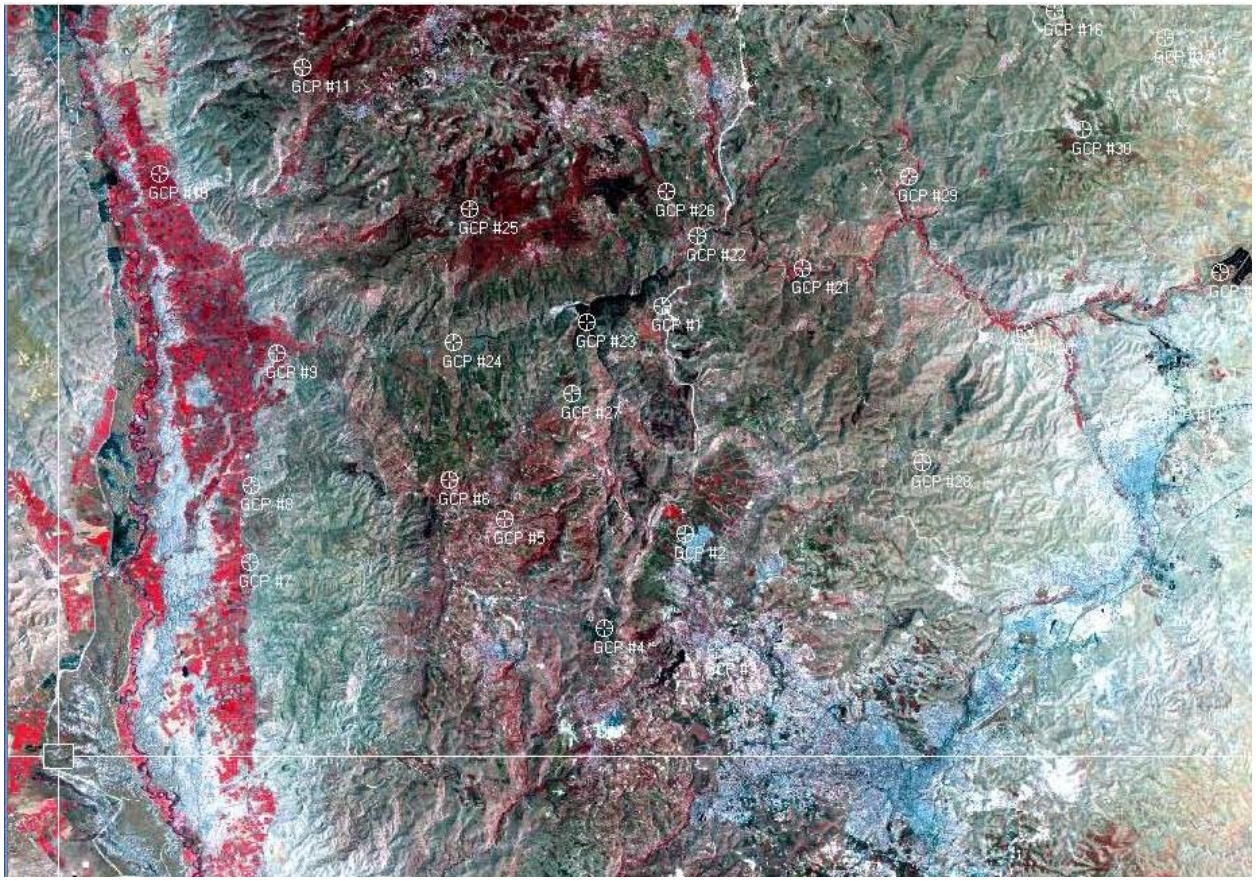

Figure 3.1. Screen shot of GCPs on reference image (Department of the Interior/USGS, 2006)

The root mean square error (RMSE) between the ground control points on each image was calculated by ERDAS software (table 3.1). The RMSE is a representation of registration accuracy, or how well each ground control point represents the actual location. It is the standard deviation of the difference between the actual and calculated positions of each GCP. For each set of points to be valid, the RMSE must be less than half a pixel (15 m) (Jensen et al., 1995). The overall average error was 9.37 m, minimum error was 3.27 m, and maximum error was 13.3 m.

Table 3.1. Ground control points and RMS error for each point on the reference image

GCP #	RMS error	GCP #	RMS error
GCP 1	11.1	GCP 11	6.86
GCP 2	8.07	GCP 12	12.4
GCP 3	13.3	GCP 13	0.75
GCP 4	7.64	GCP 14	7.95
GCP 5	10.2	GCP 15	8.21
GCP 6	12.6	GCP 16	12.9
GCP 7	12.4	GCP 17	12.5
GCP 8	3.94	GCP 18	6.40
GCP 9	12.0	GCP 19	3.27
GCP 10	1.39	GCP 20	6.64

Checkpoints were used to assess the accuracy/precision of the registration process. Checkpoints are control points where locations are known, but they are not used to calculate the registration equation, so they form a means to evaluate the precision of the registration. If the registration is robust, then the predicted locations of the checkpoint locations will be close to the known positions of the checkpoints because they were not used to prepare the registration.

The final step was to resample the images to create new images with the desired geometry based on three different methods: nearest neighbor, bilinear, and cubic convolution. The three images were compared visually with the original image to choose the most appropriate resampling technique. Figure 3.2 displays the resulting images of the three resampling methods. The nearest neighbor technique was chosen based on a visual comparison because it very closely preserves the original scene.

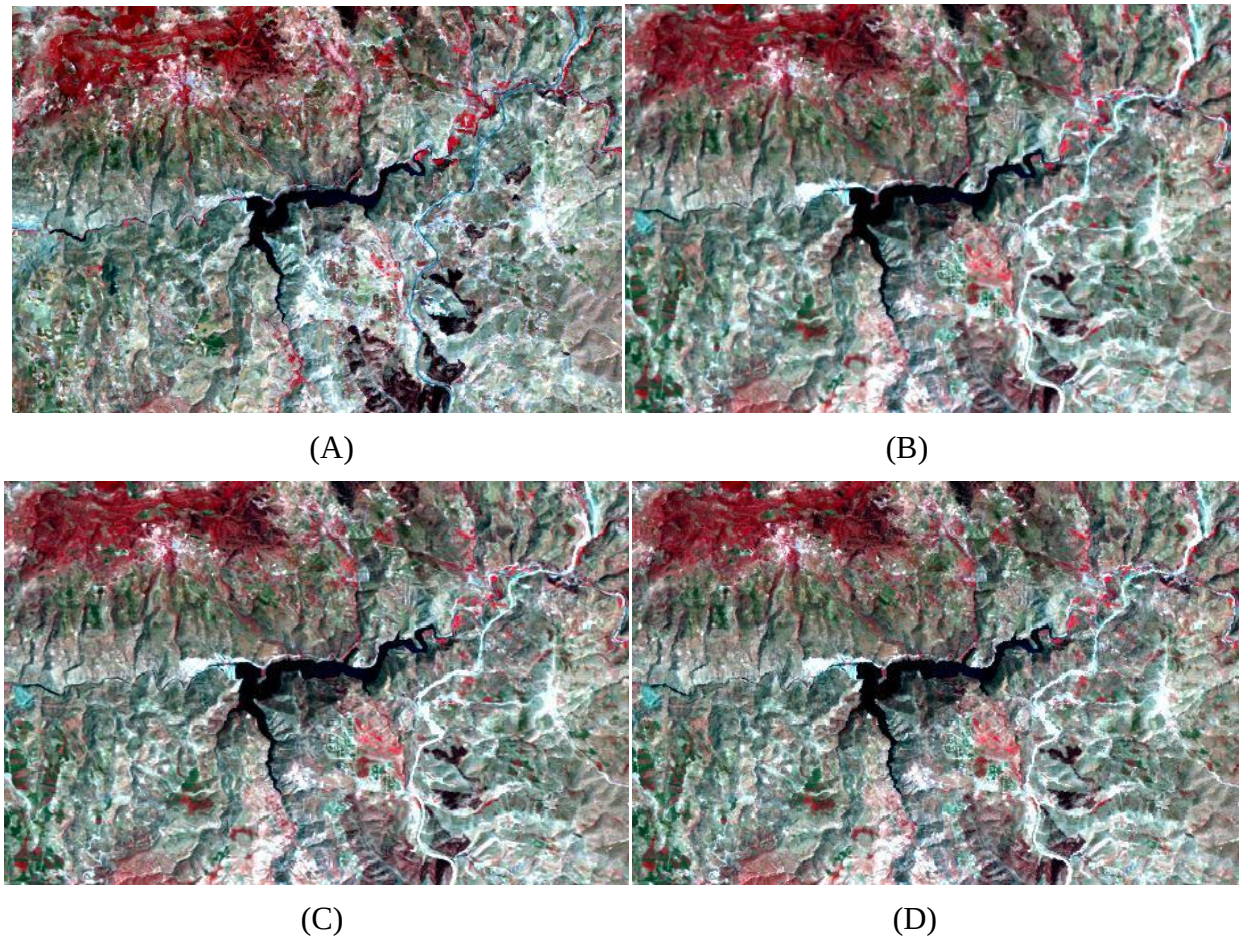

Figure 3.2. Comparison of resampling techniques (A) source image, (B) cubic convolution, (C) bilinear, and (D) nearest neighbor

For Karameh Dam, the same image of May 2006 was used, in addition to another image acquired on April 1998 and downloaded from Glovis. The April scene was selected because of the limited number of images for the dam area, and April is the closest season to May in that area. The image of 1998 was already corrected and rectified, so no correction was needed.

3.1.4 Image classification

3.1.4.1 Unsupervised classification

Unsupervised classification groups image pixels into spectral classes based on brightness values. The ERDAS software allows the analyst to choose the number of classes into which the image will be divided. The analyst also chooses the maximum number of iterations used to

divide the pixels into their respective classes. This represents the number of times the software will regroup the pixels based on a selected convergence threshold. A total of seven spectral classes with ten iterations were chosen for the first attempt, as trial and error.

A comparison of the landuse/cover types and their distribution in the reference and the source image illustrated that seven classes did not accurately divide the pixels into their respective land use classes. I tried 5, 7, 10, and 15 classes with various maximum iterations. However, none of these classes and iterations succeeded in dividing the pixels into their respective land classes. I found this method overestimated the areas of some land classes such as water and urban areas, with the classified image showing water in areas where there should not be water according to the original image. As a result, this method was not used in this research.

3.1.4.2 Supervised classification

Supervised classification is different from unsupervised classification in that the spectral classes are chosen by the user. Choosing these classes is based on previous knowledge of the data and the area represented in the reference image. To make the selection process more accurate and clear, the image was assigned the band combination of 4-3-2. This band combination was chosen because it utilizes bands in the visible and near infrared. This region of the spectrum carries important information about vegetation and is not subject to atmospheric scattering. Then training data were defined by selecting a variety of "areas of interest" (AOI) to represent each land cover type. These areas were chosen based on distinctive color, shape, and location patterns. Each AOI consists of a group of pixels representing a land cover type. Approximately 15 AOIs were chosen to represent the spectral signature for each land cover type. A variety of areas across the image were chosen based on color so that the spectral signature represented would be comprehensive.

The accuracy of each spectral signature was evaluated using spectral feature space plots. A feature space plot is a pairing of two spectral bands to represent the density of pixels occupying specific regions of data. The spectral signatures from each informational class were plotted as ellipses on the feature space plot. The ellipses were analyzed to see if all of the signatures for the informational class were located in the same place on the feature space. Large ellipses usually indicate the presence of outliers whereas smaller ellipses usually indicate a precise signature. The urban and orchard informational classes contained some large ellipses,

indicating that these two informational classes had some outliers. Some signatures were added and/or deleted to increase the accuracy of the overall spectral signature. Then classification was performed with the new spectral signature.

3.1.4.3 Recoding

Supervised classifications were performed on the four images for both reservoirs (King Talal Dam, Karameh Dam). The maximum likelihood technique was used, which assumes accurate training data and assigns all pixels based on the probabilities associated with each classification decision. The technique uses the training data to estimate the mean and variance of each class to calculate the probability that a pixel of a certain brightness value belongs to a certain class. After the technique was implemented for each image, the new images were divided into eight informational classes: 1-urban, 2-crop, 3-orchard, 4-forest, 5-rangeland, 6-desert, 7-water, and 8-salt. Each informational class was assigned a color to represent the specific land cover. For each supervised image, the following colors were assigned: light pink for urban, light green for crop, maroon for orchard, dark green for forest, orange for rangeland, gold for desert, blue for water, and tan for salt.

3.1.4.4 Image subset

Since scene-size data sets are quite large, the processing time for image analysis can be reduced by selecting only the particular area of interest for a specific project. The areas of interest (AOI) for this study were King Talal Dam and Karameh Dam and their drainage areas. A subset of both dams was created to remove all data extraneous to this study. The initial AOI selection process began by opening the “AOI > Tools” menu and drawing a polygon around the land selected for the study (Figure 3.3).

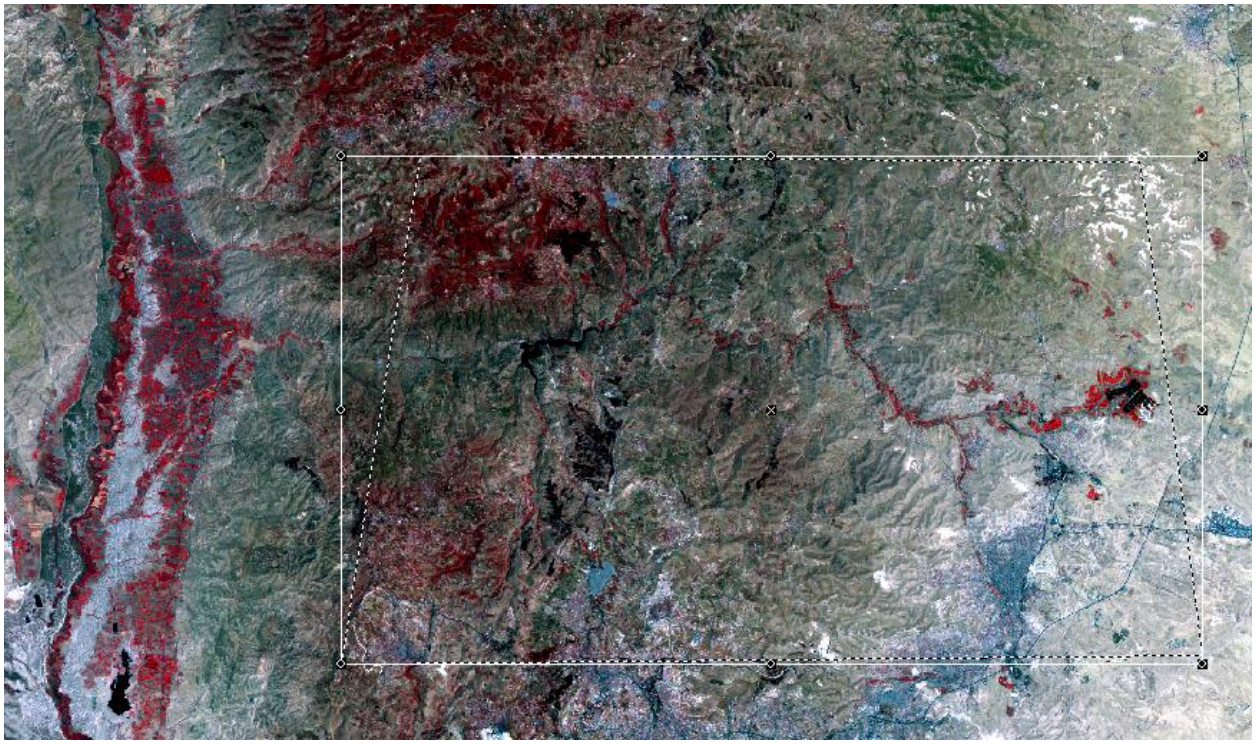

Figure 3.3. Polygon defining King Talal Area, area of the research

Next, the "Data Prep" menu was accessed to subset the four images based on the previously created AOI. The resulting reduced size image became the primary dataset for the remaining image classification procedures. The same procedure was done for each of the four images, and as a result four areas of interests were produced.

3.1.4.5 Watershed delineation and mask

Watershed delineation for both dams was useful in calculating the areas of different landuse/cover types that have impact on the water quality of the reservoir. Watershed delineation was performed for King Talal Dam using the digital elevation model (DEM). The delineation was done in ArcGIS 9.3 as follows:

a. Fill the sinks to create depressionless elevation layer.
b. Create Flow direction.
c. Create Flow accumulation.
d. Create watershed pour points (outlet).
e. Delineate watersheds.

3.1.4.6 Quantifying the change in Landuse/area

A quantitative comparison was done by calculating the area of each landuse/cover type for all images. This was done by multiplying the pixel area (900 m^2) by the number of pixels for each landuse/cover type. Then the difference between areas was calculated and the percent change to the total area was also determined.

3.1.4.7 Manual comparison of images

First, images were projected to the same coordinate system. Second, direct recognition method was used in the visual interpretation and comparison between images. This was done by applying the researcher experience, skills, and judgment to connect the image pattern with informational classes. The process is essentially a qualitative subjective analysis of the image using the elements of image interpretation as visual and logical clues. The analyst used some combination of these elements, such as image tones, texture, shadow, shape and pattern, to describe the characteristics of objects and features as they appear on the image. For example, urban areas like roads and building roofs have bright tones and distinct shape. Forest has coarse texture and dark tone, water is dark and smooth, and so on. Third, circles and rectangles were drawn to point to the changes in landuse/cover between the two images and qualitative comparison of the changes was described.

3.2 Part Two: Water-quality assessment

3.2.1 Manual method

Chromaticity is a good technique to identify and monitor changes in water turbidity and sediment distribution and concentration in water body. Various techniques are explored in the literature to study the water quality of a water body in different parts of the world, but little information exists to identify the optimal technique to use for this application in areas like Jordan. This study attempts to help fill that void, by applying the chromaticity techniques in a qualitative manner in that part of the planet, with different conditions and weather than it was done before.

Chromaticity coordinates were calculated in two ways: by manual calculation using Excel and by using ERDAS and ENVI software. Both methods used the same algorithm, as described next.

Samples were positioned a distance of 1 pixel from the nearest land boundary around the reservoir. At each sample site, a block of (3x3) pixels was used. Digital numbers (DNs) for TM bands 2, 3 and 4 were extracted for the nine-pixel block at each sample site. The average of the DNs from the nine pixels was used in the analysis. DNs were converted to calibrated radiance level, and then chromaticity coordinates were calculated and plotted in the diagram as follows:

Step 1: Extract DNs for TM bands 2, 3, and 4 using cursor in ERDAS imagine

Step 2: Convert digital numbers to radiances, using Table 3.2 and the following equations (Chander et al., 2009):

$$L\lambda = (LMAX\lambda - LMIN\lambda / Qcalmax - Qcalmin)*(Qcal - Qcalmin) + LMIN\lambda \quad \text{Equ. (3.1)}$$

OR

$$L\lambda = G\ rescale \times Qcal + B\ rescale \quad \text{Equ. (3.2)}$$

Where:

$$G\ rescale = LMAX\lambda - LMIN\lambda / Qcalmax - Qcalmin$$

$$B\ rescale = LMIN\lambda - (LMAX\lambda - LMIN\lambda / Qcalmax - Qcalmin) * Qcalmin$$

where:

$L\lambda$= Spectral radiance at the sensor's aperture [W/ (m^2 sr μm)]

Qcal= Quantized calibrated pixel value [DN]

Qcalmin= Minimum quantized calibrated pixel value corresponding to $LMIN\lambda$ [DN]

Qcalmax= Maximum quantized calibrated pixel value corresponding to $LMAX\lambda$ [DN]

$LMIN\lambda$= Spectral at-sensor radiance that is scaled to Qcalmin [W/ (m^2 sr μm)]

$LMAX\lambda$= Spectral at-sensor radiance that is scaled to Qcalmax [W/ (m^2 sr μm)]

G rescale= Band-specific rescaling gain factor [(W/ (m^2 sr μm))/DN]

B rescale= Band-specific rescaling bias factor [W/ (m^2 sr μm)]

Calculation of at-sensor spectral radiance is the fundamental step in converting image data from multiple sensors and platforms into a physically meaningful common radiometric

scale. Radiometric calibration of the MSS, TM, ETM+, and ALI sensors involves rescaling the raw digital numbers (Q) transmitted from the satellite to calibrated digital numbers (Qcal), which have the same radiometric scaling for all scenes processed on the ground for a specific period. During radiometric calibration, pixel values (Q) from raw, unprocessed image data are converted to units of absolute spectral radiance using 32-bit floating-point calculations. The absolute radiance values are then scaled to 7-bit (MSS, Qcalmax = 127), 8-bit (TM and ETM+, Qcalmax = 255), and 16-bit (ALI, Qcalmax = 32767) (Chander et al., 2009). Conversion from Qcal in Level 1 products back to at-sensor spectral radiance (Lλ) requires knowledge of the lower and upper limit of the original rescaling factors. Table 3.2 summarizes the spectral range and the post-calibration parameters for TM 4 and TM 5.

Table 3.2. Calibration scaling parameters for TM4 and TM5 (Chander et al., 2009)

Band	Spectral Range (μm)	Center Wavelength (μm)	LMIN ($W/m^2srμm$)	LMAX ($W/m^2srμm$)	$G_{rescale}$ ($W/m^2srμm$)/DN	$B_{rescale}$ ($W/m^2srμm$)/DN
L4 TM (LPGS)						
1	0.452-0.518	0.485	-1.52	171	0.6792	-2.17
2	0.529-0.609	0.569	-2.84	336	1.334	-2.20
3	0.624-0.693	0.659	-1.17	254	1.004	-4.17
4	0.776-0.905	0.841	-1.51	221	0.8760	-2.17
5	1.568-1.784	1.676	-0.37	31.4	0.1250	-2.39
6	10.42-11.66	11.04	1.237	15.3	0.0553	-0.50
7	2.096-2.347	2.222	-0.15	16.6	0.0659	-0.22
L5 TM (LPGS)						
1	0.452-0.518	0.485	-1.52	193	0.7658	-2.29
2	0.528-0.609	0.569	-2.84	365	1.448	-4.29
3	0.626-0.693	0.660	-1.17	264	1.043	-2.21
4	0.776-0.904	0.840	-1.51	221	0.8760	-2.39
5	1.567-1.784	1.676	-0.37	30.2	0.1203	-0.49
6	10.45-12.42	11.43	1.23	15.30	0.0553	1.18
7	2.097-2.349	2.223	-0.15	16.5	0.06555	-0.22

Step 3: Sum radiances for bands 2, 3 and 4.

Step 4: Find proportion of total brightness for each band:

X= radiance value of band 2/ radiance (band2+band3+band4)

Y= radiance value of band 3/ radiance (band2+band3+band4)

Z= radiance value of band 4/ radiance (band2+band3+band4)

Step 5: Use X and Y coordinates to plot on the chromaticity diagram.

Step 6: Interpret the meaning of plotted coordinates by comparing their location to the locus in the chromaticity space diagram (Figure 3.4).

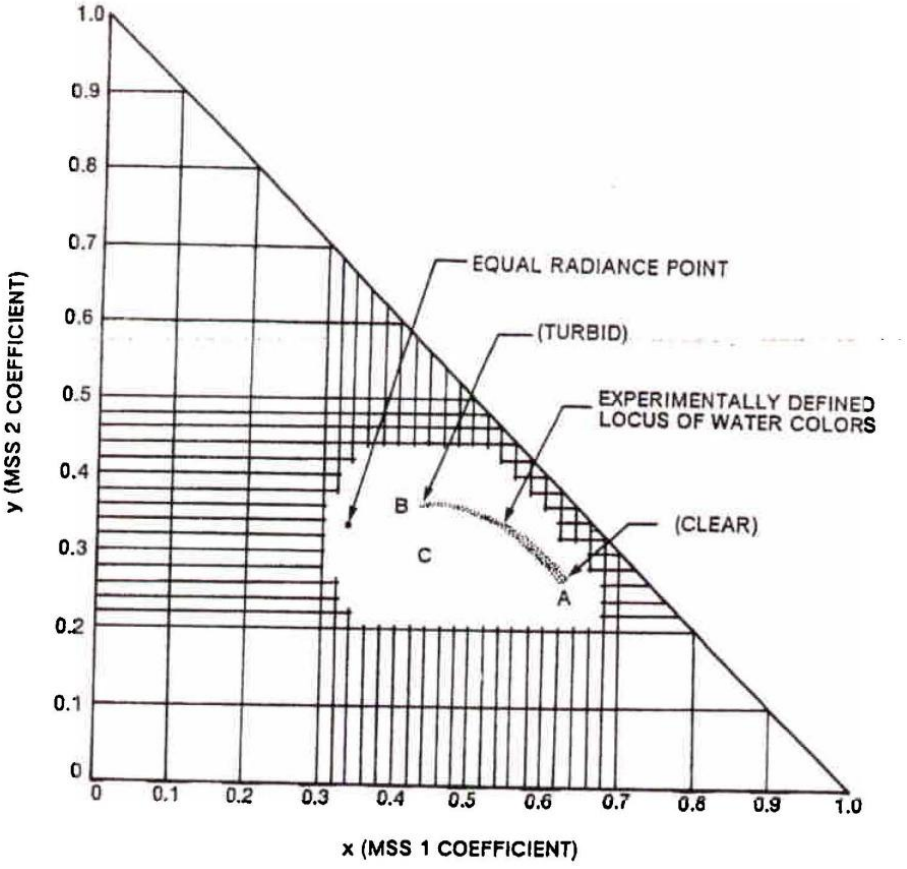

Figure 3.4. Landsat chromaticity space (Campbell, 2007).

3.2.2 Model maker in ERDAS

The term "model" is used in the field of remote sensing to refer to a series of systematic data transformation steps that will result in a new image that estimates the desired outcome. Most "remote sensing" models are deterministic (a model in which there are no random events) and have the goal of data, calibration, or estimation. A model for converting images to radiance image was built in ERDAS using the following steps:

a. A simple model was created. First, the MODELER icon from the ERDAS icon menu was selected.
b. The model maker option was selected.
c. The modeling objects, including the arrows that connect the objects, were dragged from the tool bar on the right of the modeling window.
d. The "input image object" was selected (for example, King Talal 06). Then the "output image object" was defined.
e. The "function model object" (the circle in the middle) was selected. This object allows the modeler to define the transformation process for this step in the model. In this step, the process for radiance calibration was specified.
f. Finally, the model was run by selecting the run tool from the model window icon menu. When completed, the results were displayed in a viewer. The output was the radiance image.

To calculate the chromaticity coordinates X, Y and Z, ENVI software was used to do math algebra and find the proportion of total brightness for each band by dividing each radiance image by the sum of all radiance images resulting from the previous model.

3.3 Relationship between Landuse/cover change and water quality

Turbidity levels in a reservoir can be influenced by a broad range of factors, including sediment from soil erosion, water depth and currents, wind, and meteorological events, phytoplankton, resuspended sediment from bottom, waste discharge, algae growth, and urban runoff. While there is a lack of data about many of the listed factors in the study areas, from soil erosion is affected by landuse/cover change, which was characterized in this study. One approach for estimating soil erosion as a function of landuse is the universal soil loss equation (USLE) (Al-Sheriadeh et al., 2000):

$$A = R K L S C P \qquad \text{Equ. (3.3)}$$

Where,

A = annual average soil loss (Mg/ha)

R = rainfall and erosivity index for geographic location

K = soil erodibility factor

L = slope length factor

S = slope steepness factor

C = cropping factor

P = conservation practice factor

The erodibility factor is a function of soil type. The same soil texture is dominant in both watersheds. Similarly, the rainfall index was the same for the whole watershed. The slope factor did not vary appreciably for different areas in the watershed. Because of the similarity in soil texture, slope and rainfall across the drainage area, the crop and management factor C was used as an index of erosion.

Turbidity levels as estimated by chromaticity analysis were analyzed in relation to the C factor to check if estimated turbidity levels are influenced by landuse/cover patterns.

The King Talal watershed was divided into subsheds and the changes in area in different landuse/cover were calculated between 1990 and 2006. Because the Karameh watershed area is very flat and no data are available about the stream network, it was impossible to delineate subsheds with the DEM alone. Instead of delineating subsheds, a 90-m buffer was applied around the reservoir in both years. The number of pixels changed over time for each landuse/cover class was counted using ArcGIS.

4 RESULTS

4.1 Landuse change from image interpretation (1960-2001)

Figures 4.1 and 4.2 show panchromatic images of the King Talal Dam area in Jordan, as recorded by different sensors in different years. Figure 4.1 shows an image for the year 1960 before constructing the dam. Vegetation is depicted in light and medium gray tones, with patches of forest represented in darker tones. At the dam site, Zarqa River is visible as a dark strip; roads are displayed as bright linear forms.

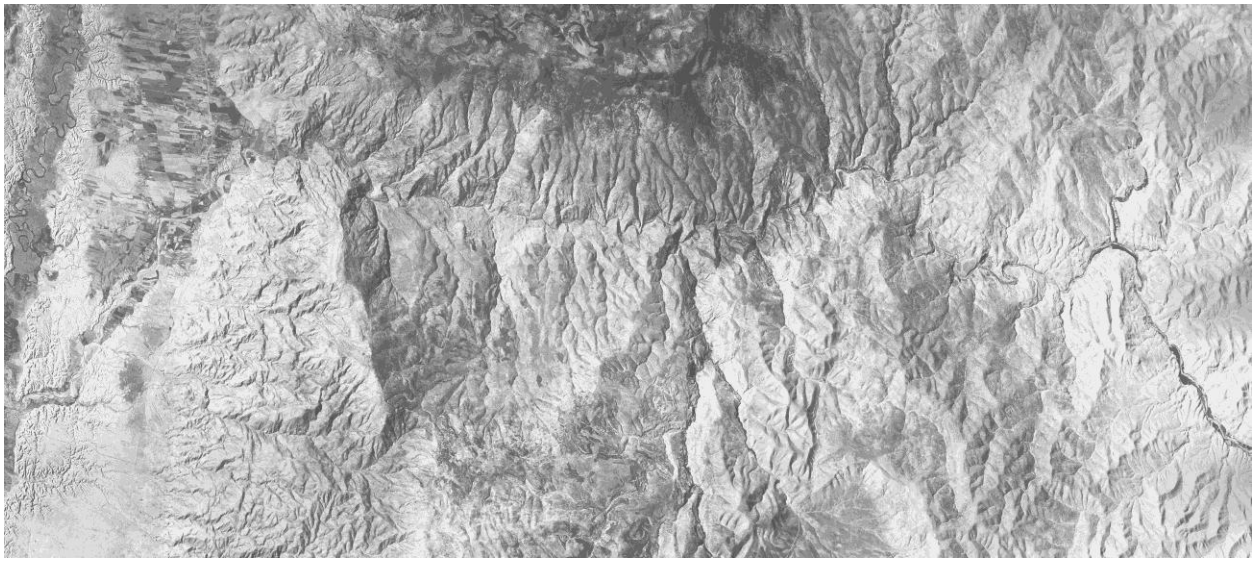

Figure 4.1. King Talal area image acquired in 1960 before building King Talal Dam (Department of the Interior/USGS, 1960)

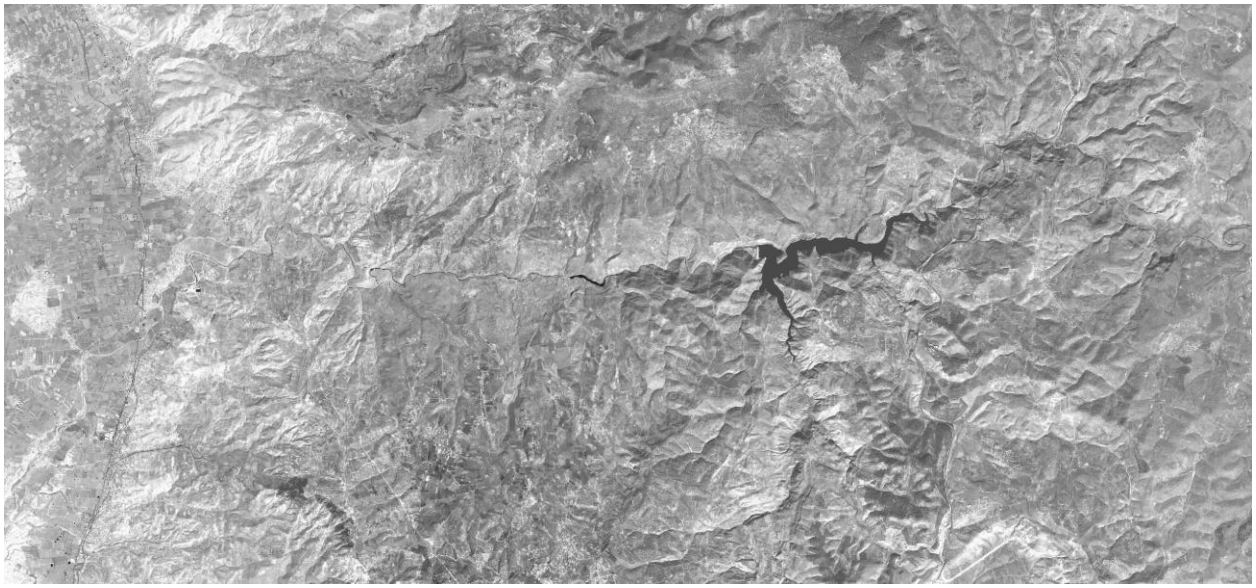

Figure 4.2. King Talal Dam area, image acquired in 2001 (Department of the Interior/USGS, 2001)

Figure 4.2 shows a panchromatic image for the same region, taken using Quick bird sensors in 2001. Here, the changes in landuse/cover can be noticed. Forested regions have light tone and cover more areas than in 1960. Open water (reservoir) is shown as smooth black tone. Topographic changes are visible in the 2001 scene after building the dam, especially after building new roads and more residential settlement. A dramatic increase in the urban and residential areas is highlighted in Figures 4.3 and 4.4. Urban land, such as that shown in 2001, is often characterized by evenly spaced rooftops and systematic patterns of paved streets and parking lots. Urbanization started to increase after the war in 1967 when many refugees came and settled in that area, especially in the capital Amman and Zarqa city. Moreover, after building the dam, many agricultural, commercial and residential lands were established in the watershed area, using the water collected by the reservoir. Today, almost 50% of the country's population lives in that region (Ministry of Water and Irrigation, 2008).

Many changes in landuse/cover occurred between 1960 and 2001. For example, the downstream area in 2001 included more residential buildings. In addition, the agricultural industry greatly expanded after building the dam. Large projects such as Abdullah Canal were constructed. This canal uses the water coming from King Talal reservoir to irrigate large areas of lands and farms in Jordan valley.

Figure 4.3 image (A) shows a region in downstream area of King Talal Dam (1960), where agricultural land is displayed in dark gray, as shown in the blue box. Image (B) shows the same region in 2001, where increased agricultural areas are displayed in light gray and with sharp boundaries, as shown in the blue box. The image also shows the dramatic increase in urban areas in 2001 as in the yellow box.

(A)

(B)

Figure 4.3. Downstream area of King Talal Dam (A) 1960, and (B) 2001(Department of the Interior/USGS, 2001)

Figure 4.4 image A and image B also show the downstream area of King Talal Dam in 1960 and 2001, respectively. Suburban areas such as those shown in figure B (yellow boxes), are characterized by spaced rooftops and a systematic pattern of paved streets, while these areas did not exist in 1960 and so do not appear in image A.

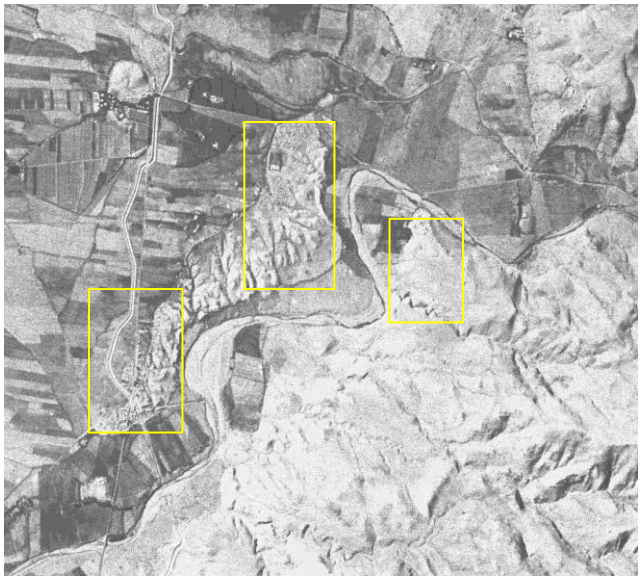

(A)

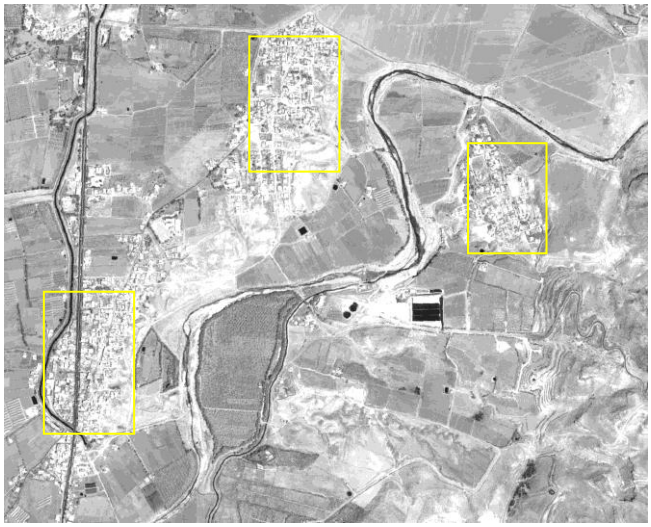

(B)

Figure 4.4. Downstream area of King Talal Dam (A) 1960 and (B) 2001 (Department of the Interior/USGS, 2001)

Figure 4.5 shows a visual interpretation of imagery for landuse/cover change of cropped agricultural land (downstream area of King Talal Dam). A distinct difference in the shape and distribution of the cropped land between the two images is evident. In 2001 (B), distinctive characteristics of the land included smooth texture and the contrast tones that distinguished varied crop and growth stages as shown in the red box.

(A)

(B)

Figure 4.5. Downstream area of King Talal Dam (A) 1960 and (B) 2001. (Department of the Interior/USGS, 1960, 2001)

Figure 4.6 shows a visual interpretation of panchromatic imagery for landuse/cover information. For example, in 2001(B), the cropped lands occupy a larger area to the south than was shown in 1960 (A) (red rectangle). In addition, in image B, Abdullah Canal (blue ellipse), which displays the linear form, was built after the construction of King Talal Dam to irrigate the agricultural lands in Jordan Valley, using the water collected in the reservoir and the water coming from Yarmouk River in the north.

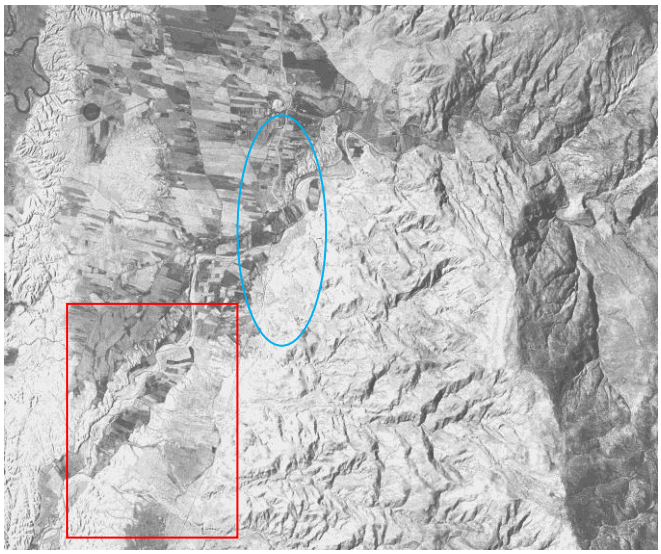

(A)

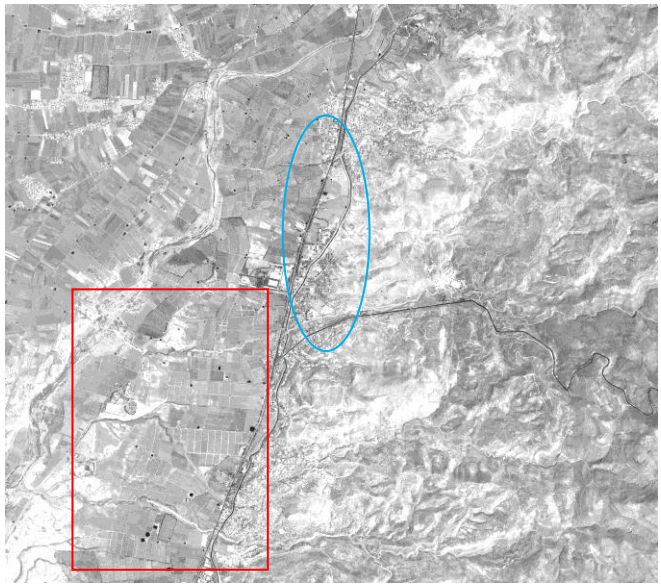

(B)

Figure 4.6. Visual interpretation of panchromatic imagery for landuse/cover information (A) 1960 and (B) 2001(Department of the Interior/USGS, 1960, 2001)

Image (A) in Figure 4.7 shows the site of the dam in 1960 as shown in the red box; (B) in Figure 4.7 shows the reservoir in 2001.

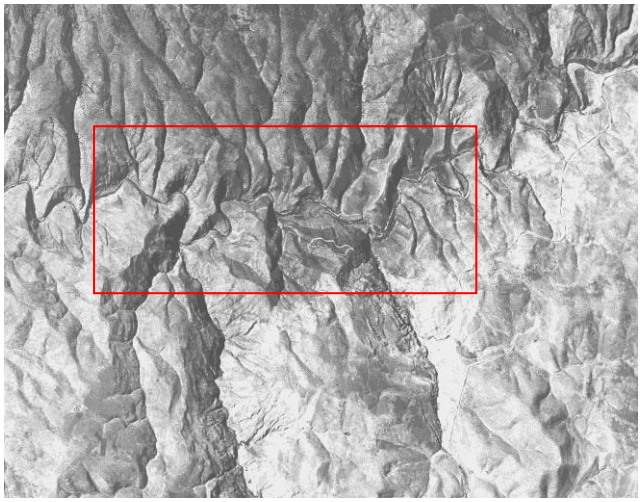

(A)

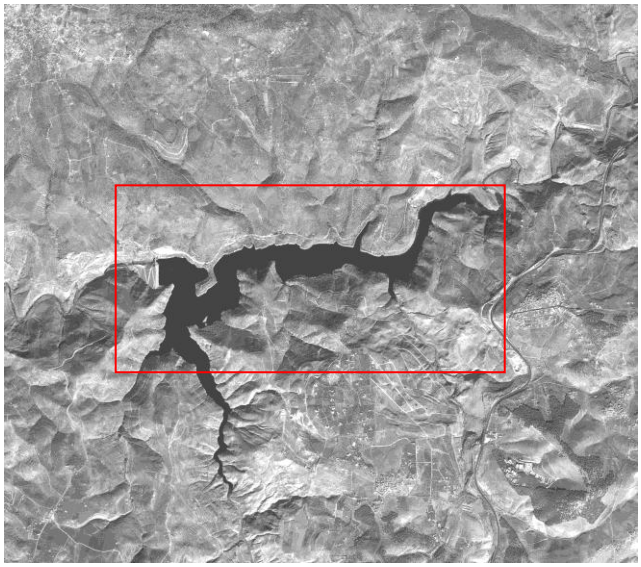

(B)

Figure 4.7. Visual interpretation of panchromatic images (A) 1960 and (B) 2001 (Department of the Interior/USGS, 1960, 2001)

Image (B) in Figure 4.8 shows the upstream areas (2001) and the changes around the reservoir. For instance, urban and residential uses are shown here by white tones and systematic streets as seen in the yellow boxes. The highway connecting Irbid city with the capital Amman

appears as a linear form in both images, however, there are changes in the size and the shape of the curves in 2001 (red ellipse).

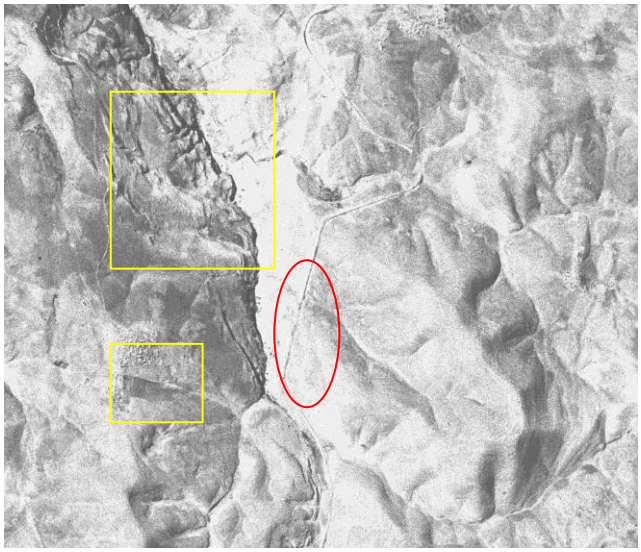

(A)

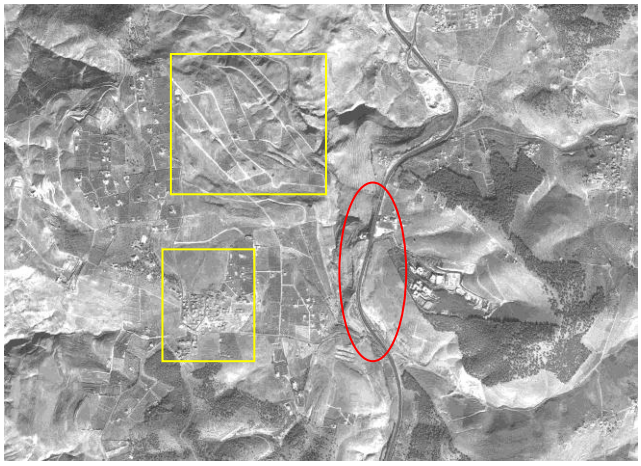

(B)

Figure 4.8. Visual interpretation of landuse/cover change (A) 1960 and (B) 2001 (Department of the Interior/USGS, 1960, 2001)

In Figure 4.9 image (A) and image (B) show the same region of upstream area of King Talal Dam. A planted forest is characterized by coarse texture (image B, red box), whereas in 1960 in image A, this forest did not exist (red box). In addition, image (B) in 2001 shows more residential areas and streets (yellow boxes).

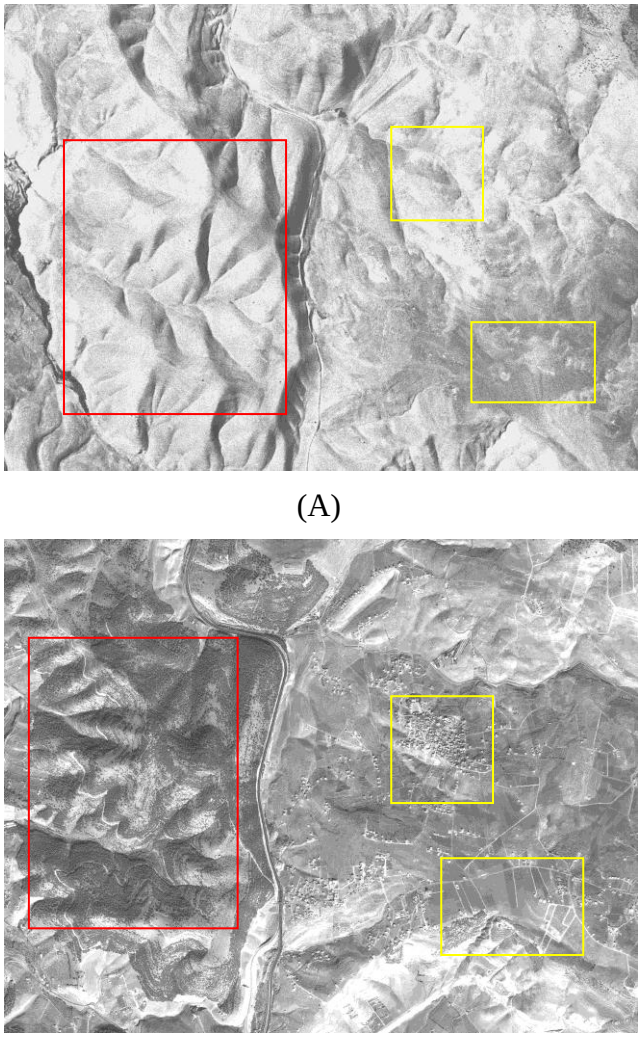

(A)

(B)

Figure 4.9. Visual interpretation of land cover changes; Forests plantation (A) 1960 and (B) 2001 (Department of the Interior/USGS, 1960, 2001)

In image (B) many changes are visible from the 1960 image (A). More urban areas and streets are shown in bright tones (yellow boxes); in addition, more cropland and farms are recognizable by their smooth texture and the contrasting tones (blue boxes). Image (A) figure 4.10 shows none of these landuse/cover types except for some trees or rangelands.

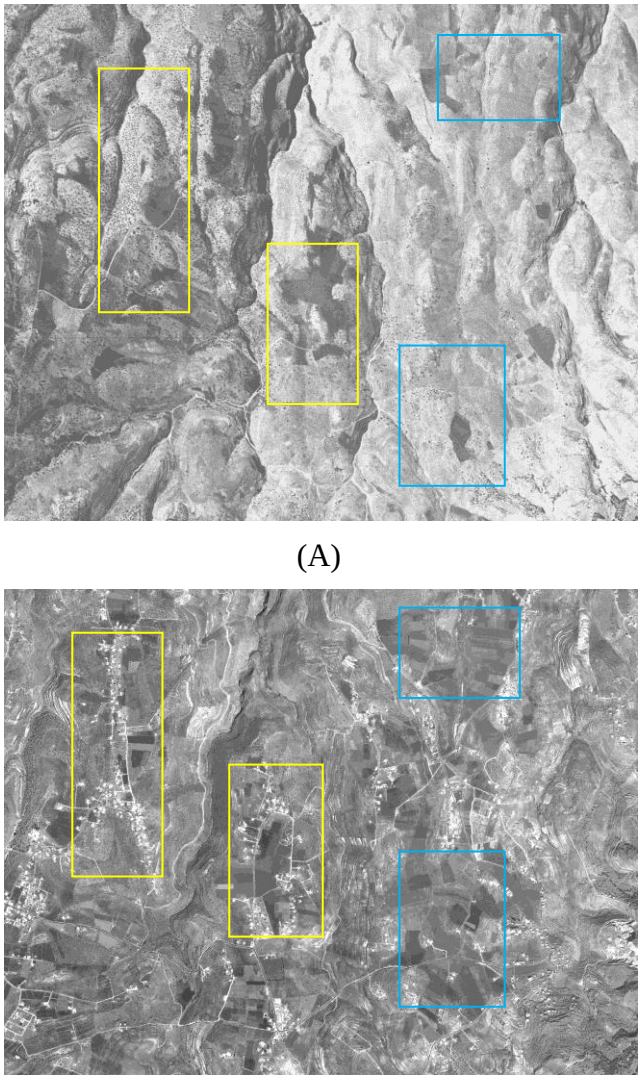

(A)

(B)

Figure 4.10. Visual interpretation of panchromatic images for landuse/cover change between (A) 1960 and (B) 2001 in King Talal upstream area (Department of the Interior/USGS, 1960, 2001)

In general, image interpretation was successful in classifying the change in land use, especially the agricultural and urban areas. Digital classification was performed (described in the next section) to give more details and quantitative analysis about the changes in different landuse/cover in this area. Image interpretation helps to establish the proper context for understanding the meaning of an image.

4.2 Landuse/cover change using digital classification

Supervised classification method was applied for all images of both dams. Then the classification technique was analyzed qualitatively and quantitatively. Each image was compared to the reference image and the other classified image to assess the accuracy of each assigned informational class. A quantitative comparison was done by calculating the difference between total percent coverage for each land cover type.

The recoded supervised images of 1990 and 2006 using the maximum likelihood technique in ERDAS are shown in Figures 4.11 and 4.12. The landuse/cover maps were classified into eight classes with total area of 3000 km^2. The two images were taken in the same season on May of 1990 and May 2006. This helped in reducing the error that may have occurred because of the seasonal influence. However, the landuse/cover types on both scenes are influenced by spring plant growth, which can cause some spectral overlap between categories. For example, spring plant growth may give the same spectral appearance in several cases as cropland. With the coarse resolution of the image, it was difficult to classify the different crops being grown. Landuse/cover including, urban, crop, orchard, forest, rangeland, desert, water, and salt are shown in Figures 4.11 and 4.12.

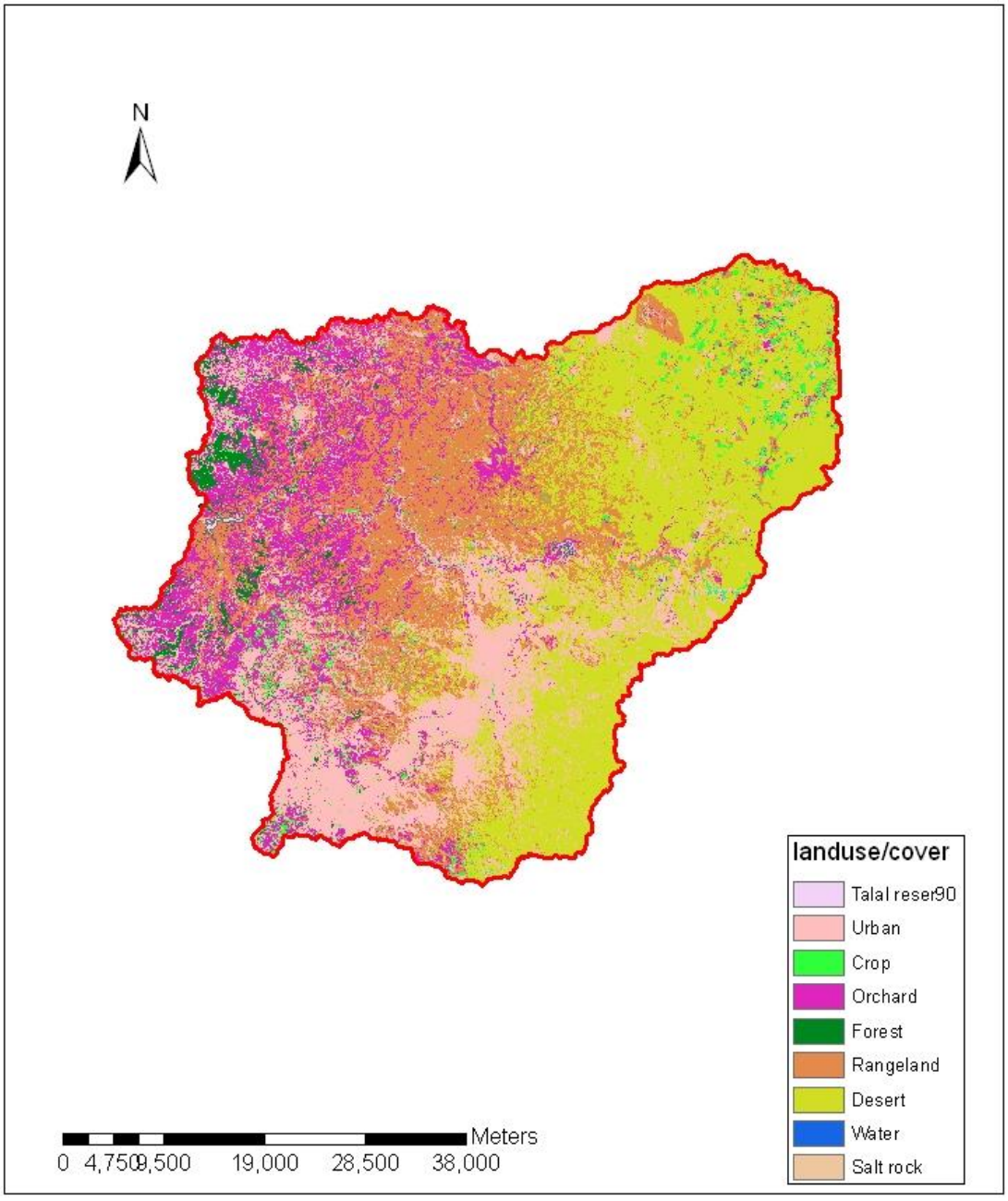

Figure 4.11. Recoded supervised image for upstream area for King Talal Dam in 1990

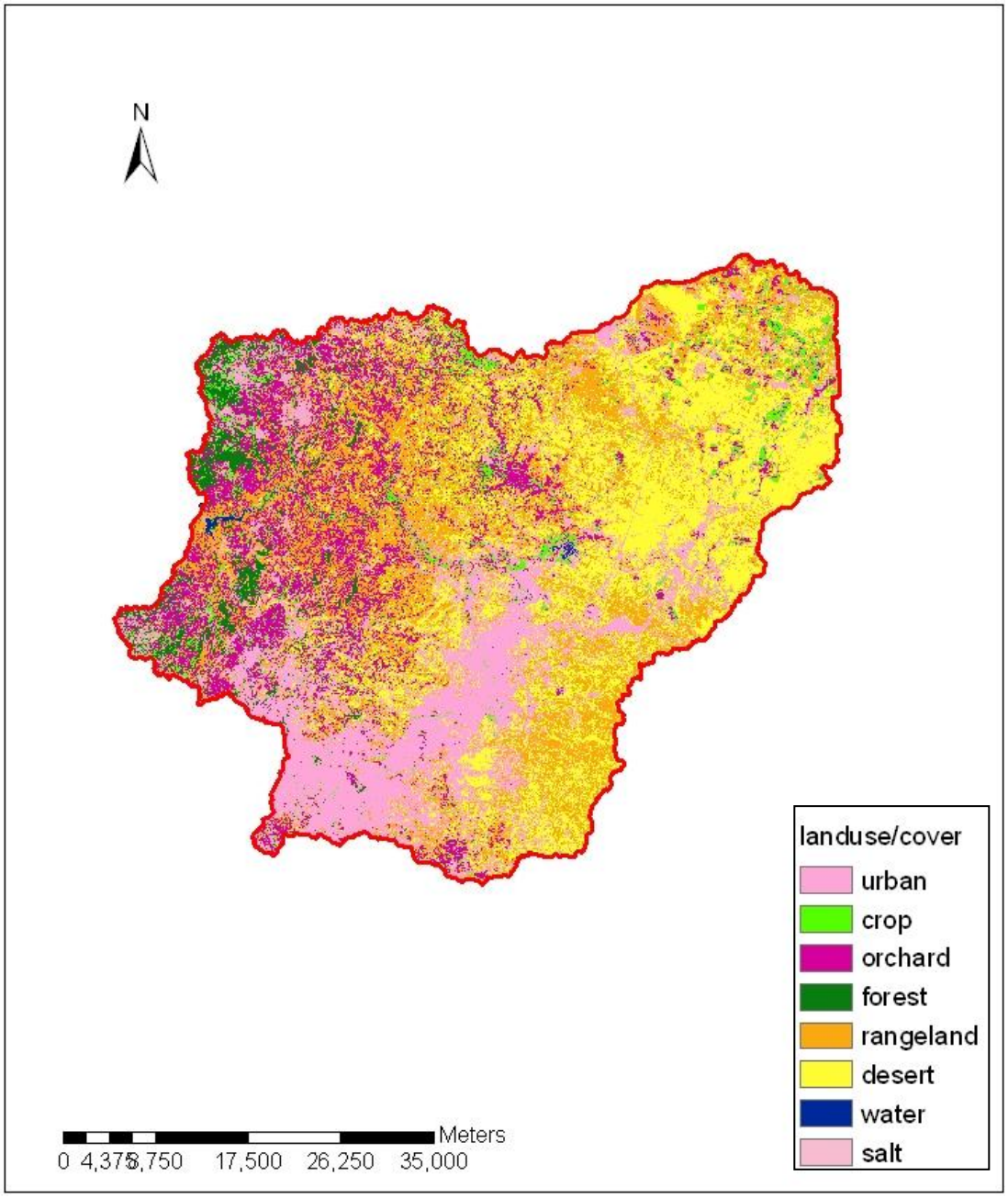

Figure 4.12. Recoded supervised image for upstream area for King Talal Dam in 2006

For supervised classification, desert represented the largest land cover, followed by rangeland, and urban. A comparison exploring the differences in the landuse/cover between 1990 and 2006 is shown in Figure 4.13. Represented in Table 4.1 are the areas of each landuse/cover type for each image and area change from 1990 and 2006 for King Talal Dam.

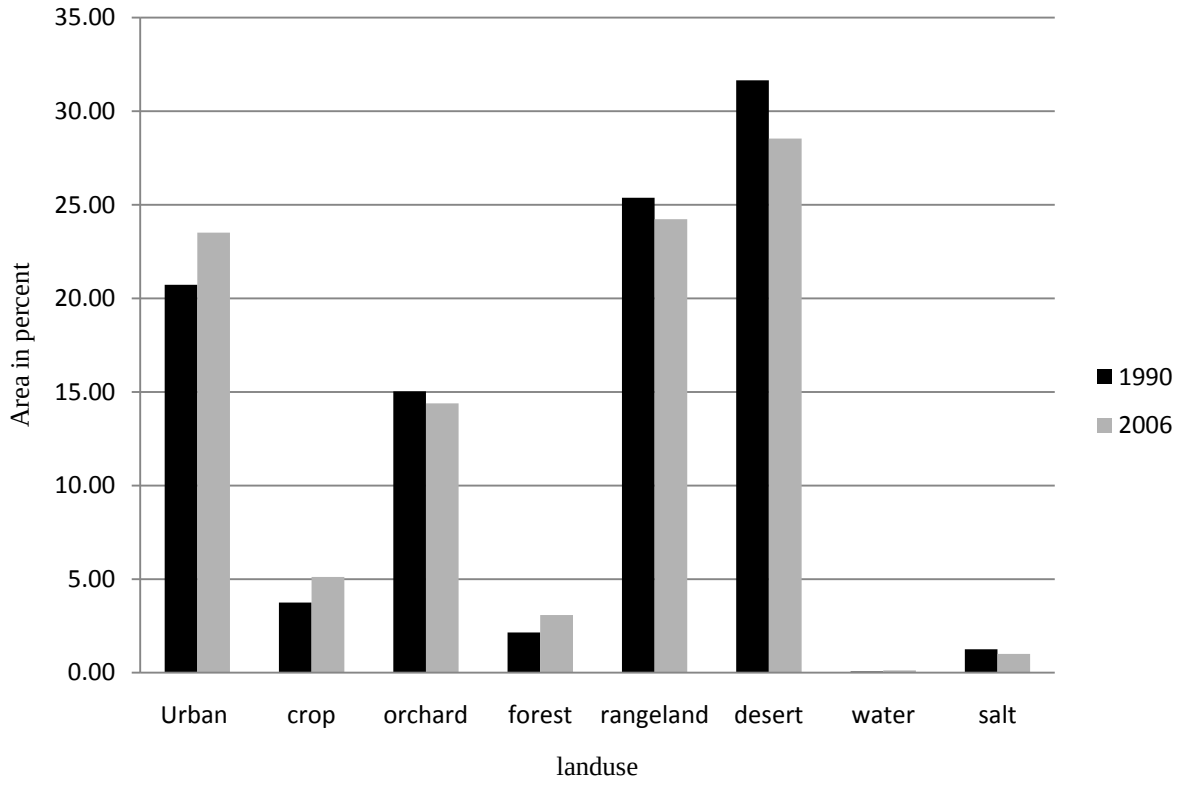

Figure 4.13. Area in percent in different Landuse for the years 1990 and 2006 for King Talal Dam

Table 4.1. Areas for different Landuse/cover type in 1990 and 2006 for King Talal Dam

Landuse/cover	Area of 1990 (Km^2)	Area of 2006 (Km^2)	Percent Area change from 1990 to 2006 (%)
urban	521	589	13.4
crop	94.2	128	36.4
orchard	377	361	-4.2
forest	54.1	77.3	79.3
rangeland	637	607	-4.5
desert	794	716	-9.8
water	1.70	3.17	85.9
salt	31.5	25.2	-19.8

4.2.1 Trend of Landuse/cover change from 1990-2006 for King Talal reservoir

During the period from 1990 to 2006, the land area in desert, rangelands, and orchard decreased. Desert decreased by about 78.0 km^2 within 16 years. Orchards appeared to decrease in area by 15.9 km^2; however, this may have been because orchard land was incorrectly identified as forest land or crop land in the 2006 image. The challenge was to identify orchard land based on the colors represented by the band combination used. It was difficult to visually discern whether land area is crop only or mixed with orchards, since the farmers in that region used to plant small crops between trees. Moreover, canopy cover of orchard areas gave the same reflectance as forest. Conversely, urban areas and crops increased from 1990 to 2006. This result implies that building the dam affected the area and increased the area of urbanized and agricultural land.

It was difficult to divide urban landuse into different categories, such as residential and industry. The coarse resolution (30 m x 30 m) of the Landsat images makes it hard to distinguish between different landuse/cover boundaries especially in urban, crop, and orchard. In addition, the maximum likelihood classification technique used in this research works best assuming accurate training data, which in this case is difficult to get because there are no field data available. However, a study done by RSS (2005) found that many factories have been built on both sides of the Zarqa River in the last 20 years. These factories were permitted to be constructed without taking into account their impact on the ecosystem of that area. In addition, more than three wastewater treatment plants were built in the same basin. The wastewater treatment plants discharge water to King Talal reservoir.

Forest area increased from 54.1 km^2 in 1990 to 77.3 km^2 in 2006 as a result of the government policy to plant evergreen trees in the upstream area of the reservoir and in the lands around the Zarqa River. In addition, a small increase in the forest area occurred after building Kherbt Al Samra Waste Treatment Plant.

Finally, the salt area was decreased in 2006 to 25.2 km^2; this informational class was added after the first trial of the digital classification. It was noticed that salt areas were overlapping with urban areas which caused the urban areas to be overestimated. As a result, a new informational class with new training data was added to both images. Then a second

classification trial was performed to reduce the error, and to distinguish between urban areas and salt areas. This was successfully achieved in the output images.

The main increase in landuse was in the urban area of the King Talal watershed. One of the major reasons for this expansion was the migration from rural areas following a drop in the prices of agricultural products. A second reason was the migration from other urban areas, such as Irbid city, to the capital Amman. The process of fast growing urban settlements lacks adequate planning. This fast growth may negatively affect other landuse/cover types in this area. For example, most of the urban areas were located on lands occupying former agricultural land.

4.2.2 Landuse classification for Karameh Dam

The recoded supervised images of 1998 and 2006 for Karameh Dam using the maximum likelihood technique in ERDAS are shown in Figures 4.14 and 4.15. The landuse/cover maps were classified into eight classes with total area of 62.35 Km^2. The 1998 image was taken in April, while the 2006 image was taken in May. The difference in time may increase the error that could occur because of the seasonal influence. However, the landuse/cover types on both scenes were influenced by spring plant growth, which can cause some spectral overlap between categories. For example, spring plant growth may give spectral appearance as cropland especially in the April scene. This condition makes category separation difficult and causes underestimation or over estimation of the area of other categories.

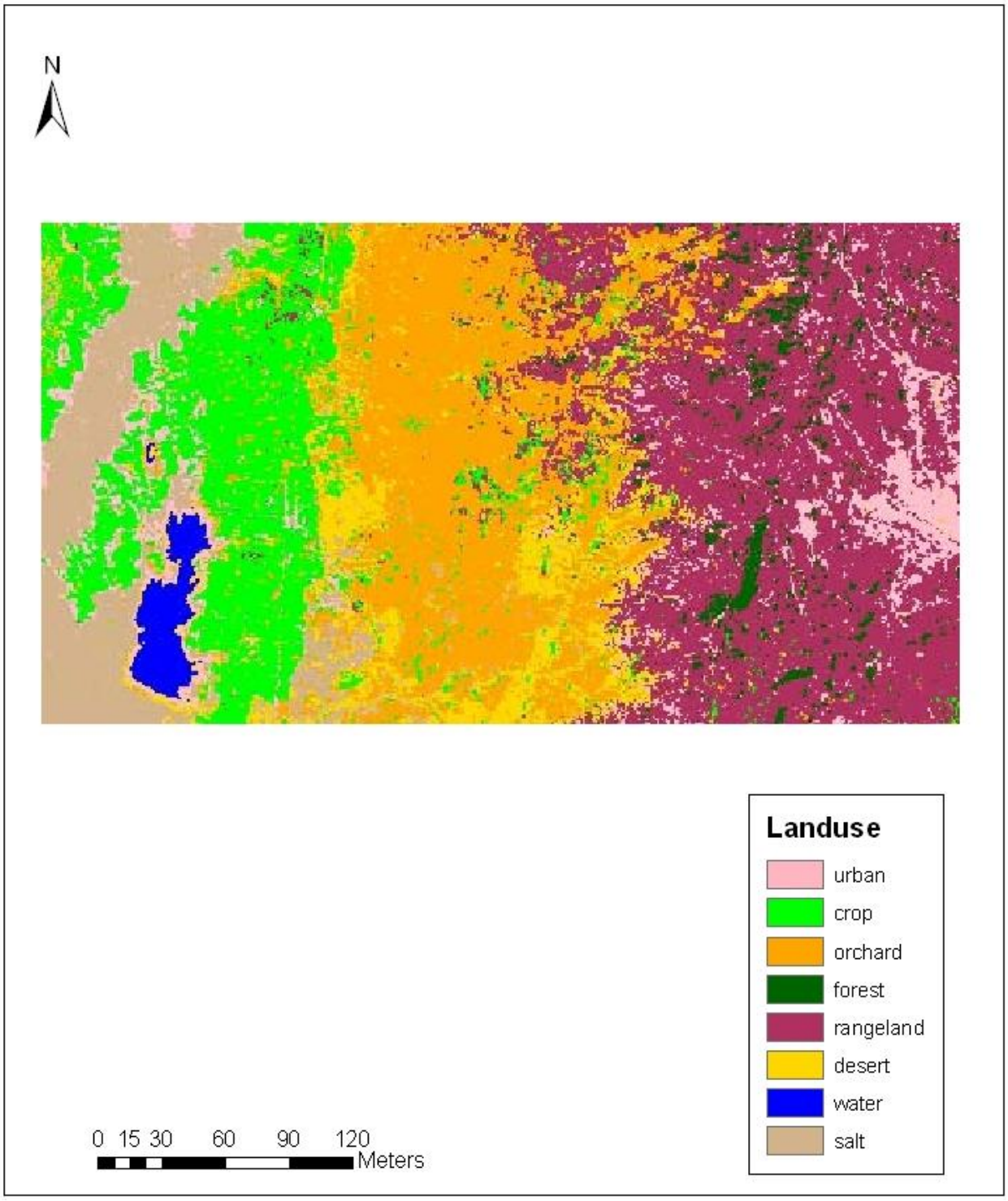

Figure 4.14. Recoded supervised image for Karameh Dam watershed in 1998

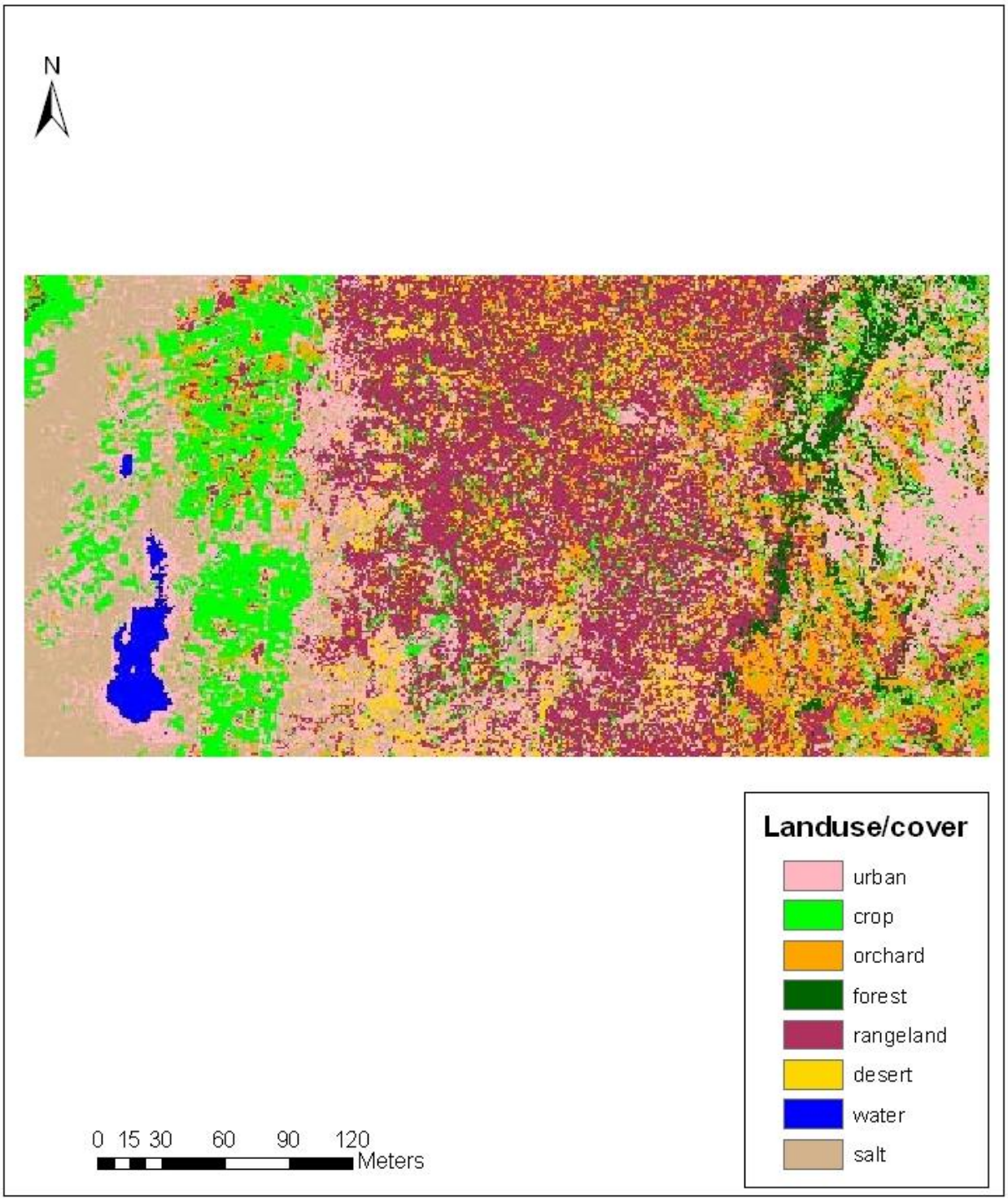

Figure 4.15. Recoded supervised image for Karameh Dam watershed in 2006

Rangeland in both years represented the largest landuse/cover type. There were significant changes in landuse/cover in 2006. The comparison of the different landuse/cover in 1990 and 2006 is shown in Figure 4.16.

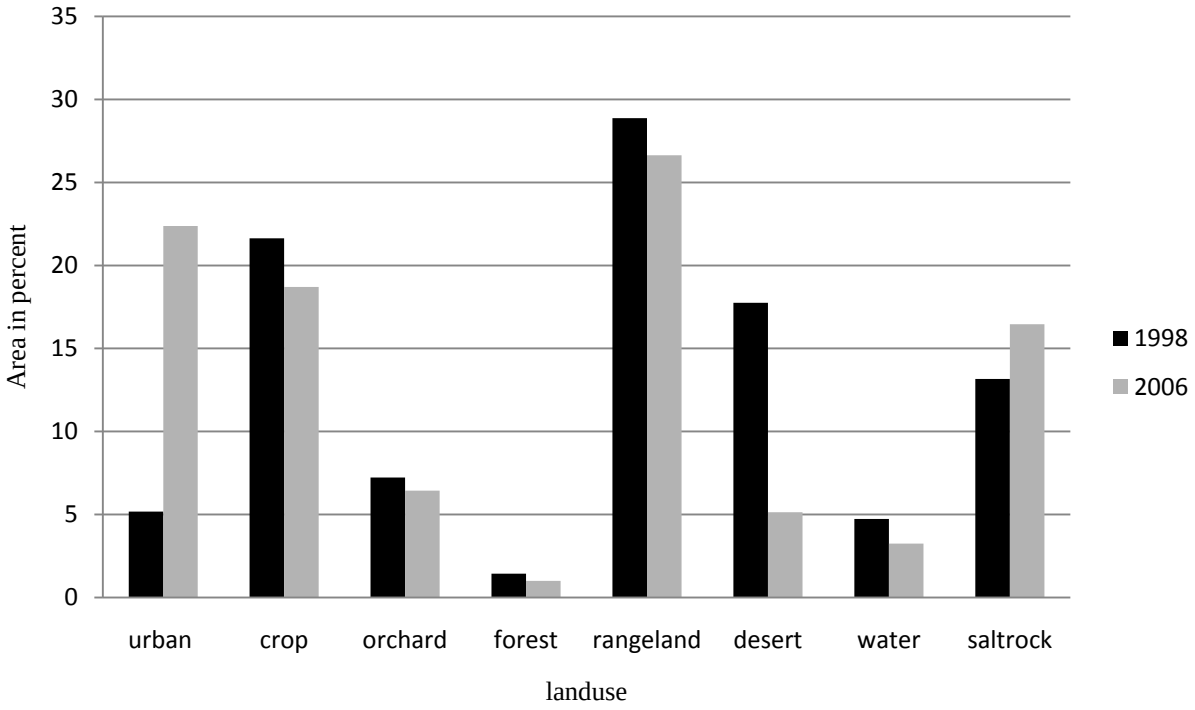

Figure 4.16. Area in percent in different landuse for Karameh Dam in 1998 and 2006

Table 4.2, which gives the area in each class from each image, shows significant changes in desert and urban lands from 1998 to 2006.

Table 4.2. Differences in the area of Landuse/cover type between the years 1998 and 2006 for Karameh Dam

Landuse/cover	Area of 1998 (km^2)	Area of 2006 (km^2)	Percent area change from 1998 to 2006 (%)
urban	3.21	13.9	333.3
crop	13.4	11.6	-13.6
orchard	4.49	4.00	-10.9
forest	0.894	0.62	-30.2
rangeland	17.9	16.6	-7.8
desert	11.1	3.19	-70.7
water	2.94	2.02	-31.3
salt	8.19	10.2	25.0

4.2.3 Trend of Landuse/cover change from 1998-2006 for Karameh Dam

Table 4.2 shows the changes in landuse/cover from 1998, one year after building the dam, to 2006. Rangeland and desert decreased, with desert losing 7.82 km^2 from 11.1 km^2 within eight years. Crops decreased by 1.82 km^2. This might have happened because it was difficult to differentiate between crops and spring plants. As a result, spring plants in 1998 might have been incorrectly classified as crops and increased the estimated area. Finally, water decreased from 2.94 km^2 to 2.02 km^2 due to the drought year after year (1998, 1999, and 2000) (Ministry of Water and Irrigation, 2008). No water entered the reservoir during the drought, except a small amount from small streams around the reservoir and groundwater.

On the other hand, urban areas dramatically increased by 10.7 km^2 and salty rocks geological formation increased by 2.05 km^2. It is obvious that rapid and uncontrolled urbanization occurred in that area after building the dam. Many people started to settle in that area looking for an opportunity to work; especially since one of the purposes of building the dam was to establish a recreational and tourism area. This purpose was not met, however, for many reasons to be mentioned later in this study. Salt rocks increased around the reservoir due to high

salinity of the formation around the reservoir (Salameh, 2004) and high evaporation in that area. This resulted in shrinkage of the reservoir area and increased the salt rocks area. A study by Refaat (2002) confirmed the increase and the salinity of the rocks in the Karameh Dam area.

In 2006, the main increase in landuse/cover was in urban. As mentioned above, most of the urban areas were residential. Farmers and workers tended to move and settle randomly around the dam hoping that new job opportunities would be available after the operation of the dam. However, the increase in urban areas in 2006 may be overestimated. There were some areas around the reservoir that were classified as urban but might actually be salt rocks. This was due to the spectral overlap between the salt rocks and urban classes. Many trials were done to reduce this overlap by choosing more areas of interests around the reservoir and reclassifying, but the problem remained. This may be solved by field visits to help in determining more accurate areas of interest.

4.2.4 Discussion

The specific study presented used Landsat-4 TM and Landsat-5 imagery and a simple remote sensing classification technique to identify areas and assess landuse/cover change within the King Talal watershed between 1990 and 2006 and within the Karameh Dam watershed between 1998 and 2006. The work was based upon supervised image classification analysis, which provides low-cost solutions for establishing maps for monitoring past and current landuse/cover change. One of the major difficulties in this study arose from the classification of land cover in both supervised images. Without a field visit, it was difficult to distinguish between areas of some land covers; for example, it was challenging to identify all areas of agriculture and forest based on the various colors representing those land types. Another challenge was the identification of orchard land. For example, it was hard to know whether some areas were forest or orchard, especially on the mountain areas, based on the colors represented by the band combination used. To increase the accuracy of the supervised image, more assessment of the ellipses located on the feature space plot was done to prevent misidentification of land cover.

The findings of the study were consistent with previous research (Shammout, 2003), which found that there was an increase in urban areas and crops and decrease in desert land. Also the findings were visible on the satellite scenes that urban and crop increased between 1990 and

2006. Refaat (2002) and Salameh (2004) studied the Karameh Dam and confirmed the increase in the salt rocks forming the Karameh Dam and its reservoir site. They also noticed a presence of salt water springs at the bottom of the reservoir area. Assessing the overall accuracy of this classification is beyond the scope of this study, because of the lack of validation data and the lack of field observation. However, a detailed comparison of selected areas from satellite images within the watershed to aerial photographs revealed the classification scheme to be accurate in separating different landuse/cover types and identifying the changes.

4.2.5 Water quality analysis using remote sensing data

4.2.5.1 Manual calculation for King Talal Dam

Water quality sample data were extracted from the two Landsat scenes. Sample sites from different places such as the body of the lake and tributaries were selected (Figure 4.17). This was done as a preliminary check to determine if the chromaticity technique is appropriate to be applied for both reservoirs using the techniques developed by Munday et al. (1970).

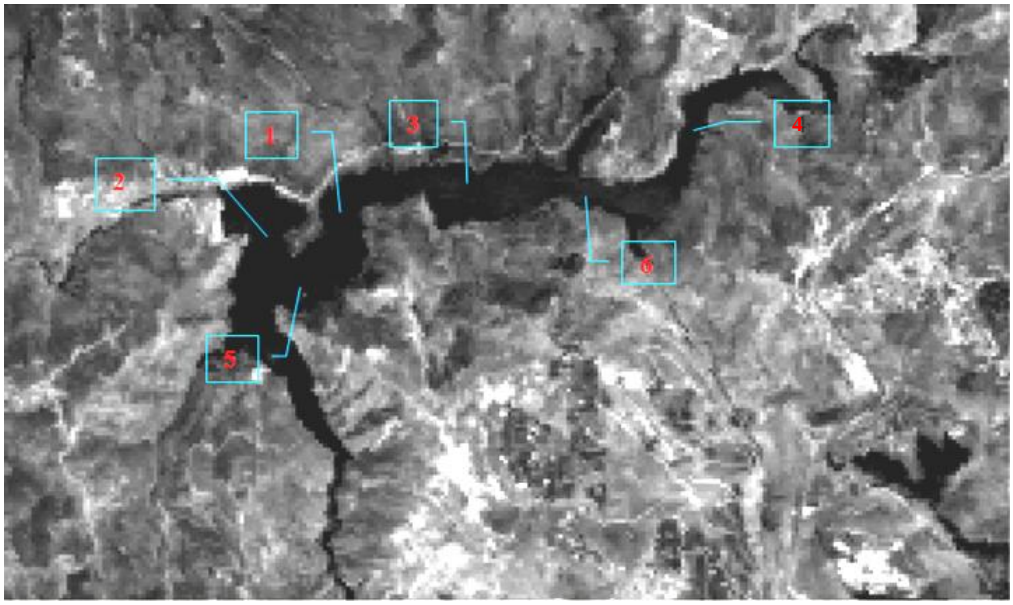

Figure 4.17. Sample sites on the Landsat image of King Talal Dam

Tables 4.3 and 4.4 show the numbers of samples identified on the satellite scenes for King Talal reservoir in 1990 and 2006, respectively. In addition to the average DNs of TM bands 2, 3 and 4 that were extracted for the nine-pixel block (3x3 pixels), Tables 4.3 and 4.4 show radiance values and X and Y chromaticity coordinates. The value of the X coordinate for each sample decreased from 1990 to 2006. In addition, the variability of the values increased. In 1990, the values of the X coordinate were almost the same (within 0.0164) for all samples, while in 2006; the values of the X coordinate varied more (by 0.098). Values of the Y coordinates also changed but only slightly, with some increasing and some decreasing. The change in X values indicates turbidity levels were increased.

Table 4.3. Results of the chromaticity analysis performed manually on excel spread sheet for May 1990 dataset

Sample No.	TM band 2	TM band 3	TM band 4	Radiance 2	Radiance 3	Radiance 4	Sum	X coordinate	Y coordinate
1	30.75	26.25	13.75	0.4372	0.2707	0.1187	0.8266	0.5289	0.3275
2	31.00	26.25	13.00	0.4408	0.2707	0.1122	0.8237	0.5351	0.3286
3	39.00	36.5	16.75	0.5901	0.3996	0.1446	1.134	0.5202	0.3523
4	41.5	38.75	16.75	0.5901	0.3996	0.1446	1.134	0.5202	0.3523
5	30.50	26.25	15.25	0.4337	0.2707	0.1317	0.8360	0.5187	0.3238
6	36.75	32.75	17.00	0.5225	0.3377	0.1468	1.007	0.5189	0.3354

Table 4.4. Results of the chromaticity analysis performed manually on excel spread sheet for the May 2006 dataset

Sample No.	TM band 2	TM band 3	TM band 4	Radiance 2	Radiance 3	Radiance 4	Sum	X coordinate	Y coordinate
1	34.00	31.00	15.50	0.4834	0.1397	0.1338	0.9369	0.5159	0.3412
2	42.33	39.67	19.00	0.6019	0.4091	0.1640	1.175	0.5123	0.3481
3	35.50	36.00	24.75	0.5048	0.3713	0.2137	1.089	0.4632	0.3407
4	26.00	24.67	14.33	0.3697	0.2544	0.1237	0.7478	0.4944	0.3402
5	38.00	40.67	26.33	0.5403	0.4194	0.2273	1.187	0.4552	0.3533
6	38.00	40.67	26.33	0.4453	0.3723	0.2480	1.065	0.4179	0.3494

Sediment loci were calculated for chromaticity coordinates of both images for King Talal reservoir in 1990 and 2006. For each locus, the end nearest E is an indication of turbid water, whereas the opposite end of the locus is an indication of clearer water (figure 3.4). The sediment locus forms an indication of relative turbidity. Water in King Talal reservoir showed high levels of turbidity. As shown in Figure 4.18, some coordinates (circles) from Landsat TM 1990 fall in the middle part of the locus and some toward the upper end (more turbid) of the sediment locus. The location of the plotted coordinates varied with respect to their location on the locus. As seen in the diagram some of the plotted coordinates fall below the locus, while one plotted coordinate falls above the locus in the chromaticity diagram. A position below or above the sediment locus is an indication of spectral impurity as mentioned before and may be caused by atmospheric effects as in samples 4 and 5 in 1990 (blue circles). In addition, the sediment locus constructed by Munday et al. (1979) was for a specific site. Ideally, every site should define its own locus. The chromaticity coordinates for King Talal Dam on May 2006 are plotted as red squares in Figure 4.18. Most coordinates also fall on the upper end of the locus; however, the plotted coordinates this time fall closer to the sediment locus, and shifted more toward the upper end than the coordinates in 1990. Samples in both years were taken from the same place. Figure 4.18 shows variation in the position of samples with respect to the locus position from 1990 and 2006. For example, samples 6 and 5 changed dramatically in 2006 and shifted more to the upper end of the locus, an indication of increase in turbidity.

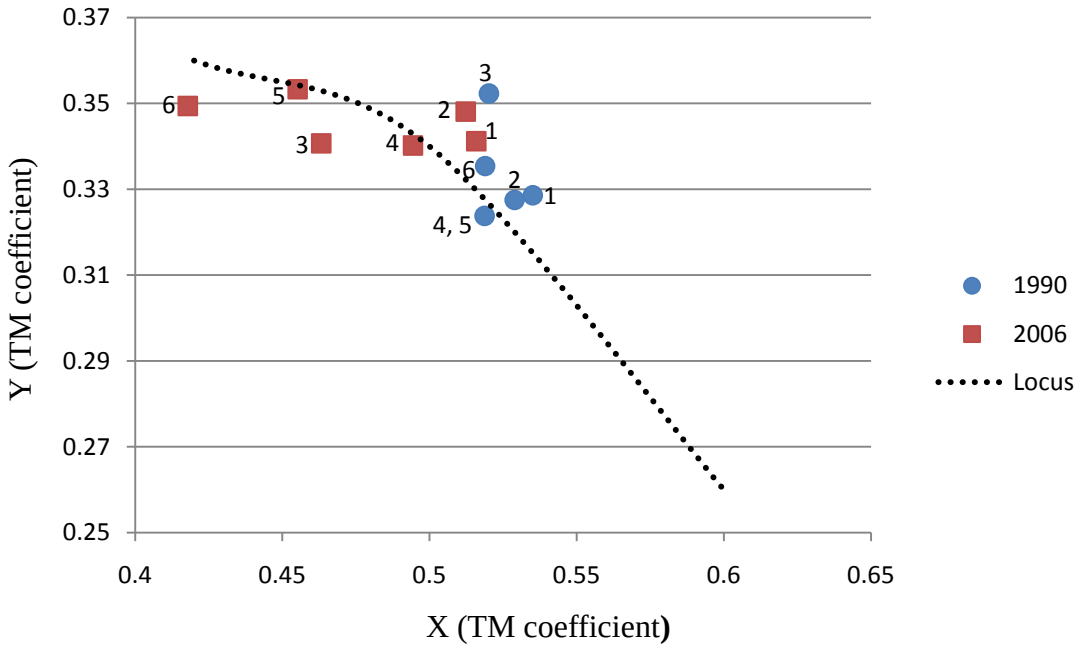

Figure 4.18. Chromaticity coordinates for samples taken for King Talal reservoir in 1990 and 2006. Dashed line is the sediment locus approximated from Munday et al. (1979)

Results showed that King Talal reservoir had the problem of high level of turbidity in 1990 and increased turbidity level in 2006 based on the chromaticity coordinates positions. However, this is a preliminary test of the chromaticity technique to check if this test is applicable for King Talal reservoir and needs to be done for the whole reservoir, not for averaged samples. In addition, to make it more meaningful, the results should be compared to field measurement in the same sites where the Landsat samples were taken.

4.2.5.2 Manual calculation for Karameh Dam

Water quality sample data were extracted from the two Landsat scenes selected for Karameh Dam (1998, and 2006). Pixel values were extracted from Landsat data using ERDAS software. The sample sites were taken from different places of the reservoir as shown in Figure 4.19.

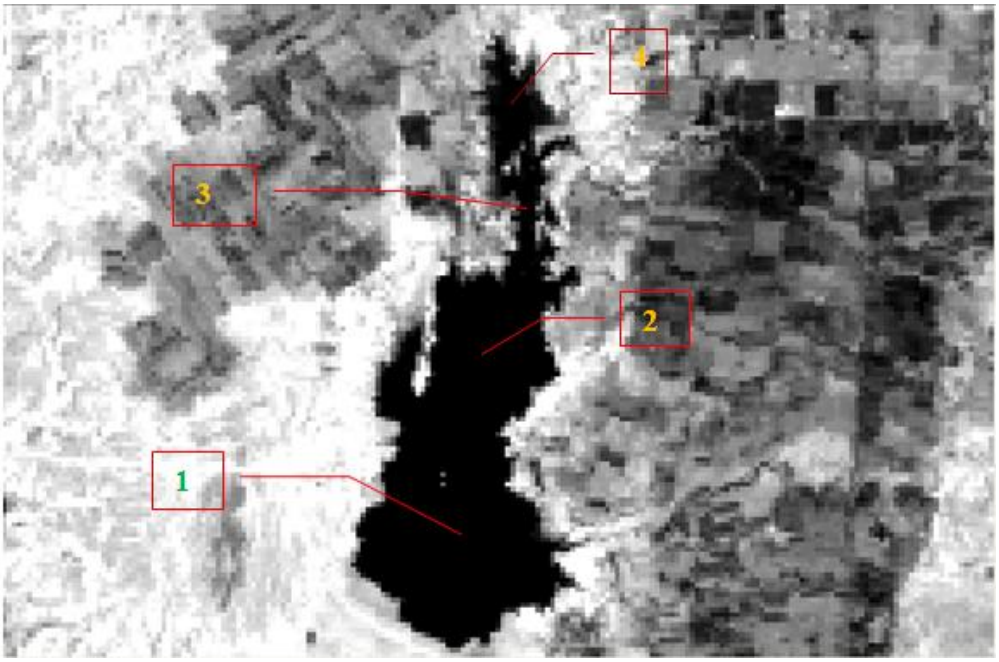

Figure 4.19. Reservoir show the sample sites on the Landsat image

As mentioned previously, samples were positioned the distance of 1 pixel from the nearest land boundary around the reservoir; this was accurately done by using ERDAS software. Tables 4.5 and 4.6 show the average DNs of the samples identified on the satellite scenes and X and Y chromaticity coordinates in 1998 and 2006. The X coordinate varied between 0.49 and 0.56 in 1998, while in 2006, the X coordinate was almost the same, about 0.49, for all samples. The X coordinates in 2006 shifted to the turbid end of the locus (Figure 4.20), meaning the turbidity level had increased. The same trend was seen for the Y coordinates. The values in 1990 were about 0.30, while in 2006 the values ranged between 0.325 and 0.336. This means values shifted more toward the locus because of the increase in turbidity.

Table 4.5. The results of the chromaticity analysis performed manually on excel spread sheet for 1998 dataset of Karameh Dam

Sample No.	Band 2 DN	Band 3 DN	Band 4 DN	Radiance 2	Radiance 3	Radiance 4	Sum	X coordinate	Y coordinate
1	40.00	30.00	15.00	0.5687	0.3094	0.1295	1.008	0.5645	0.3070
2	34.00	25.00	15.00	0.4834	0.2578	0.1295	0.8707	0.5552	0.3004
3	31.00	22.00	14.00	0.5119	0.3403	0.1812	1.033	0.4953	0.3000
4	32.00	24.00	15.00	0.4692	0.3094	0.1727	0.9513	0.4933	0.3020

Table 4.6. The results of the chromaticity analysis performed manually on excel spread sheet for 2006 dataset of Karameh Dam

Sample No.	Band 2 DN	Band 3 DN	Band 4 DN	Radiance 2	Radiance 3	Radiance 4	Sum	X coordinate	Y coordinate
1	30.00	27.00	17.00	0.4266	0.2784	0.1468	0.8517	0.5008	0.3269
2	32.00	30.00	18.00	0.4550	0.3094	0.1554	0.9198	0.4947	0.3364
3	36.00	33.00	21.00	0.5119	0.3403	0.1812	1.033	0.4953	0.3293
4	33.00	30.00	2.00	0.4692	0.3094	0.1727	0.9513	0.4933	0.3252

Sediment loci were calculated for chromaticity coordinates of both images for Karameh reservoir. In 1998, as shown in Figure 4.20, the chromaticity coordinates (blue circles) fall in different parts of the sediment locus. Two plotted samples fall toward the left end, the other two fall in the middle, an indication of relatively turbid water. Some of plotted coordinates also fall below the locus and some above it. A position below or above the sediment locus is an indication of spectral impurity caused by atmospheric effects. An explanation for that effect might be that Karameh Dam area had high level of dust in the atmosphere due to relatively high speed wind (Refaat, 2002). Presented in the same Figure 4.20, the sediment locus in 2006 is an indication of

high turbidity in Karameh reservoir, with most chromaticity coordinates falling toward the upper end of the sediment locus. The plotted coordinates for 2006 fall closer to the sediment locus than in 1998 and are shifted more toward the upper end. Since the samples were taken from the same location each year, the results indicate that there was an increase in the turbidity of the water in the reservoir nine years after the dam was built. Figure 4.20 shows the change in the position of each point from the locus between 1990 and 2006. For example, the change in the position of samples 1 and 2 indicates a shift toward the turbid end of the locus.

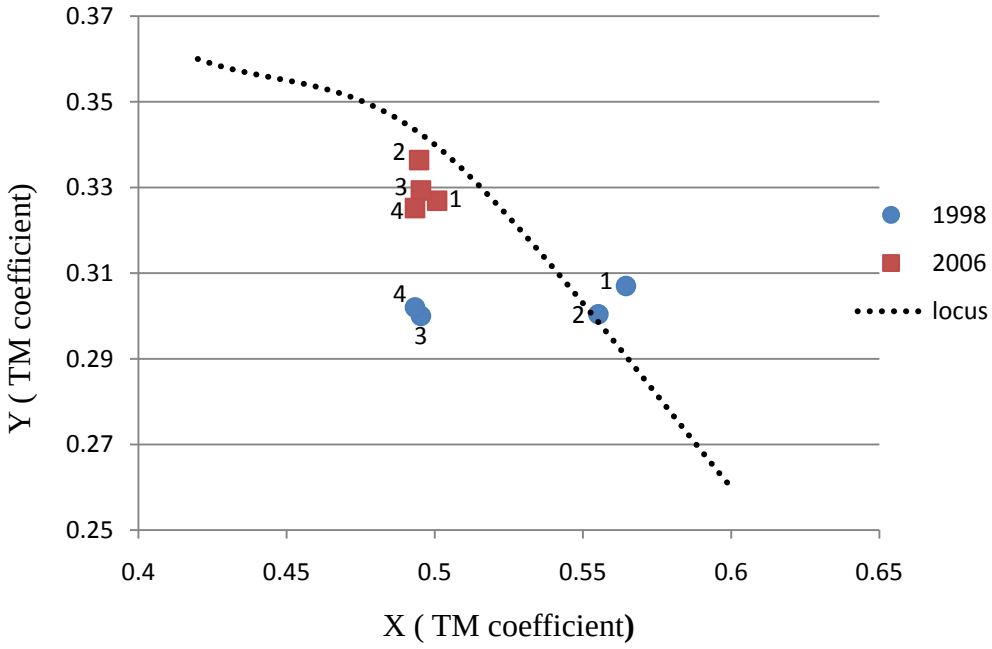

Figure 4.20. Chromaticity coordinates for samples taken for Karameh Dam in 1998 and 2006. Dashed line is the sediment locus approximated from Munday et al. (1979)

The X and Y coordinates showed that the turbidity level in Karameh reservoir has increased from moderately turbid in 1998 to highly turbid in 2006, based on the position of the coordinates in relation to the sediment locus. That was nothing more than a preliminary check of the chromaticity technique. The results of the chromaticity analysis for the whole reservoir are presented in the next section.

4.2.6 Chromaticity analysis using model maker in ERDAS 9.2

4.2.6.1 Qualitative chromaticity analysis

A model (Figure 4.21) was set up in ERDAS Imagine to perform chromaticity analysis for King Talal Dam (1990 and 2006 images) and Karameh Dam (1998 and 2006 images). This model was designed to implement the radiance conversion technique described in section 3.2.1.

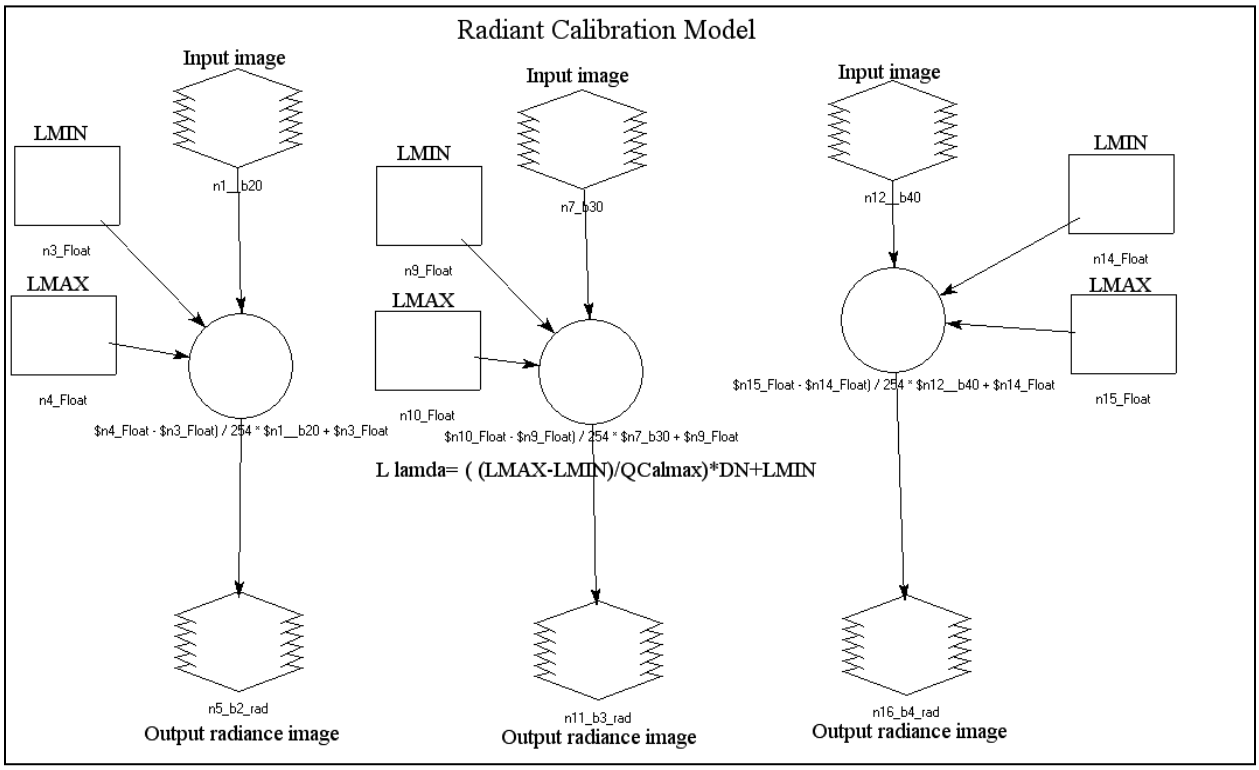

Figure 4.21. Radiant Calibration model built in ERDAS

The model created three output images, one image for band 2 with pixels converted to radiance values, another image for band 3 and the last radiance image for band 4. The subsequent operations, including summation of the output radiance values and finding the chromaticity coordinates, were done in ENVI software using the band algebra method.

The last step was to combine the output images to get the final map of the reservoir that shows the distribution of turbidity, as shown in Figures 4.22 and 4.23. Both images are shown in the color image display. The orange and yellow colors represent the turbidity level in the water, with orange representing high turbidity. The different distribution of colors indicates that

turbidity distribution changed from 1990 to 2006. A little change in the distribution of turbidity was noticed in 2006. As seen in Figures 4.22 and 4.23, red circles show higher turbidity than other areas.

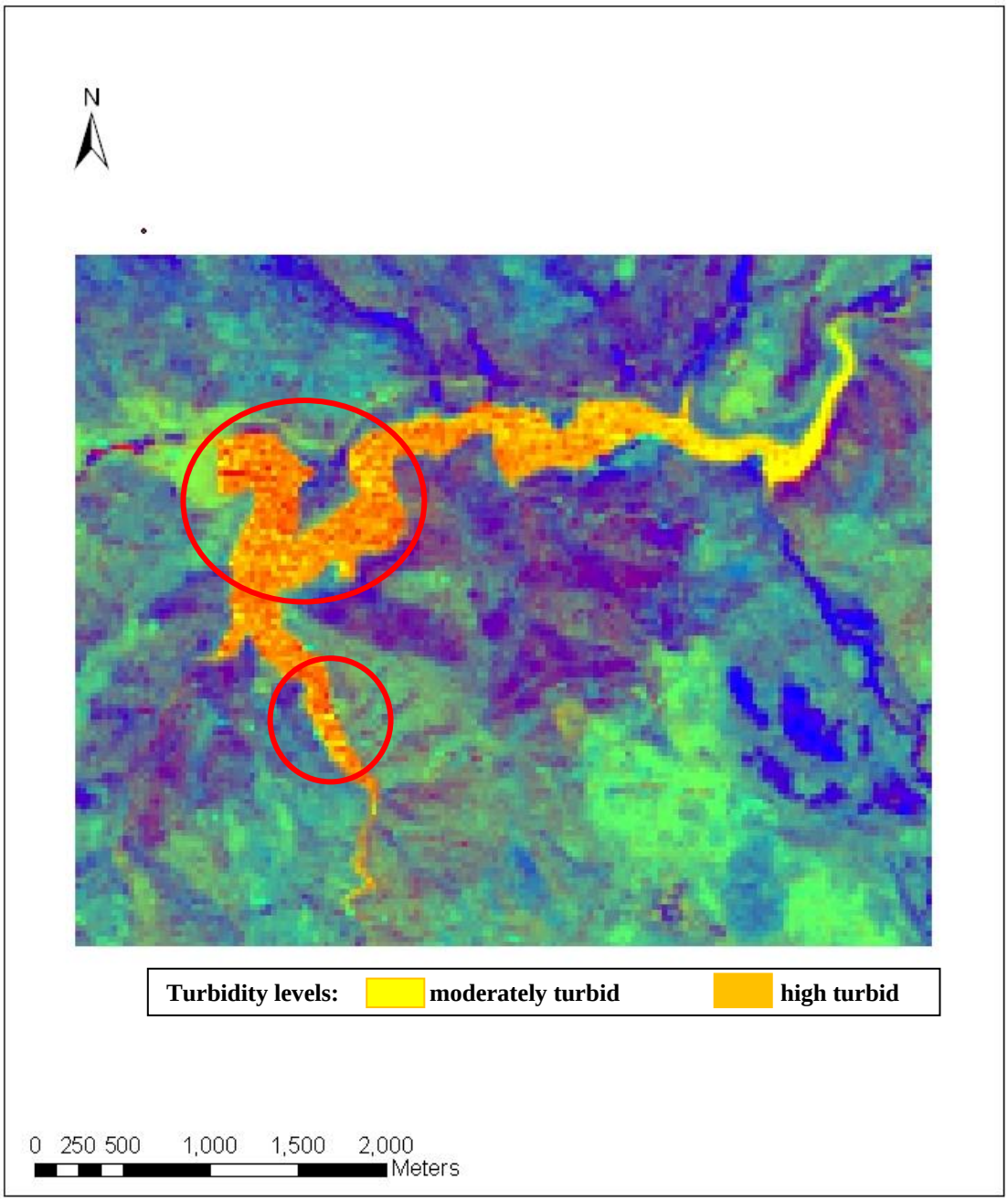

Figure 4.22. Final map for King Talal Dam shows the distribution of turbidity in 1990. Red circles highlight areas with high turbidity.

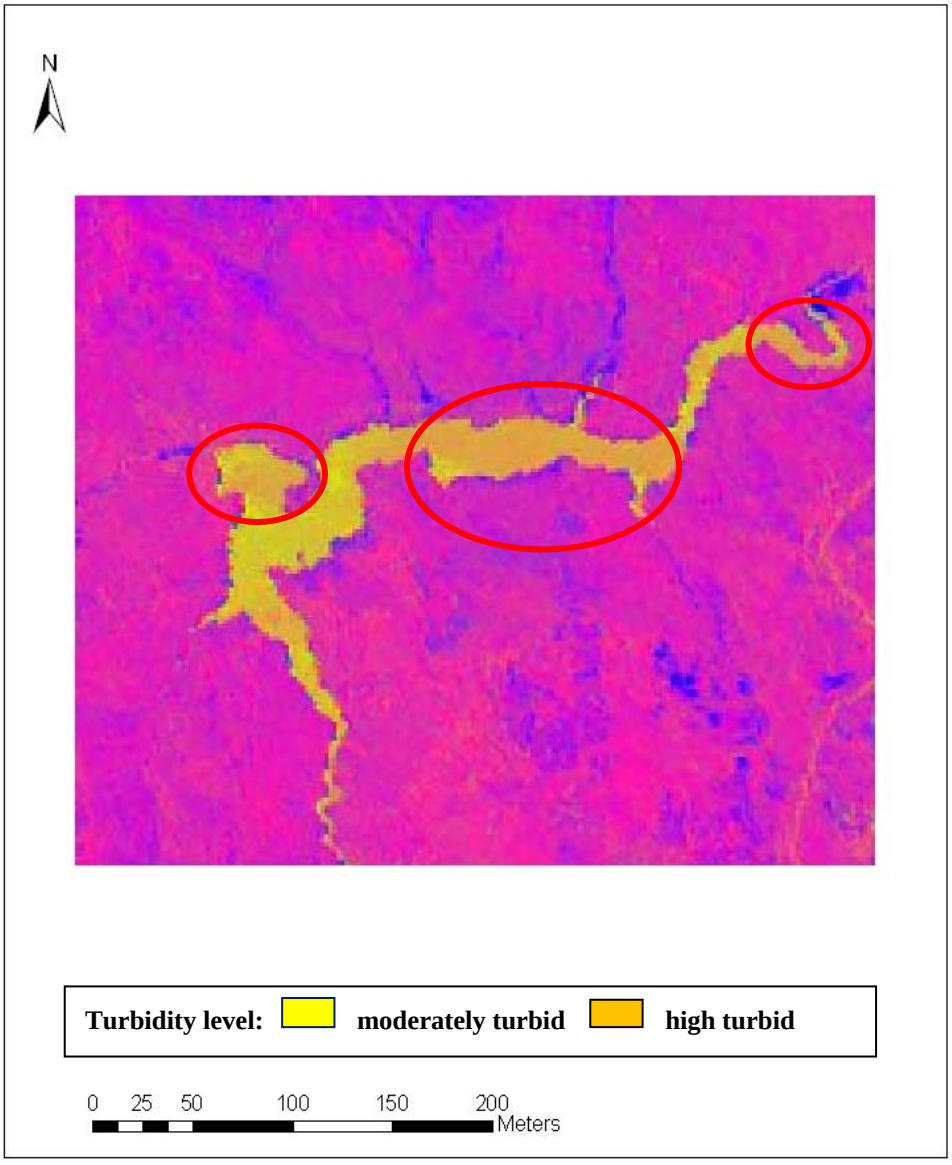

Figure 4.23. Final map of King Talal Dam shows the distribution of turbidity in 2006. Red circles highlight areas with high turbidity.

Figures 4.24 and 4.25 show the distribution of turbidity in 1998 and 2006 for Karameh Dam. Both images are shown in the color image display. The orange and yellow colors represent the turbidity level in the water. The different distribution of colors indicates that turbidity distribution changed from 1998 to 2006. The distribution and the level of turbidity changed from 1998 to 2006. As seen in Figure 4.24, a big plume of sediment was observed in the southern part

of the lake. In 2006, the distribution of sediment had changed and the surface of the reservoir became all turbid (Figure 4.25).

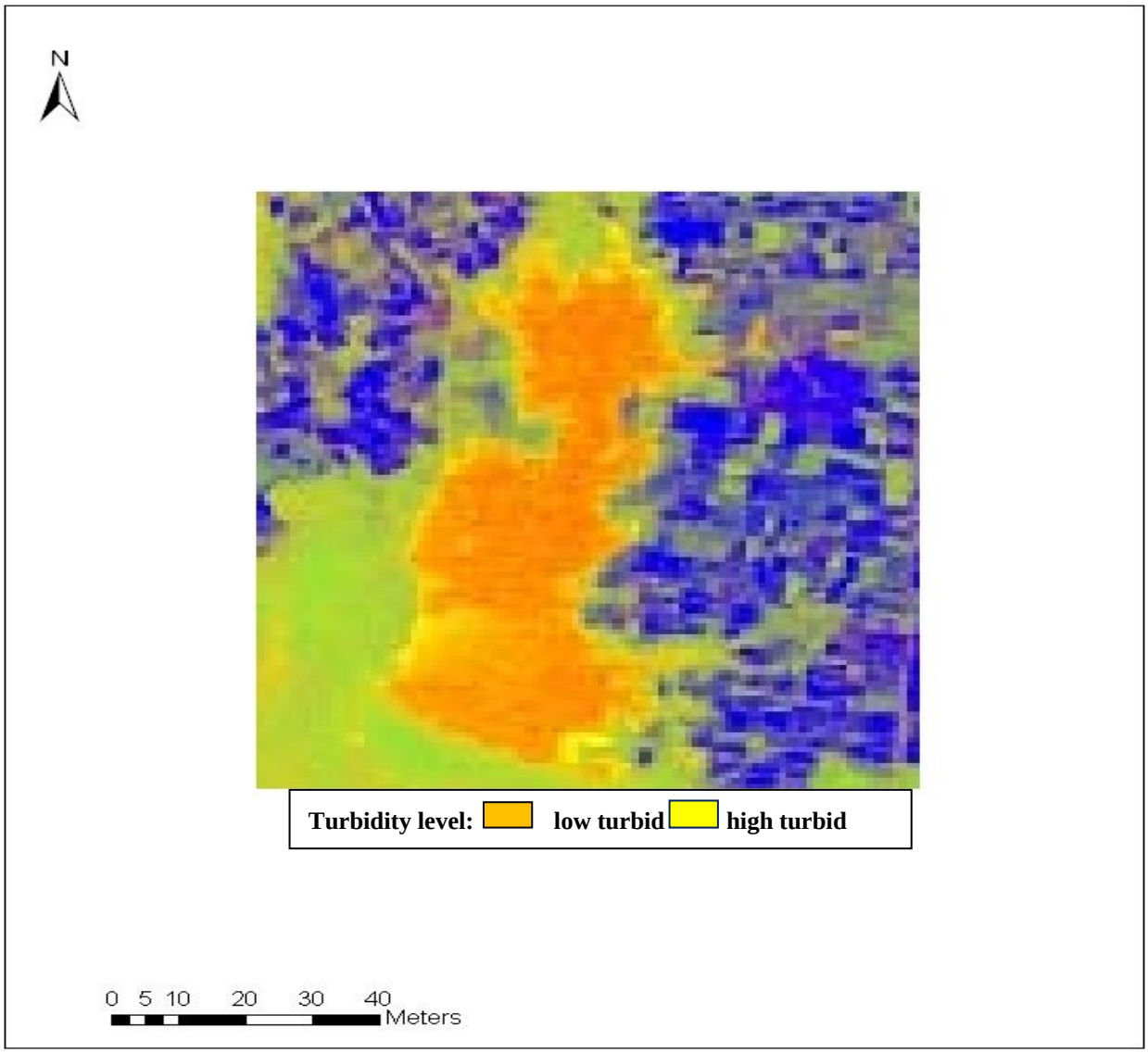

Figure 4.24. Final map of Karameh Dam shows the distribution of turbidity in 1998

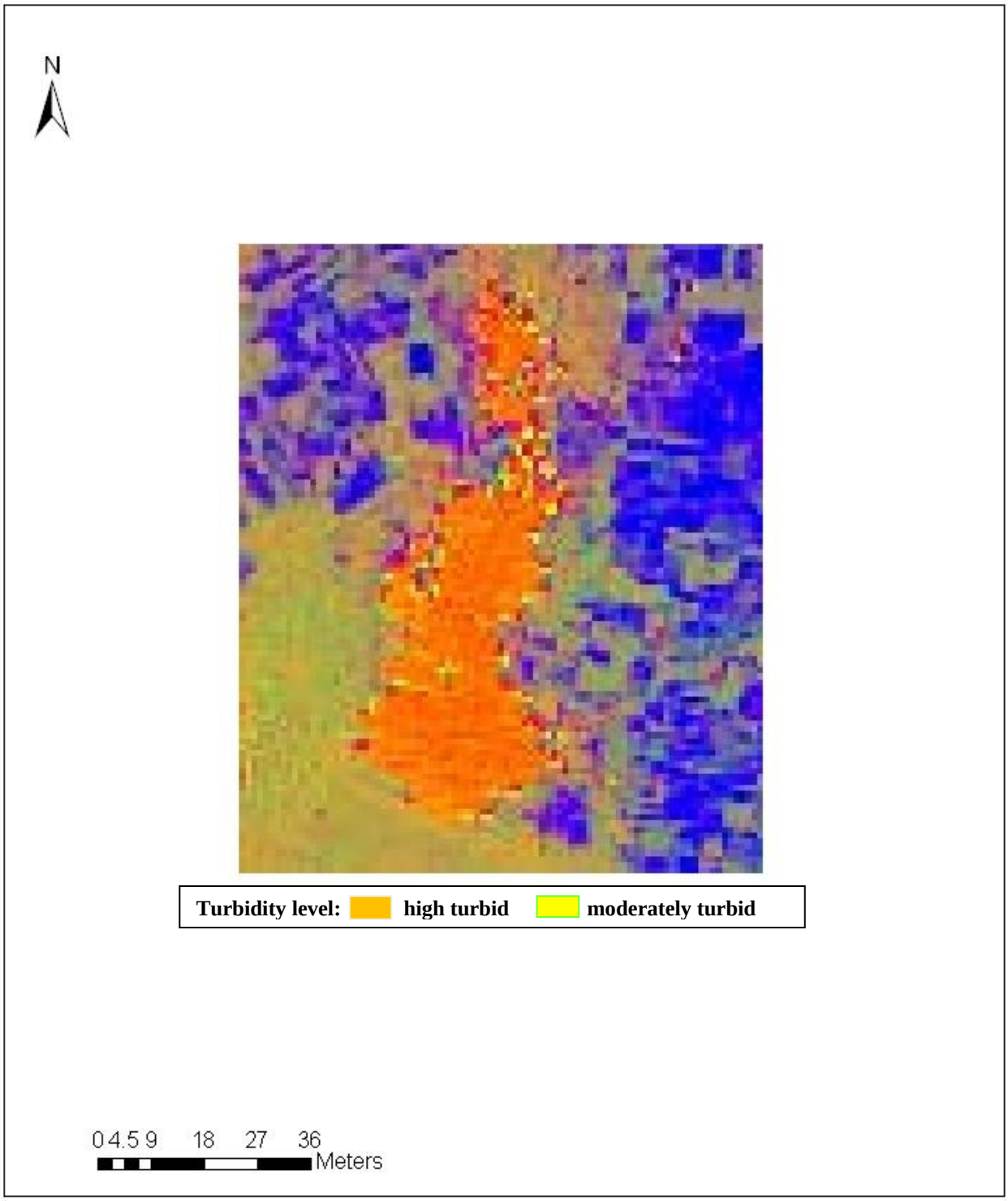

Figure 4.25. Final map of Karameh Dam shows the distribution of turbidity in 2006

4.2.6.2 Discussion

Satellite remote sensing information has been found to be useful for determining turbidity in King Talal and Karameh reservoirs in Jordan. The availability of cloud-free images in the Jordan region increases the potential for using satellite remote sensing technologies for determining turbidity or other water quality parameter in reservoirs on a systematic basis.

Although the chromaticity technique relating Landsat data and turbidity was performed before over large areas, the ability of this model to be used in different regions and areas was confirmed. Further research is required to establish the reliability of predictive models using more satellite images and the best regression estimates for regions with a wide range of turbidity values. In-situ measurement of reflectance using spectro-radiometers in conjunction with other water quality ground measurements during the satellite overpass will help to estimate the concentration of different parameters in water.

It is possible to determine the turbidity in other reservoirs using only one satellite image. Indeed, satellite remote sensing might have an effective role in reducing the cost, labor, and time required to monitor water quality and provide information over the full surface area of an inland water body. This is perceived as offering the considerable advantage of providing an early warning of quality changes anywhere within the impounded water reservoir that could have negative impacts on subsequent water treatment processes. It has the potential to be used as a tool to develop synoptic assessments that are currently not practical using traditional field operations.

4.2.6.3 Limitations of applying chromaticity technique

The major limitations and issues have identified. First, it was not possible to estimate the concentration of sediment in the reservoir because of the lack of water quality samples at the same time and dates as the satellite image. Second, while other researchers have successfully used chromaticity analysis to estimate turbidity levels, their studies included large open water, such as the Bay of Fundy. This study attempted to estimate turbidity levels in small man-made reservoirs. Several characteristics of small man-made reservoirs, such as King Talal Reservoir, might influence the accuracy of chromaticity analysis of water quality. For example, the narrow arms of this reservoir might influence the spectral purity of water pixels. Although all samples

were taken from a distance more than one pixel from the nearest land edge, spectral overlap between land and water pixels could affect the pixel value.

4.2.6.4 Comparison between chromaticity results and measured data for King Talal Dam

Munday et al. (1979) tested the accuracy of chromaticity analysis by correlating the coordinate X with the log of turbidity. This procedure could not be followed in this study because no surface samples were available at the time of the satellite pass. As mentioned before, the results of chromaticity analysis for both scenes of King Talal Dam showed high level of turbidity, which means that turbidity is a significant issue in this reservoir. A study by (JVA, 1988) expected an increase in the amount of sediment entering the reservoir. According to Jordan Valley Authority (1988) the estimated average annual inflow of suspended sediment into the reservoir was 1.0 million m^3. Further, it is assumed that sediment will be deposited until the remaining active storage equals the reservoir volume contained between the elevation of the mid-point of the spillway gates and the maximum controlled reservoir level. Under these assumptions, the accumulated sediment will reach a maximum for the raised dam in 2050.

A more recent report by Royal Scientific Society (2006) showed that the sediment in King Talal reservoir has increased from year to year. For example, sediment accumulation increased from 3.15 MCM in 1980 to 13.00 MCM in 2000 (Figure 4.26).

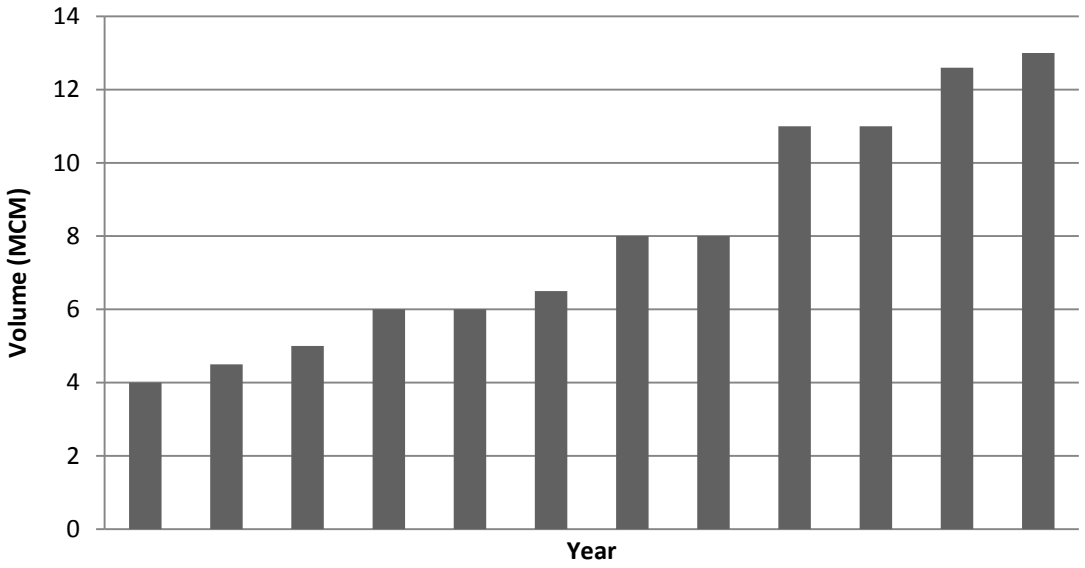

Figure 4.26. Sediment accumulation in King Talal Dam from (1980-2000)

The study by the Royal society confirmed that there is an increase in sediment volume in the reservoir. The results of chromaticity gave a qualitative estimate of turbidity in the reservoir; these results showed that the problem of turbidity is present and increasing.

4.2.6.5 Comparison between chromaticity results and measured data for Karameh Dam

The results of chromaticity analysis for both scenes of Karameh Dam showed an increase in the level of turbidity during the nine years between dates on which the images were taken. Reefat (2002) studied the Karameh reservoir and came to a conclusion that the reservoir has become an ecological disaster and a source of pollution and diseases in that area. The study confirms the findings of this research that the sediment concentration increased dramatically in the lake, due to many reasons including the rocks forming the reservoir and its site. These rocks consist mainly of salt rocks, sand stones, clay, and gravel, which reach the reservoir by runoff from small reaches. Urban and agricultural areas carry sediments and fertilizers to the reservoir. And, finally, the strong wind in that area (26 m/s) carries fine sediments to the lake and causes currents that make the water turbid.

Reefat (2002) also confirmed that there was an increase in the amount of suspended sediment in the bottom of the lake, where fine sediments deposited by gravity, in addition to the presence of suspended plants and algae. Moreover the amount of sediments was calculated and it was found that the volume of the reservoir was decreased by 1.5568 MCM between 1997 and 2002 due to the sediments that entered the reservoir.

4.2.7 Relationship between landuse/cover change and water quality

Tables 4.7 and 4.8 identify the changes in landuse/cover from 1990 to 2006 in King Talal area and changes in landuse/cover in Karameh dam area between 1998 and 2006. Inspection of table 4.7 shows how the classification represents actual change in areas on the land from 1990 to 2006. For example, 84 pixels were classified as urban, reading the third row, six pixels changed from crop in 1990 to urban in 2006. In table 4.8, 91 pixels were classified as urban and the biggest change in landuse/cover was from salt in 1998 to urban in 2006. For more accurate results validation data are needed to check if the classification results are reasonable. However, these validation data are not available for this research which means errors in classification are expected. For example, desert area on ground may be assigned to rangeland on classified map.

Error for one category will be tabulated as error for other. In addition, the supervised classification method refers to informational categories first then to spectral property. Area that is one hundred percent rangeland may be accurate with respect to the rangeland designation, but may still be very diverse with respect to density and other spectral properties.

Table 4.7. Changes, in terms of number of pixels, in Landuse/cover between each class from 1990 to 2006 in King Talal Dam

Landuse/cover		Remain the same in 2006	Changed to urban (2006)	Changed to crop (2006)	Changed to orchard (2006)	Changed to forest (2006)	Changed to rangeland (2006)	Changed to desert (2006)
Urban (1990)	Total 171	84	---	7	11	34	33	2
Crop (1990)	Total 22	4	6	---	2	9	1	0
Orchard (1990)	Total 120	23	21	0	---	41	34	1
Forest (1990)	Total 82	49	9	0	14	---	9	1
Rangeland (1990)	Total 265	55	115	5	49	39	---	2
Desert (1990)	Total 2	1	0	0	0	0	1	---

Table 4.8. Changes, in terms of number of pixels, in Landuse/cover between each class from 1998 to 2006 in Karameh Dam

Landuse/cover		Remain the same in 2006	Changed to urban (2006)	Changed to crop (2006)	Changed to Orchard (2006)	Changed to Forest (2006)	Changed to Rangeland (2006)	Changed to Desert (2006)	Changed to Salt (2006)
Urban (1998)	Total 105	91	---	8	5	0	1	0	0
Crop (1998)	Total 27	7	20	---	0	0	0	0	0
Orchard (1998)	Total 27	3	20	0	---	4	0	0	0
Salt (1998)	Total 671	163	501	0	0	0	2	5	---

Three subwatersheds draining into the reservoir were selected to study the relationship between landuse/cover changes and turbidity in King Talal Dam for each year in 1990 and 2006 as shown in figures 4.27, 4.28 and figure 4.29. The C-factor in the USLE equation was used as an erosion index for each subwatershed. The three figures show the subwatersheds with different landuse/cover distribution and changes.

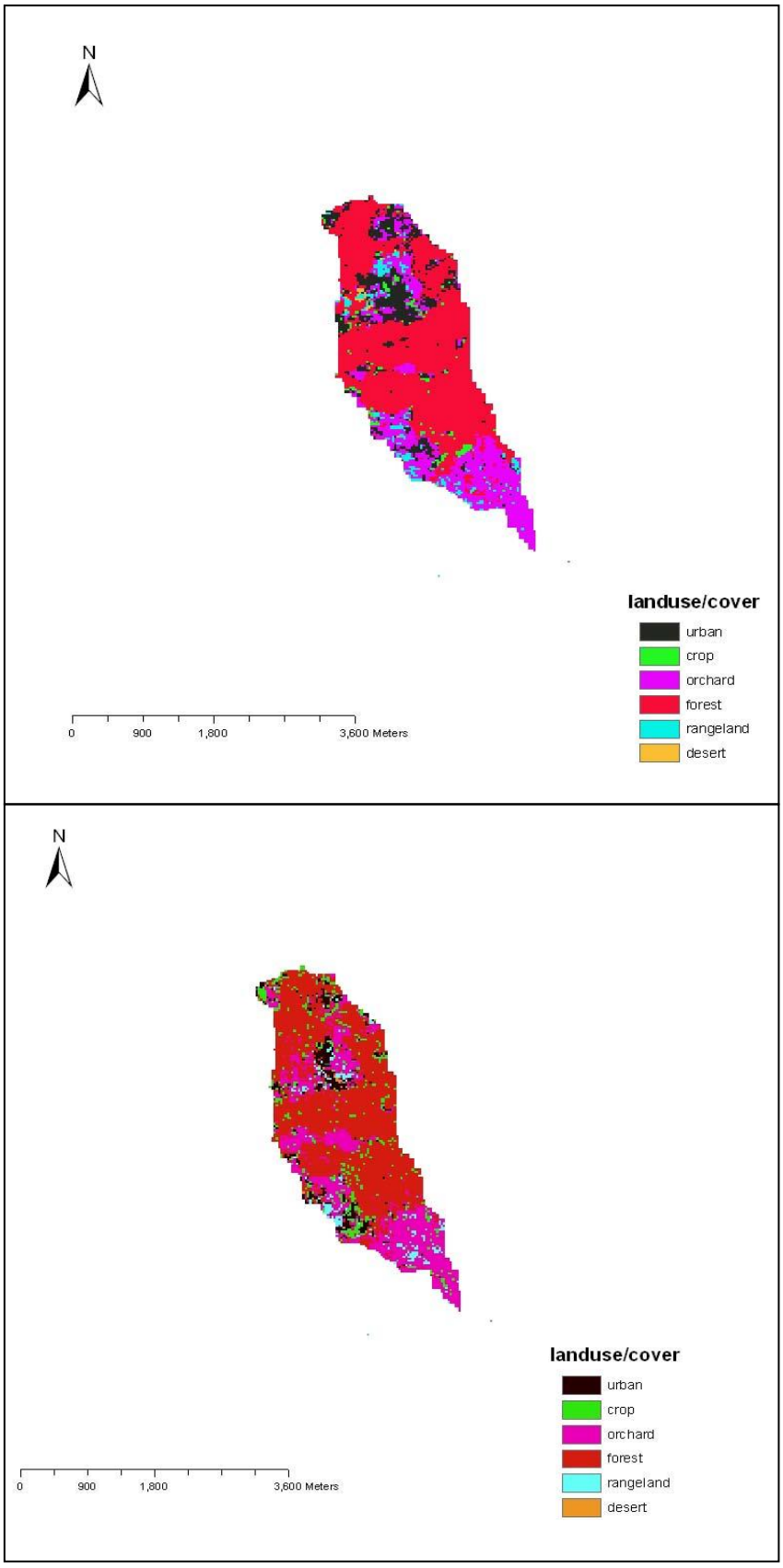

Figure 4.27. Subwatershed 1 for King Talal Dam (A)in 1990 and (B) in 2006

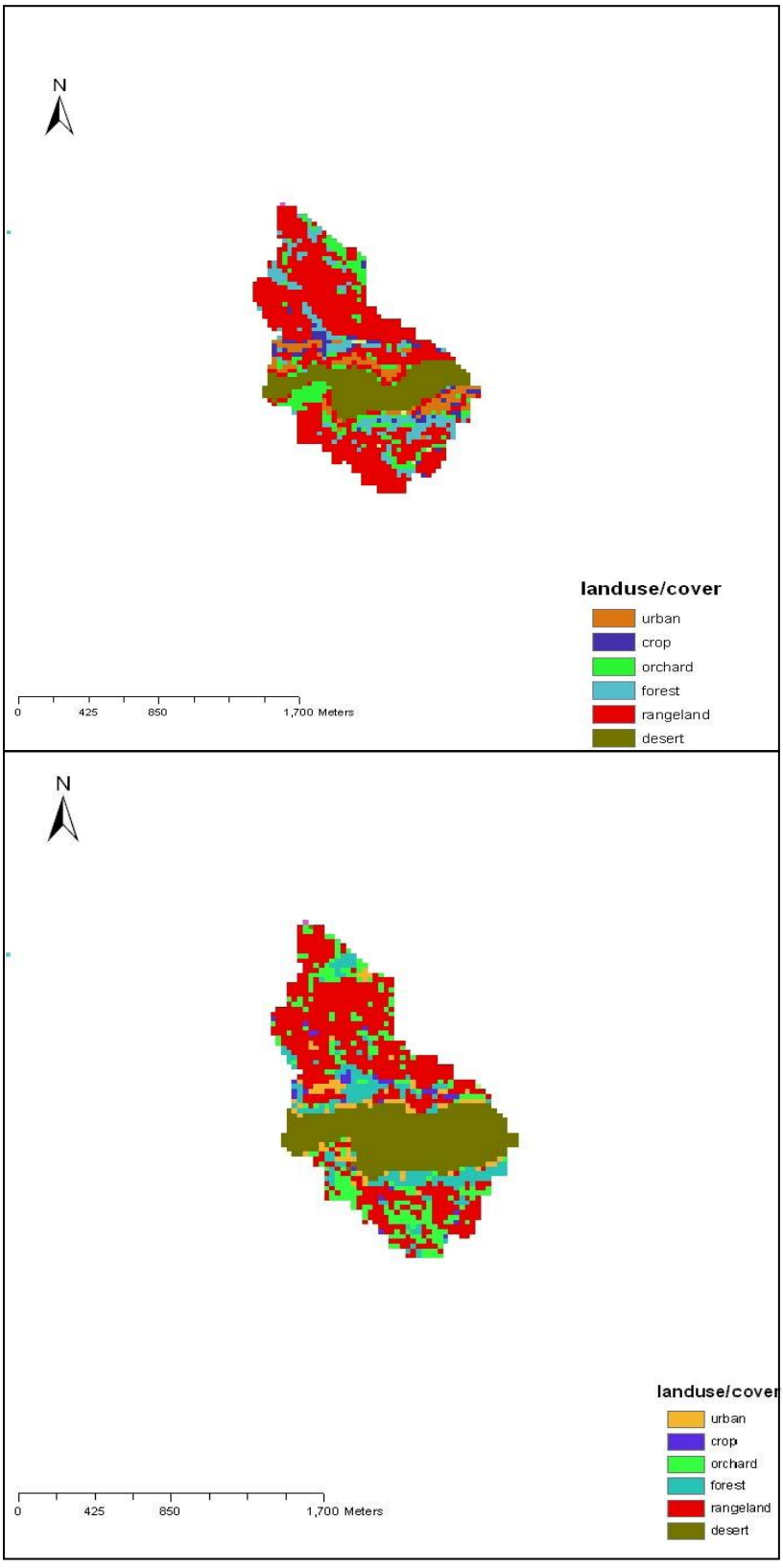

Figure 4.28. Subwatershed 2 for King Talal Dam (A) in 1990 and (B) in 2006

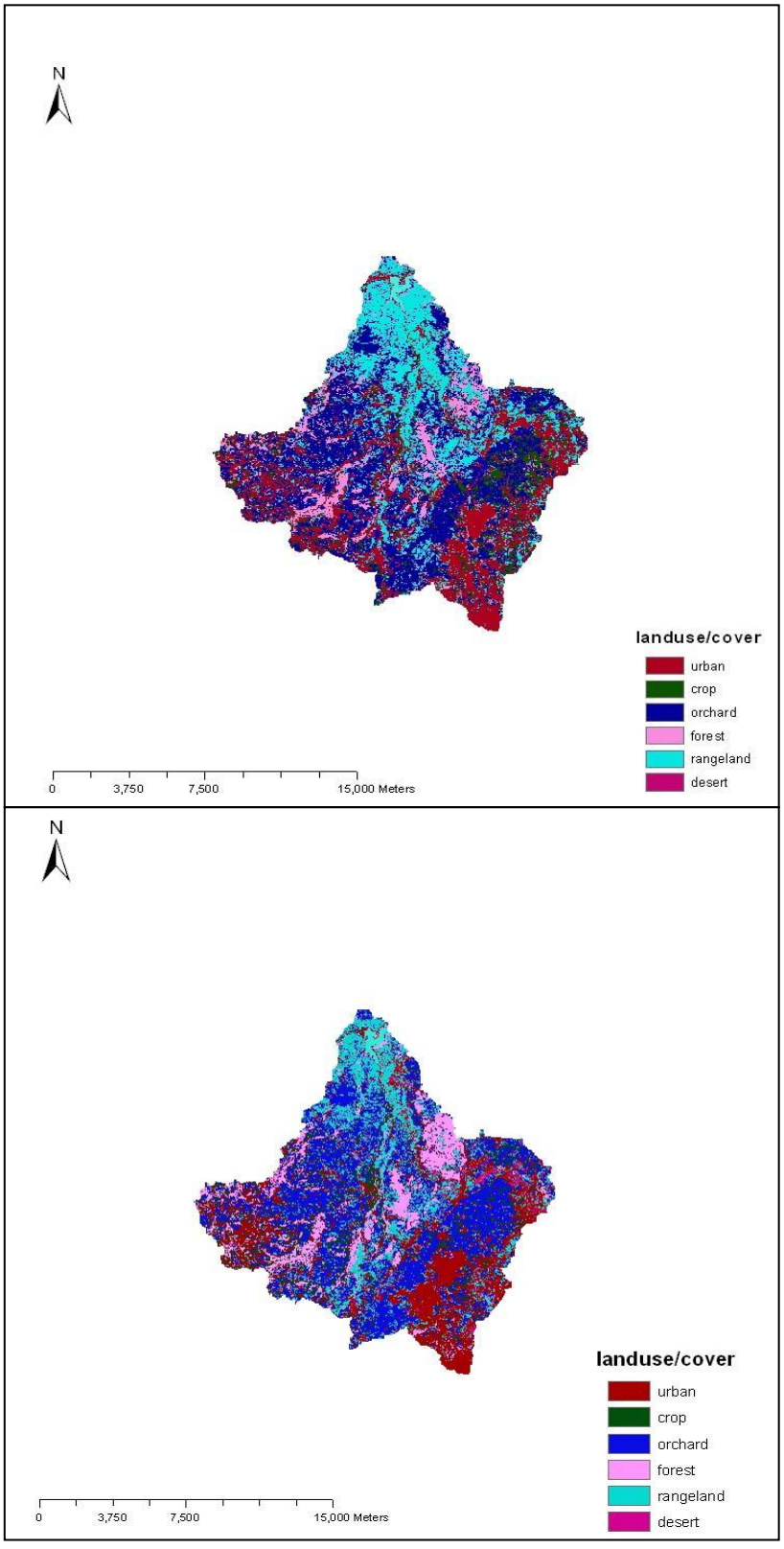

Figure 4.29. Subwatershed 2 for King Talal Dam (A) in 1990 and (B) in 2006

Table 4.9 shows the values of C-factor for each landuse/cover type and sources of these values. These values were taken from studies conducted in areas with the same semi-arid and dry conditions as Jordan. For example, the C-factor value for orchard was taken from a study by Rousseva (2003) for the common summer fruit recognizing by separate stages and development like grapes, peaches, and nectarines. These summer fruits are dominant in both areas of study between June and August.

Table 4.9. C-factor for different Landuse/cover from different sources

Landuse/cover	C-factor	Source
Urban	0.01	Tollner and Saleh (2008)
Crop	0.013	Tollner and Saleh (2008)
Orchard	0.35	Rousseva (2003)
Forest	0.006	Tollner and Saleh (2008)
Rangeland	0.036	Tollner and Saleh (2008)
Desert	0.038	Renard (1982)

The area-weighted average C-factor was calculated for the three subwatersheds in 1990 and 2006 for King Talal dam. The number of pixels for each specific area was determined as shown in tables 4.10, 4.11, and 4.12. The area-weighted average C-factor was compared between 1990 and 2006. Results showed that the C-factor in 2006 was a little higher than it was in 1990 for both subsheds 1 and 2, which means these two subsheds were susceptible to more erosion in 2006. The same results were found by the chromaticity analysis where turbidity levels had increased in these two areas in 2006. However, for subshed 3, the average C-factor in 2006 was less than that in 1990, which means subshed 3 was less susceptible to erosion in 2006 than in 1990. Conversely, the chromaticity analysis found that turbidity levels increased in that area in 2006.

Table 4.10. Number of pixels for each Landuse/cover and area-weighted average C-factor for subwatershed 1 for King Talal Dam

Landuse/cover	Number of Pixels	
	1990	**2006**
Urban	939	431
Crop	178	563
Orchard	1603	1901
Forest	4109	3966
Rangeland	274	223
Desert	31	16
Area-weighted average C-factor	0.0741	0.0865

Table 4.11. Number of pixels for each Landuse/cover and area-weighted average C-factor for subwatershed 2 for King Talal Dam

Landuse/cover	Number of Pixels	
	1990	**2006**
Urban	105	80
Crop	62	333
Orchard	177	237
Forest	173	188
Rangeland	881	706
Desert	296	470
Area-weighted average C-factor	0.05336	0.0619

Table 4.12. Number of pixels for each Landuse/cover and area-weighted average C-factor for subwatershed 3 for King Talal Dam

Landuse/cover	Number of Pixels	
	1990	**2006**
Urban	48570	46240
Crop	14821	19856
Orchard	74896	69768
Forest	16163	25738
Rangeland	45942	33676
Desert	883	5832
Area-weighted average C-factor	0.1239	0.1155

As described in chapter 3, it was impossible to delineate the Karameh watershed based on the DEM because the area is very flat. The relationship between landuse/cover and turbidity was examined by creating a buffer zone around the reservoir and comparing the C-factor for selected areas 1 and 2 as shown in figures 4.30 and 4.31 in both years 1998 and 2006 with the chromaticity analysis results. As shown in both figures, more landuse/cover types were found in 2006. For example, the dominant landuse/cover type in 1998 was the salt rocks, while in 2006 the dominant landuse/cover was urban.

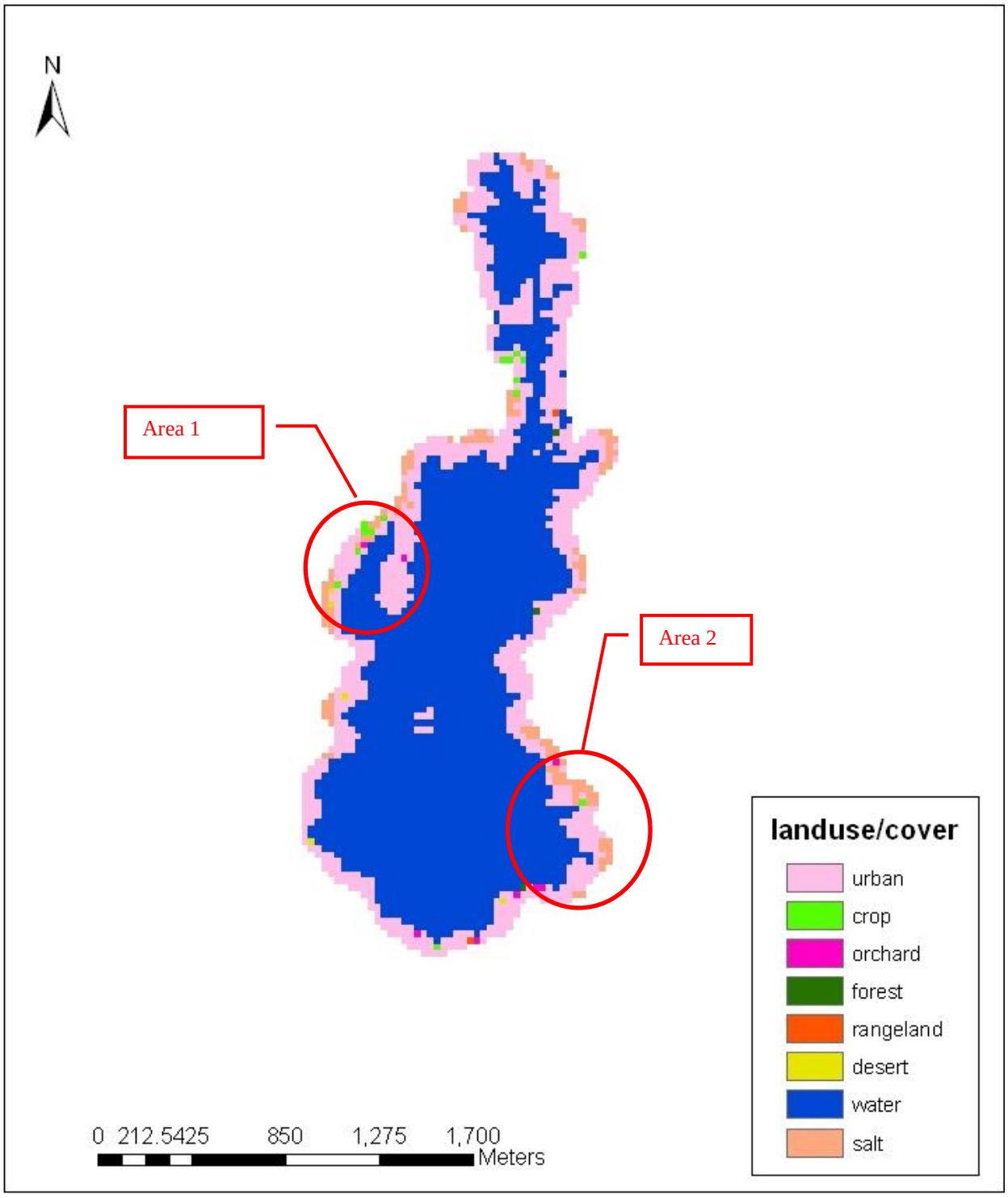

Figure 4.30. Buffered area for Karameh Dam in 2006

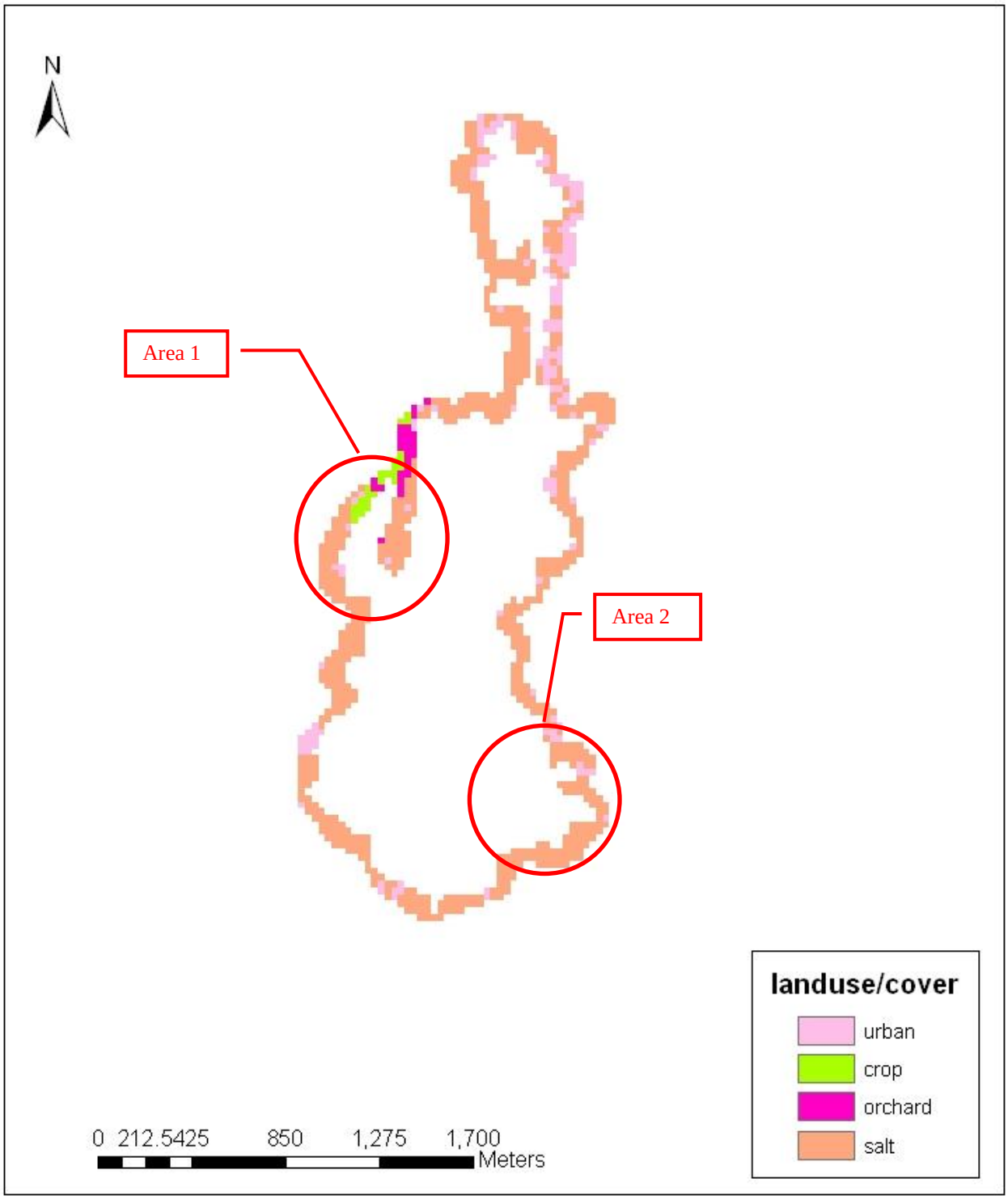

Figure 4.31. Buffered area for Karameh Dam in 1998

The number of pixels for each specific area was determined as shown as in tables 4.13 and 4.14. Results showed that the c-factor weighted average in 2006 was 0.016 that is less than it was in 1998 for area 1. For area 2 average c-factors was 0.025 in 2006 which is also less than average c-factor in 1998. This means these two areas produced less turbidity in 2006. Conversely, chromaticity analysis found that turbidity levels had increased in these two areas in 2006.

Table 4.13. Number of pixels for each Landuse/cover for area 1 in Karameh Dam

Landuse/cover	1998	2006
Urban	11	99
Crop	20	6
Orchard	23	2
Forest	0	0
Rangeland	0	0
desert	0	2
salt	84	30

Cw- avg (1998) = 0.075

Cw- avg (2006) = 0.016

Table 4.14. Number of pixels for each Landuse/cover for area 2 in Karameh Dam

Landuse/cover	1998	2006
Urban	11	84
Crop	0	1
Orchard	0	3
Forest	0	1
Rangeland	0	0
desert	0	0
salt	113	35

Cw avg (1998) = 0.036

Cw avg (2006) = 0.025

The objective of this research was to identify if a relationship exists between turbidity levels and landuse/cover patterns. TM data were transformed to chromaticity coordinates to estimate turbidity levels in both reservoirs. The chromaticity analysis found that there was an increase in turbidity level in 2006 in both reservoirs. It was difficult to directly find a relationship between turbidity levels as estimated by chromaticity analysis and the change in C-factor as an index of erosion in both areas. Many factors may affect turbidity levels besides landuse/cover, as mentioned in chapter 3. The methodology of this research, the use of Landsat TM data to study the relationship between landuse/cover patterns and turbidity was not enough to find this relationship. Field data are needed for the future studies of such relationship.

A study by Royal Scientific Society (2006) found that during the past 20 years, many factories have been built on the Zarqa River bank, the main water supply for King Talal reservoir. These factories got the permission without evaluation of the negative impact upon the river. These factories started to discharge their waste to the river and ended in King Talal reservoir. Moreover, many WWT plants were built in the catchment area including, Al Samra

WWTP Jerash, and Baka'a, which discharge in the tributaries of the reservoir. According to Royal Scientific Society (2006) the outflow of these WWTP is estimated to be about 50% of the water that enters the reservoir.

5 SUMMARY AND CONCLUSIONS

The purpose of this research was to extend the use of Landsat TM by focusing on the following objectives:

1) to evaluate the potential for developing landuse/cover maps for Jordan by using remote sensing techniques;
2) to quantify the changes in landuse/cover in dam areas in Jordan;
3) to determine if changes in water quality can be detected using remote sensing techniques; and
4) to determine if there is a relationship between the changes in landuse/cover and reservoir water quality over a period of time using remote sensing data.

The first and second objectives were accomplished by identifying the pattern of landuse/cover change in the study area using supervised classification technique. The use of remote sensing proved to be powerful in documenting the amount of growth, spatial distribution and changes in landuse/cover. The supervised classification technique was useful in quantifying eight different landuse/cover types. The main increase in landuse/cover in 2006 for both dam watersheds was in urban.

For objective (3), TM was used successfully to detect turbidity levels within two reservoirs by the chromaticity technique and the results were related to previous reports and results based on ground data. Estimated turbidity levels correlated moderately well with surface data; both types of data found that turbidity levels increased in both reservoirs over time.

The C-factor in the USLE equation was used as an index to estimate turbidity in an effort to determine a relationship between landuse/cover patterns and turbidity levels. The area-weighted average C-factor was calculated for different subsheds for both reservoirs. For King Talal reservoir, the average C-factor for subsheds 1 and 2 increased in 2006, indicating the potential erosion from these two subsheds increased in 2006. For subshed 3 in King Talal reservoir, the average C-factor decreased in 2006, however, the turbidity levels increased according to chromaticity analysis. Similar results were found for Karameh reservoir. These inconsistencies made it difficult to relate particular landuse/cover patterns and turbidity levels for both King Talal and Karameh reservoirs. Because landuse/cover patterns did not relate to the

results of chromaticity analysis, other factors such as water depth and currents, wind, metrological events, and waste discharge should be considered when studying turbidity.

The resulting data can provide a baseline on which to base future studies of both areas for tracking the changes and the negative impacts to the environment. To minimize the negative impacts to the environment, and make a control means for population growth, there is a need for accurate, reliable and up to date data at regular intervals. Remote sensing technology can serve as a basic data source for this need.

Governmental organizations and private agencies in Jordan should cooperate and work together, rather than attempting isolated solutions on an individual basis. Adaptation of protection strategy to the current status requires certain, urgent and short-term measures. Future generations should be considered, and landuse activities, which can result in irreversible changes, should be kept under control.

As proven through this study and many of the studies mentioned before, remote sensing imagery analysis is an effective way to analyze data in a low-cost and efficient manner. This study proved that using remote sensing can be applicable to study topics like landuse/cover changes and water quality assessment. The existence of systems like Landsat allow for efficient, consistent data collection for use in temporal studies. The wide availability of this satellite imagery along with the availability of higher spatial resolution imagery for comparison makes the use of this data effective for time series analysis, especially when no field data are available, like the situation in Jordan.

The increasing availability of worldwide imagery coverage by different sensors (e.g., TM and QuickBird) provides a wealth of information viewed from a variety of spatial, spectral, temporal, and directional scales. Such information could assist in determining vulnerable areas and prioritizing land-use planning as well as engaging collaborative thinking and cooperation in conservation initiatives that would be beneficial among different sectors in Jordan such as universities, schools, and ministries.

5.1 Limitations and implications

A combination of practical and conceptual problems influenced the results of this research. Practical problems were defined in this research as data collection problems and can be classified into three categories: date difference, data availability, and Landsat system problems. For example, Landsat TM samples a larger area of the water body than the surface sample which could account for the differences between turbidity estimated levels. Problems within these categories can be solved by collecting new or different kinds of data.

Conceptual problems were based on theoretical issues of using Landsat TM data for watershed assessment purposes and remain even after the practical problems have been solved. Conceptual problems can be classified into two broad-categories: technique application problems and constraints of the Landsat system. Problems within these two categories indicate that Landsat data are not a substitute for surface data. Instead, Landsat data can more probably supplement surface water quality data. The practical and conceptual problems can be summarized as follows:

1) Dates availability and date difference: it was not easy to get images for both reservoirs in the same year and month to avoid seasonal difference, especially for Karameh Dam
2) Data availability: The lack of water quality data and the lack of images made it difficult to extract reflectance data and calculate the concentration of the sediments in reservoir and even to expand this to other reservoirs. The relationship between landuse/cover and turbidity was difficult to identify using just two scenes for each dam. Sufficient high quality imagery would be difficult to acquire for more in depth study.
3) System problems: the coarse resolution of Landsat prevents a more specific analysis for landuse/cover change.

In the end, the Landsat system is limited by the type of information that it can provide about the earth's resources and by atmospheric conditions. The Landsat system can provide spectral information about water bodies, but because of meteorological conditions, this information might not be available on a regular basis. However, by reducing the conceptual problems, and using one or two high quality scenes per year, it may be possible to delineate

landuse/cover patterns within a watershed. Therefore, meteorological events and atmospheric haze would not be as problematic for this technique. Data from this technique, combined with a broad base of surface data, permit watershed assessment and gross landuse/cover information and water quality relationships.

5.2 Recommendation and extension of research

From the results of this research, several recommendations can be suggested:

1) New regulations and restrictions should be applied on the use of land and areas in the watershed, especially within unused areas, to reduce the sources and amount of pollution that reach the reservoir.
2) It is important to have a regular monitoring program to monitor and protect the water in reservoirs in Jordan.
3) Conduct an environmental impact assessment for the landuse/cover activities within the watershed and study their effects on water quality of the reservoir.
4) Acquire sufficient high-quality imagery for in-depth study, with better temporal and spatial resolution.
5) Efforts should be made to include a broader range of surface samples which should be collected on the same date as the satellite overpass.
6) For accuracy assessment purposes, field data are needed to support the results from remotely sensed data. This can be achieved by involving the stakeholders, universities and local organizations to perform the field work.
7) Recent images would be necessary to monitor the recent changes.
8) Automate the process: If the above procedure were proven by further research, the next logical step would be to automate the procedure to make it more efficient and practical to use. Once the process becomes time tested and automated, the main goal of producing maps that show the changing dynamics of a reservoir and landuse would be more easily attained. In addition, this could be extended to other reservoirs and study other water parameters like phosphorus, nitrogen and chlorophyll.
9) Run other models to help understand the relationship between landuse/cover and water quality.

6 REFERENCES

Agricultural Research Service. 2010. Remote sensing/GIS/modeling. Washington DC, U.S.: Department of Agriculture, U.S. Available at: http://www.ars.usda.gov.

Ahern, F. J., D. G. Goodenough, S. C. Jain, V. R. Rao, and G. Rochon. 1977. Landsat atmospheric corrections at CCRS. In *Proceedings of the Fourth Canadian Symposium on Remote Sensing*, Quebec City, Canada, May 1977, pp. 583-595.

Al-Tamimi, S., and J. T. Al-Bakri. 2005. Comparison between supervised and unsupervised classifications for mapping land use/cover in Ajloun area. *Jordan Journal of Agricultural Sciences* 1:73-83.

Alföldi, T. T., and J. C. Munday. 1977. Progress toward a Landsat water quality monitoring system. In *Proceedings of the Fourth Canadian Symposium on Remote Sensing*, Quebec City, Canada, pp. 325-340.

Campbell, J. B. 2007. *Introduction to Remote Sensing*. 4th ed. Guilford Press, New York.

Center for Biodiversity and Conservation. 2010. Image Interpretation and Classification. American Museum of Natural History. Available at: http://biodiversityinformatics.amnh.org.

Central Intelligence Agency. 2009. The World Factbook: Jordan. Central Intelligence Agency. Available at: https://www.cia.gov.

Chander, G., B. L. Markham, and D. L. Helder. 2009. Summary of current radiometric calibration coefficients for Landsat MSS, TM, ETM+, and EO-1 ALI sensors. *Remote Sensing of Environment* 113(5):893-903.

Chauhan, P., S. Nayak, R. Ramesh, R. Krishnamoorthy, and S. Ramachandran. 1996. Remote sensing of suspended sediments along the Tamil Nadu coastal waters. *Journal of the Indian Society of Remote Sensing* 24(2):10.

Chavez, P. S. 1975. Atmospheric, solar and M.T.F. corrections for ERTS digital imagery. In *Proceedings American Society of Photogrammetry Fall Conference*, Phoenix, AZ, p. 69.

Chavez, P. S. 1988. An improved dark-object subtraction technique for atmospheric scattering correction of multispectral data. *Remote Sensing of Environment* 24(3):459-479.

Choubey, V. K. 1994. Monitoring water quality in reservoirs with IRS-1A-LISS-I. *Water Resources Management* 8(2):121-136.

Coskun, H. G., A. Tanik, U. Alganci, and H. K. Cigizoglu. 2008. Determination of environmental quality of a drinking water reservoir by remote sensing, GIS, and regression analysis. *Water, Air, & Soil Pollution* 194:275–285.

Dai, X., and S. Khorram. 1998. The effects of image misregistration on the accuracy of remotely sensed change detection. *IEEE Transactions on Geoscience and Remote Sensing* 36(5):1566-1577.

Department of the Interior/ USGS. 1960. U.S Geological Survey. Available at: http://glovis.usgs.gov. Accessed May 2010.

Department of the Interior/ USGS. 2001. U.S Geological Survey. Available at: http://glovis.usgs.gov. Accessed May 2010.

Department of the Interior/ USGS. 2006. U.S Geological Survey. Available at: http://glovis.usgs.gov. Accessed May 2010.

Detwiler, R. P., and C. A. S. Hall. 1988. Tropical forests and the global carbon cycle. *Science* 239(4835):42-47.

Gildea, J. J. 2000. Relationships Between Land Use, Land Use Change, and Surface Water Quality Trends in Virginia. MS thesis. Virginia Polytechnic Institute and State University, Environmental Science and Engineering, Blacksburg.

Goel, M. K., and S. K. Jain. 1996. Evaluation of reservoir sedimentation using multi-temporal IRS-1A LISS II data. *Asian-Pacific Remote Sensing and GIS Journal* 8(2):39-43.

Gorsevski, P. V. 2008. Assessment of Land Use and Land Cover Changes around Ohrid and Prespa Lakes Using Landsat Imagery. In *Proceedings of BALWOIS 2008 Symposium*. Ohrid, Republic of Macedonia: BALWOIS.

International Commission on Illumination. 1931. CIE 1931 color space. Available at: www.cie.co.at. Accessed April 2010.

Itten, K. I., and P. Meyer. 1993. Geometric and radiometric correction of TM data of mountainous forested areas. *Geoscience and Remote Sensing, IEEE Transactions* 31(4):764-770.

Jain, S. K., P. Singh, and S. M. Seth. 2002. Assessment of sedimentation in Bhakra Reservoir in the western Himalayan region using remotely sensed data. *Hydrological Sciences Journal* 47(2):10.

Jensen, J. R. 2006. *Remote Sensing of the Environment: An Earth Resource Perspective*. 2nd ed. Prentice Hall Publications, New Jersey.

Jensen, J. R., K. Rutchey, M. S. Koch, and S. Natumalani. 1995. lnland wetland change detection in the Everglades water conservation area 2A using a time series of normalized remotely sensed data. *Photogrammetric Engineering & Remote Sensing* 61(2):199-209.

Khorram, S., H. Cheshire, A. L. Geraci, and G. L. Rosa. 1991. Water quality mapping of Augusta Bay, Italy from Landsat-TM data. In *International Geoscience and Remote Sensing Symposium*. British Columbia: University of British Columbia.

Kondratyev, K. Y., and A. P. Cracknell. 1998. *Observing Global Climate Change*. Climatic Change. 1st ed. Springer Netherlands.

Kovalick, W. M. 1983. The effect of selected preprocessing procedures upon the accuracy of Landsat derived classification of a forested wetland. MS thesis. Virginia Polytechnic Institute and State University, Blacksburg, VA.

Lindeli, T., B. Karisson, M. Rosengren, and T. Afoldi. 1986. A further development of the chromaticity technique for satellite mapping of suspended sediment load. *Photogrammetric Engineering and Remote Sensing* 52(9):1521-1529.

Liu, J., M. Liu, D. Zhuang, Z. Zhang, and X. Deng. 2003. Study on spatial pattern of land-use change in China during 1995–2000. *Science in China Series D: Earth Sciences* 46(4):373-384.

Lugo, A. E., and S. Brown. 1992. Tropical forests as sinks of atmospheric carbon. *Forest Ecology and Management* 54(1-4):239-255.

Manavalan, P., P. Sathyanath, and G. L. Raiegowda. 1993. Digital lmage Analysis Techniques to Estimate Waterspread for Capacity Evaluation of Reservoirs. *Photogrammetric Engineering & Remote Sensing* 59(9):1389-1395.

Ministry of Water and Irrigation, Jordan. 2008. Water situation in Jordan: 2007. Amman, Jordan.

Moran, E. 1993. Deforestation and land use in the Brazilian Amazon. *Human Ecology* 21(1):1-21.

Munday, J. C. 1974. Lake Ontario water mass delineation from ERTS-1. In *International symposium on remote sensing of environment*. Michigan, United States.

Munday, J. C., and T. T. Alföldi. 1975. Chromaticity changes from isoluminus techniques used to enhance multispectral remote sensing data. *Remote Sensing of Environment* 4:221-236.

Munday, J. C., T. T. Alföldi, and C. L. Amos. 1979. Bay of Fundy verification of a system for multidate LANDSAT measurement of suspended sediment. In *Proceedings of the Fifth Annual*

William T. Pecora Memorial Symposium on Remote Sensing. Sioux Falls, United States: CSA Illumina.

Nayak, S. 1983. Orbital monitoring of suspended sediments in water body. In *National Sympsium of Remote Sensing in Development and Management of Water Resources*.

Nelson, S. A. C., P. A.Soranno, K. S. Cheruvelil, S. A.Batzli, and D. L.Skole. 2003. Regional assessment of lake water clarity using satellite remote sensing. *Journal of Limnology* 62:27-32.

Olmanson, L., P. Brezonik, S. Kloiber, M. Bauer, and E. Day. 2000. Lake water clarity assessment of Minnesota's 10,000 lakes: a comprehensive view from space. In *Virginia Water Research Symposium*. Virginia, United States: CSA Illumina.

Otterman, J., and C. J. Robinove. 1981. Effects of the atmosphere on the detection of surface changes from Landsat Multispectral scanner data *International Journal of Remote Sensing* 2(4):351- 784.

Pyne, S. J. 2003. *Ecological Restoration of Southwestern Ponderosa Pine Forests*. The Science and Practice of Ecological Restoration Series. Island Press.

Rowan, L. 1974. *Discrimination of rock types and detection of hydrothermally altered areas in south-central Nevada by the use of computer enhanced ERTS images*. U.S. Govermnet Print Office, Washington DC.

Royal Scientific Society. 2001. Monitoring the water in King Talal Dam. Royal Scientific Society. Amman, Jordan.

Royal Scientific Society. 2006. Monitoring the water in King Talal Dam. Royal Scientific Society. Amman, Jordan

Ruan, R., Y. Zhang, and Y. Zhou. 2008. Change detection of wetland in Hongze lake using a time series of remotly sensed imagery. *The International Archives of the Photogrammetry, Remote Sensing and Spatial Information Sciences* XXXVII(B 7):1545-1548.

Salameh, E. 1996. *Water Quality Degradation in Jordan: Impact on Environment Economy and Future Generations Resources Base*. Royal Society for Conservation of Nature, Amman, Jordan.

Salameh, E. 2004. The tragedy of the Karama Dam project/ Jordan. *Acta Hydrochimica et Hydrobiologica* 32(3):249−258.

Schalles, J. F., A. A. Gitelson, Y. Z. Yacobi, and A. E. Kroenke. 1998. Estimation of chlorophyll a from time series measurements of high spectral resolution reflectance in an eutrophic lake. *Journal of Phycology,* 34(2):383-390.

Schiebe, F. R., and J. C. Ritchie. 1975. Color measurements and suspended sediments in north Mississippi reservoirs. *Remote Sensing of Earth Resources* 4:543-553.

Sharp, J. M. 2009. Jordan: Background and U.S. Relations. Congressional Research Service. C. R. Service.

Shukla, J., C. Nobre, and P. Sellers. 1990. Amazon deforestation and climate change. *Science* 247(4948):1322-1325.

Singh, A. 1989. Digital change detection techniques using remotely-sensed data. *International Journal of Remote Sensing* 10(6):989-1003.

Skole, D., and C. Tucker. 1993. Tropical deforestation and habitat fragmentation in the Amazon: satellite data from 1978 to 1988. *Science* 260(5116):1905-1910.

Smith, S. E., K. H. Mancy, and A. F. A. Latif. 1980. The application of remote sensing techniques towards the management of the Aswan High Dam reservoir In *14th International Symposium on Remote Sensing of Environment*. San Jose, Costa Rica; United States: CSA Illumina.

United States Geological Survey. 2010. Remote Sensing Resources. United States Geological Survey Available at: http://www.usgs.gov/pubprod/aerial.html#remote.

Vignoloa, A., A. Pochettino, and D. Cicerone. 2006. Water quality assessment using remote sensing techniques: Medrano Creek, Argentina. *Journal of Environmental Management* 81(4):429–433.

Vincent, R. K. 1972. An ERTS multispectral scanner experimental for mapping iron compounds. In *8th International Symposium on Remote Sensing of Environment*. Ann Arbor, MI, U.S.

Vitousek, P. M. 1992. Global environmental change: an introduction. *Annual Review of Ecology and Systematics* 23(1):1-14.

Wayman, J. P. 2000. Landsat TM-based forest area estimation using iterative guided spectral class rejection. MS thesis. Virginia Polytechnic Institute and State University, Department of Forestry, Blacksburg, VA

Welby, C. W. 1975. Use of ERTS imagery in the study of the Cape Fear Plume. *Southeastern Geology* 16(4):189-203.

Weng, Q. 2001. Land use change analysis in the Zhujiang Delta of China using satellite remote sensing, GIS and stochastic modelling. *Journal of Environmental Management* 64 (3):273–284.

Yuan, F., K. E. Sawaya, B. C. Loeffelholz, and M. E. Bauer. 2005. Land cover classification and change analysis of the Twin Cities (Minnesota) Metropolitan Area by multitemporal Landsat remote sensing. *Remote Sensing of Environment* 98(2-3):317-328.

Zhenqiang, M., W. Jing, and L. Yanxia. 2004. Anlysis of land cover change and land degradation in HengShan County Based on RS and GIS. *IEEE International* 5(20-24):3444-3447.

Zilioli, E., and P. A. Brivio. 1997. The satellite derived optical information for the comparative assessment of lacustrine water quality. *Science of The Total Environment* 196(3):229-245.